

Aus der Medizinischen Klinik II

der Universität zu Lübeck

Direktor: Prof. Dr. H. Schunkert

Histological and molecular genetic analysis
of mice with genetic predisposition to
dystrophic cardiac calcification in response to injury.

Inauguraldissertation

zur

Erlangung der Doktorwürde

Der Universität zu Lübeck

- **Aus der Medizinischen Fakultät** -

Vorgelegt von

Zouhair Aherrahrou

aus Rich (Marokko)

Lübeck 2003

1. Berichterstatter: Prof. Dr. med. Heribert. Schunkert

2. Berichterstatter: Prof. Dr. rer. Nat. Reiner Johannisson

Tag der mündlichen Prüfung: 18.10.2004

Zum Druck genehmigt. Lübeck, den 18.10.2004

Gez. Prof. Dr. med. Peter Dominiak

- Dekan der Medizinischen Fakultät -

Contents

Contents	i
List of Figures	iv
List of Tables	v
List of abbreviation	vi
1. Introduction	1
1.1. Pathophysiological mechanisms of cardiovascular calcification	1
1.2. Histological investigations	4
1.3. Molecular genetic studies	6
1.4. Aims of the study	6
2. Material and Methods	8
2.1 Material	8
2.1.1 Reagents	8
2.1.2 Enzyme, Inhibitors and Antibodies	8
2.1.3 Kits	10
2.1.4 Buffers and Solutions	10
2.1.5 Laboratory materials	11
2.1.6 Instruments	11
2.1.7 Oligonucleotides	12
2.2 Animal housing	14
2.3 Molecular biological methods	14
2.3.1 Genomic DNA isolation from mouse tail	14
2.3.2 Cytoplasmic RNA isolation from myocard	15
2.3.3 DNA free, Dnase treatment	15
2.3.4 Total RNA quality control	16
2.3.5 Gel electrophoresis	16
2.3.6 Determination of DNA and RNA concentrations	16
2.3.7 Genotyping of polymorphic microsatellite markers in BXH strains	16
2.3.8 Restriction fragment length polymorphism (RFLP) analysis	17
2.3.9 Radiation Hybrid (RH) analysis	18

2.3.10	Reverse transcription (RT)	19
2.3.11	One step RT-PCR	19
2.4	Freeze-thaw injury	20
2.5	Immunohistological methods	20
2.5.1	Histological analysis	20
2.5.1.1.	Light microscopy	20
2.5.1.2.	Transmission Electron Microscopy (TEM)	21
2.5.2	Immunological analysis	21
2.5.3	Enzyme linked immunosorbent assay (Elisa)	22
2.6	Clinical chemistry	22
3.	Results	24
3.1.	Mapping <i>Dyscalc1</i> in BXH RI strains.	24
3.2.	Identification of candidate genes	24
3.2.1.	Typing of intragenic RFLPs in BXH RI strains	26
3.2.2.	Radiation hybrid mapping of potential candidate genes	28
3.2.3.	Candidate gene expression analysis	30
3.3.	Histopathological investigations	36
3.3.1.	Calcein staining	36
3.3.2.	Alizarin red S staining	38
3.3.3.	Transmission Electron Microscopy	40
3.4.	Bone related proteins expression	40
3.4.1.	Osteopontin	40
3.4.1.1.	Myocardial osteopontin expression	40
3.4.1.2.	Osteopontin concentrations in plasma	48
3.4.2	Transforming growth factor-beta 1, Tgfβ1	49
3.4.3	Osteocalcin	52

3.4.4	Osteonectin.	54
3.4.5	Ca ²⁺ , Mg ²⁺ , phosphor, and Troponin T concentrations in Plasma.	56
4.	Discussion	59
4.1.	Gene targeting	59
4.2.	Pathology	60
4.3.	Initiation and progression of calcium phosphate deposits	60
4.4.	DCC and biological bone mineralisation	63
4.5.	The genetic background	66
5.	Summary	73
	Reference list	76
	Acknowledgement	89
	Curriculum Vitae	90

List of Figures

<u>Fig. 1:</u>	Hypothetical model for dystrophic calcification	3
<u>Fig. 2:</u>	Genetic-environment complexity of DCC	5
<u>Fig. 3:</u>	RFLPs obtained from different BXH RI strains	27
<u>Fig. 4:</u>	Quality control of RNA degradation	31
<u>Fig. 5-1:</u>	Determination of the standard curves and melting temperature for 18S	32
<u>Fig. 5-2:</u>	Determination of the standard curve for Hrc and Etfb	33
<u>Fig. 5-3:</u>	Determination of the standard curve for Bax	34
<u>Fig. 6:</u>	Candidate gene expression analysis after injury	35
<u>Fig. 7:</u>	Calcium deposition analysis at day 1 after injury	37
<u>Fig. 8:</u>	Progression and development of calcium deposits	38
<u>Fig. 9:</u>	Calcium deposition using Alizarin red S staining	39
<u>Fig. 10:</u>	Macroscopic observation of calcium depositions	39
<u>Fig. 11-1:</u>	TEM of C3H/He and C57BL/6 myocardium 1 day after freeze-thaw injury	41
<u>Fig. 11-2:</u>	TEM of C3H/He myocardium 3 days after freeze-thaw injury	42
<u>Fig. 11-3:</u>	TEM of C3H/He myocardium 4 days after freeze-thaw injury	43
<u>Fig. 12:</u>	Detection of macrophages infiltration	45
<u>Fig. 13:</u>	Osteopontin protein expression	46
<u>Fig. 14:</u>	Standard curve for Opn mRNA	47
<u>Fig. 15:</u>	Opn mRNA induction in C57BL/6 and C3H/He mice	47
<u>Fig. 16:</u>	Opn plasma concentration	48
<u>Fig. 17:</u>	Tgf β 1 protein expression	50
<u>Fig. 18:</u>	Standard curves for Tgf β 1 mRNA.	51
<u>Fig. 19:</u>	Tgf β 1 mRNA expression	51
<u>Fig. 20:</u>	Osteocalcin mRNA induction in C3H/He mice	53
<u>Fig. 21:</u>	Osteocalcin protein expression	53
<u>Fig. 22:</u>	Standard curve for osteonectin mRNA	55
<u>Fig. 23:</u>	Osteonectin mRNA expression in C57BL/6 and C3H/He mice	55
<u>Fig. 24:</u>	Ca ²⁺ , Mg ²⁺ and PO ₄ plasma concentration	57
<u>Fig. 25:</u>	Hypothetical pathogenetic model for DCC	72

List of Tables

<u>Tab. 1:</u> Alphabetical list of restriction enzymes	9
<u>Tab. 2:</u> List of polymorphic microsatellite markers	12
<u>Tab. 3:</u> List of oligonucleotide primers used for PCR-amplification for intra-gene RFLP analysis	13
<u>Tab. 4:</u> List of oligonucleotide primers used to amplify PCR products for Radiation Hybrid analysis	13
<u>Tab. 5:</u> List of oligonucleotide primers used to amplify PCR products for RT-PCR analysis	14
<u>Tab. 6:</u> Genotype and DCC phenotype determination in BXH RI strains	25
<u>Tab. 7:</u> Data obtained by genotyping various loci on chromosome 7 using template DNA from cell lines 1-100 of the Radiation hybrid panel	29

1. Introduction

1.1. Pathophysiological mechanisms of cardiovascular calcification

Calcification is known as a process that lead to calcium phosphate crystal formation during bone formation from calcium and phosphate. This physiological event is well known in vertebrates during the formation of skeleton essential for the rigidity of their body. The skeleton alone comprises up to 99% of the total body calcium. The remaining 1% calcium is distributed in blood, extracellular fluid and cells where calcium, as signaling factor, mediate, initiate or inhibit many biochemical processes. Therefore, the homeostasis of calcium is very important for many physiological processes. The mechanism of mineralisation in bone is seen where bone formation take place. The so-called matrix vesicles (MV) are the initial sites of apatite mineral deposition. Once the calcification begun, $\text{Ca}(\text{PO}_4)$ crystal serve as nuclei for the formation and growth of new crystals and no more need for MV to support mineralizing. This process is activated by the availability of Ca^{2+} , $\text{PO}_4^{(3-)}$ and collagen, and inhibited by proteoglycans and several non-collagenous proteins such as osteocalcin (Osc), osteonectin (Osn) and phosphoproteins (Anderson, 1989).

Pathological tissue calcification is a well known finding in various organs. Calcium phosphate precipitation and hydroxyapatite deposits may severely affect patients and determine their quality of life. Several forms of calcification can be distinguished (reviewed in Seifert, 1997): 1) metastatic calcification of soft tissues in the presence of abnormally high extracellular calcium and phosphate concentrations, which may be linked to a disturbed calcium homeostasis due to renal disease, abnormal Vitamin D or parathyroid hormone levels or other forms of metabolic disease; 2) dystrophic calcification associated with focal tissue necrosis, which occur in chronic degenerative or inflammatory conditions usually without influence on extracellular calcium concentrations, and, 3) rare inherited mendelian defects producing mostly premature calcification of cartilage or other bradytrophic tissues such as chondrocalcinosis articularis (Bjelle and Sundstroem, 1975) and chondrodystrophia calcificans congenita (Bosman et al., 1977).

Dystrophic calcium deposition is a hallmark of cardiovascular disease occurring in the coronaries (Catellier et al., 1990), the cardiac valves (Mohler, 2001) as well

as in pericardial or (endo)myocardial tissue, sometimes even in fetal myocardium (Veldtman et al., 1999). Calcium deposits may indicate the severity of cardiac disease similar to calcified plaques, which usually characterize an advanced stage of atherosclerosis (Stallion et al., 1994). Consistent with this, calcification is observed after severe myocardial damage e.g. in patients with ischemic myocardial infarction (D'Agostino and Chiga, 1970; Bloom and Peric-Golia, 1989; Lockard and Bloom, 1991). Interestingly, these reports also discuss a potential relation with mitochondrial function and serum magnesium concentrations.

Although dystrophic cardiac calcification was first described decades ago the disease-causing mechanisms are still not fully understood today. Recent experimental evidence highlighting potential candidate genes and pathways has been contributed from groups studying vascular (Boskey, 1996; Kim, 1995) and osseous calcification (Anderson, 1989) as well as osteoporosis. Studies in transgenic or gene-targeted mouse models have emphasized the roles of calcium binding proteins (Luo et al., 1997) and bone-related proteins, such as osteopontin (Opn), which appear to influence calcium precipitation and cell signaling in injured and necrotic tissue (Giachelli and Steiz, 2000).

Dystrophic cardiac calcification (DCC) may also occur spontaneously in aging mice of certain inbred strains with a genetic predisposition including DBA/2, C, C3H, BALB/c, A, CBA and CHI (Van Vleet and Ferrans, 1987). Studies with the aim to optimize the diet of laboratory animals have shown that a high-fat or low-protein diet (Eaton et al., 1978, Van Vleet and Ferrans, 1987; Highman and Daft, 1965; Everitt et al, 1988), as well as a high-phosphorus or low-magnesium diet (Van den Broek et al., 1997) may produce premature or enhanced DCC. Other factors such as infectious agents including Coxsackie virus A and B, Cytomegalovirus or the Encephalomyocarditis virus were also reported to cause DCC (Gang et al., 1986; Matsumori et al., 1991). Moreover, experiments employing cryopexy to produce a direct myocardial freeze-thaw injury have demonstrated that DCC actually occurs after irreversible cell injury and necrosis irrespective of the etiology (Vracko and Thorning, 1985; Brunnert and Altman, 1990; Brunnert et al., 1997).

Although the pathogenesis of DCC is still not known, ultrastructural evidence suggested that calcium precipitation originated in swollen mitochondria and progressed to include the entire sarcoplasm of the irreversibly injured

myocyte. These mineral deposits were described as very-electron-dense granules, spicular deposits, and needle-like crystals, reflecting their hydroxyapatite crystal nature and were compared with bone calcification (Christoffersen and Landis, 1991). It is now believed that dystrophic calcification is an active process that might be regulated and evidence including structure resembling bone and bone marrow (Bostrom and Demer, 2000; Bostrom, 2000) and matrix vesicles (Kim, 1976) supported this hypothesis. A hypothetical model for dystrophic calcification was proposed by Cotran et al., (1994) (Fig. 1).

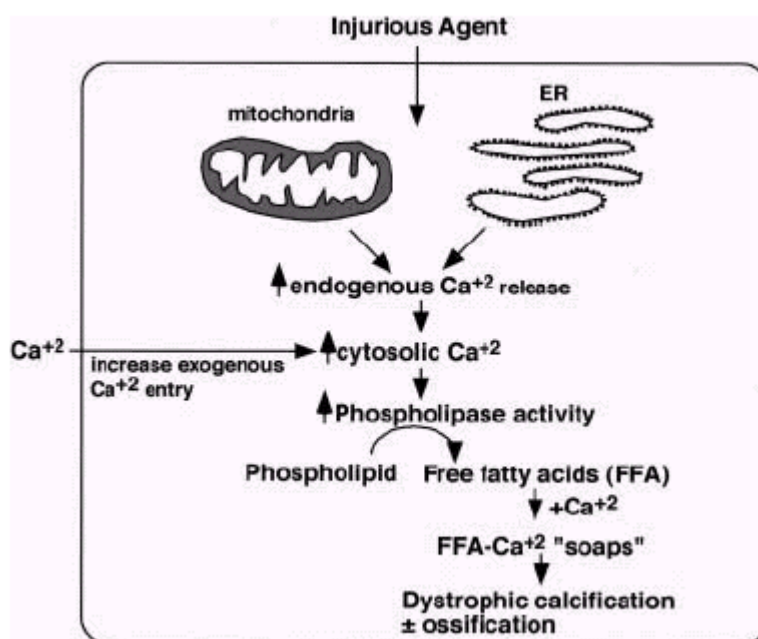


Fig. 1: Hypothetical model for dystrophic calcification. Injury or inflammation stimulate release of Ca^{2+} from mitochondria, endoplasmic reticulum and exogeneous Ca^{2+} entry. This result in elevated cytosolic calcium concentration that in turn will stimulate the activity of phospholipase that lead to fatty acids liberation. Finally, calcium binds to fatty acids and serves as nidus for further calcification progression. Modified from Cotran et al., (1994).

Insights into the biology of dystrophic calcification were obtained from studies exploiting the mouse as a genetic model of complex mammalian disease. A polygenic basis of recessively inherited DCC was proposed first in 1978 (Eaton et al., 1978). Examining an F2 intercross of resistant C57BL/6J (B6) and susceptible C3H/He (C3H) Ivandic et al., (1996) finally identified by quantitative trait locus (QTL) analysis a major locus, *Dyscalc1*, on proximal chromosome 7. Later, this locus was shown to be responsible for DCC in susceptible DBA/2 strains as well (Van den Broek et al., 1998, Brunnert et al., 1999). Recently, additional *Dyscalc* loci were identified: *Dyscalc2*, *Dyscalc3*, and *Dyscalc4* were mapped to chromosome 4, 12, and 14, respectively. These loci exhibited

epistasis and modified the penetrance and expression of DCC (Ivandic et al., 2001). These genetic studies led to a hypothetical disease model, Fig. 2, in which various agents may cause irreversible cell injury subsequently leading to cell death and necrosis. Ensuing tissue repair is characterized by scarring and calcium deposition, which is determined by *Dyscalc1*. In addition, *Dyscalc2*, a modifier locus, which itself is not sufficient to cause DCC, may enhance the influence of *Dyscalc1* (Fig. 2). Although the *Dyscalc1* locus has been refined to a chromosomal interval of about 10 cM (corresponding to approx. 20 million bp) the underlying gene has not been cloned so far (Ivandic et al. 2001, Colinayo et al. 2002).

Present studies were carried out to improve our rather limited understanding of the observed phenotype of DCC in order to identify potential candidate genes, which had to be located in the *Dyscalc1* interval to be potentially identical with the *Dyscalc1* gene. Therefore, a comprehensive approach was chosen, including both the histological analysis of DCC as well as molecular genetic studies with the aim to map precisely a number of genes on proximal chromosome 7, which are involved in calcium homeostasis, inflammation, wound healing and apoptosis.

1.2. Histological investigations

Histological investigations were carried to compare calcium deposition in response to tissue injury with physiological bone mineralisation. First hints that both conditions might share common elements was derived from a report of Murry and co-workers, who observed an induction of osteopontin after myocardial freeze-thaw injury in rats (Murry et al. 1994). They demonstrated osteopontin induction throughout several days after myocardial damage in a subpopulation of macrophage-like cells infiltrating the necrotic tissue. Opn is a

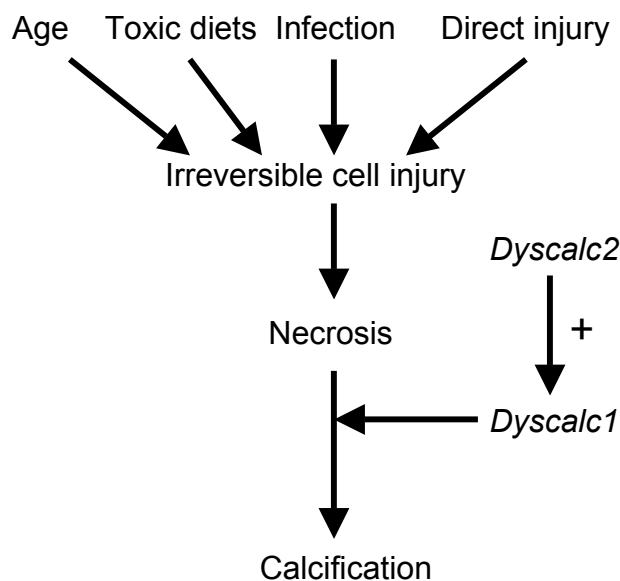


Fig. 2: Genetic-environment complexity of DCC. Genetic background of *Dyscalc* play a determinant role in the initiation and development of dystrophic calcification that result from irreversible cell injury and necrosis enhanced by various environmental agents.

multi-functional calcium binding protein with an RGD motif interacting with osteoclasts through CD44, the $\alpha_v\beta_3$ integrin receptor (Miyachi et al., 1991; Flores et al., 1992). A marked chemotactic effect on macrophages has been shown for Opn in wound healing (Giachelli et al., 1998). Thus, Opn may not only attract macrophage-derived osteoclasts, but also immobilize them on calcium deposits and thus enable bone resorption (Ross et al., 1993). Therefore, the primary aim of the histological examination was to test, whether Opn was also induced in myocardial freeze-thaw necrosis in mouse strains predisposed to DCC and if so, to examine its regulation employing immunohistochemical and mRNA analysis to reveal strain-specific differences. Additional bone-related proteins including alkaline phosphatase, Osn and Osc were also tested as markers for osteoblasts and would relate DCC with biological bone mineralisation (secondary aims). This linkage has been shown for vascular calcification (Demer, 1995). Histological analyses were performed in groups of susceptible C3H/He and resistant C57BL/6 (control) mice 1, 2, 3, 5, 9, and 21 days after freeze-thaw injury in order to elucidate the time course of calcium deposition and gene induction in the necrotic myocard.

1.3. Molecular genetic studies

Many potential candidate genes for *Dyscalc1* were located on proximal chromosome 7. The current genetic maps display many genes – some were only roughly mapped – that encode for proteins which are involved in intracellular calcium homeostasis (skeletal ryanodine receptor, Ryr1; histidine-rich calcium binding protein, Hrc; Na⁺-Ca⁺⁺ exchanger, Slc8a2), inflammation (nuclear factor of kappa light chain gene enhancer in B cells inhibitor, Nfkbib), wound healing (transforming growth factor-beta 1, Tgfβ1), apoptosis (bcl2-associated death protein, Bax) as well as certain marker genes of growth and differentiation (FBJ osteosarcoma oncogene B, Fosb; myogenic differentiation 1, Myod1). These genes may be considered candidate genes for *Dyscalc1*, if they can be located in the *Dyscalc1* interval either by segregation analysis of intragenic restriction fragment length polymorphisms (RFLP) in recombinant inbred BXH strains (derived from C57BL/6 and C3H/He strains) or by high-resolution mapping employing radiation hybrid (RH) mapping techniques. Potential candidate genes were then examined by quantitative RT-PCR to reveal strain-specific differences in gene regulation in response to freeze-thaw injury, which might support their consideration as a relevant candidate gene.

1.4. Aims of the study:

The specific aim of the present study was to combine pathological and molecular genetic approaches to highlight the complex environment-genetic complex interaction leading to the initiation and progression of DCC using mice with genetic predisposition. For this reason potential candidate genes on proximal chromosome 7 and bone related proteins were extensively investigated.

Strategy of the work

- 1.) Narrow the interval containing *Dyscalc1* on proximal chromosome 7 using BXH-recombinant inbred strains.
- 2.) Identify and re-map with more accuracy potential candidate genes on proximal chromosome 7 employing RFLP and RH mapping strategies.
- 3.) Study the differential expression of selected potential candidate genes after freeze-thaw injury.

- 4.) Compare the development of necrotic tissue calcification in susceptible C3H/He mice and resistant C57BL/6 mice after freeze-thaw injury.
- 5.) Compare DCC with bone mineralization by analyzing the expression at mRNA and protein level of:
 - Opn, the secreted acid phosphoprotein known to act as physiological inhibitor of mineralization and chemotactic cytokine.
 - Other bone related proteins including Osc and Osn.

2. Material and Methods

2.1. Materials

2.1.1. Reagents

Acetone p.a	Merck
Agarose: QA-Agarose TM (standard)	Q.Bio.gene
Metaphor [®] Agarose(High resolution)	BMA
Alizarin Red S	Fluka
Boric acid	Sigma
Bromphenolblue	Sigma
Calcein	Sigma
Chloroform p.a.	Merck
EDTA (Ethyldiaminetetraacetic Acid)	Sigma
Ethanol p.a	Merck
Ethidium bromide	Sigma
Hämatoxylin	Pharmacy
Isofluran	Curamed
Isopropanol	Sigma
Kaisers Glyceringelatine	Merck
Magnesiumchloride	Sigma
Methanol (HPLC reagent)	Baker
Phenol:chloroform:Isoamyl (25:24:1)	Sigma
Trizma [®] Base	Sigma

2.1.2. Enzyme, Inhibitors and Antibodies

Enzymes

ProofSprinter [™] Taq/Pwo Mix	Hybaid-AGS
Proteinase K	Sigma
Taq DNA Polymerase	Amersham
Reverse transcriptase (M-MLV RT)	Gibco

Restriction enzymes

Restriction enzyme	Recognition sequence	Supplier
BamH I	G [^] GATCC	Hybaid-AGS
Bgl II	A [^] GATCT	Hybaid-AGS
Bsp 1431	[^] G A T C	Hybaid-AGS
Dde I	C [^] T N A G	Biolabs
Dra I	TTT [^] AAA	Hybaid-AGS
Eco24 I	G R G C Y [^] C	Hybaid-AGS
EcoR I	G [^] AATTC	Hybaid-AGS
EcoR V	GAT [^] ATC	Hybaid-AGS
Hae III	GG [^] CC	Hybaid-AGS
Hind III	A [^] A G C T T	Stratagene
Hinf I	G [^] A N T C	Hybaid-AGS
Hsp92 II	C A T G [^]	Promega
Kpn I	G G T A C [^] C	Hybaid-AGS
Mbo II	G A A G A N N N N N N N [^]	Hybaid-AGS
Mnl I	C C T C N N N N N N N [^]	Stratagene
Msp I	C [^] C G G	Hybaid-AGS
Nci I	CC [^] SGG	Stratagene
Nco I	C [^] CATGG	Hybaid-AGS
Nde I	CA [^] TATG	Hybaid-AGS
Nde II	[^] G A T C	Hybaid-AGS
Pst I	CTGCA [^] G	Hybaid-AGS
Rsa I	G T [^] A C	Hybaid-AGS
Sal I	G [^] TCGAC	Hybaid-AGS
Taq I	T [^] C G A	Hybaid-AGS
Xba I	T [^] CTAGA	Hybaid-AGS
Xho I	C [^] TCGAG	Hybaid-AGS

Tab. 1: Alphabetical list of restriction enzymes. This set of restriction enzymes were employed to identify intragenic RFLPs as described in section 2.3.8. (^), specify site of action of the restriction endonucleases.

Primary Antibodies

Rat anti-macrophage Monoclonal antibody (MOMA-2)	BMA
Rabbit anti-Bax polyclonal antibody	Santa Cruz
Rabbit anti-Myod1 polyclonal antibody	Santa Cruz
Rabbit anti-Tgfb1 polyclonal antibody	Santa Cruz
Goat anti-osteopontin polyclonal antibody	R&D systems
Goat anti-osteocalcin polyclonal antibody	Biotrend Chemikalien
Rabbit anti-osteonectin polyclonal antibody	Chemicon

Secondary Antibodies

Goat anti-rabbit	SantaCruz
Goat anti-rat	SantaCruz
Donkey anti-goat	SantaCruz

Inhibitors

Ribonuclease-Inhibitor (RNA-Guard)	Amersham
------------------------------------	----------

2.1.3. Kits

Cardiac Troponin ^T Quantitative	Roche Diagnostics
Display Thermo-RT TM	Quantum Appligene
DNA-free TM Kit	Ambion, Technologies
Elisa Kit for mouse osteopontin	Immuno-Biol. Lab
ImmunoCruz Staining System	SantaCruz.
LigthCycler-DNA Master SYBR Green I	Roche Diagnostics GmbH
LigthCycler-RNA Master SYBR Green I	Roche Molecular Biochemicals
ProofSprinter TM Taq/Pwo Mix	Hybaid-AGS

2.1.4. Buffers and Solutions

For routine use, buffers and solutions were performed according to Sambrook et al., 1989. Dissolution and dilutions were carried out by Aqua Bidest. sterile water.

<u>TBE-buffer</u> : pH8.7	1M Tris-Base
	1M Boric acid
	10mM EDTA

<u>TE-buffer</u> : pH8.0	10mM Tris-HCl,
	1mM EDTA

<u>Lysis-buffer</u> :	0.2 % (w/v) SDS
	5 mM EDTA, pH 8.3
	100 mM Tris-HCl, pH 8.5
	200 mM NaCl
	100 µg/ml Proteinase K

Phosphate buffer saline (PBS)	Biochrom KG
Pd(N6) primer	Amersham
Ultrapure dNTP set	Amersham
RNA-clean solution	Hybaid-AGS

2.1.5. Laboratory materials

Filters: Folded Filters (125 mm)	Schleicher & Schuell
Disposable Syringe Filters (0.45 µm)	Nalgene®
Lithium heparin tubes (400-600 µl)	BD Microtainer™
Microscope slides and coverslips	Menzel-Gläser
Plastic-ware	Greiner, Sarstedt, Falcon
Scalpel (sterile, disposable)	Feather
Reaction tubes 0,2; 1,5; and 2 ml	Eppendorf

2.1.6. Instruments

Cardiac Reader™ System	Roche Diagnostics
Cryotome® SME	Shandon
Gel-documentation system	MWG-Biotech
Microscope: Fluorescence	Zeiss
Light	Zeiss
Microwave	Siemens
Touch Down PCR-machine	Hybaid-AGS
pH-meter	Knick
Plate reader	Dynex Technologies
Tab. centrifuge: Biofuge, pico	Heraeus
Cooler EBA 12R	Hettich
Thermomixer	Eppendorf
Vortex	Bender & Hobein
UltraTurrax Homogenizer T8	Omnilab
UV-Transilluminator	MWG-Biotech

2.1.7. Oligonucleotides

Except polymorphic microsatellite markers, all oligonucleotide primers described under this section were designed using the primer3 software (http://www-genome.wi.mit.edu/cgi-bin/primer/primer3_www.cgi; Dated from Jan. 2001 to Jul. 2002).

Marker	Position (cM)	Oligonucleotide Primers (Forward / Reverse)
D7Mit56	4,0	AATGAAGATACCCACAGAAGCTG / GATGGGAACTGGGAACTTAGC
D7Mit266	10,0	TCAGGGATGTCTTAAACTGGG / CGCTGTAAAGCGTATTCTGCG
D7Mit224	15,0	CCATGCAGAGGTTTGGAAAGT / CCAATGTTCTTGATTCCCA
D7Mit247	16,0	TCTTTTGACTTGATTTTGGCG / TGGAGGAGACATATCTTTGCG
D7Mit309	16,0	TGATAAGGACCCTACAAGCACC / CACAGAGATGGACAGATACAGACA
D7Mit227	16,0	GAGTCCTCAGCAGATATTACTCAGC / CTGATGTCTCATCATTTGGGG
D7Mit25	16,0	AGGGGCACATGTTCAACTATG / GGTTGTTCCAGCTTTGGG
D7Mit310	18,0	GGGCTCGAAAGACACAGAAA / ATGTAGTGTTAACGGAACATAACTGG
D7Mit270	18,0	CCCTCCATCATCCTCCTTC / TCTCAAAAAGTCAATGGTGCC
D7Mit228	18,0	ATTCTTGCCTTTTCTTGTAACA / AAACCTCCCACTGACTTCCA
D7Mit229	23,0	GGTTCTCTTTCCTTGTTGCC / TACTGGTTACATCTGGTGGGTG
D7Mit158	23,5	CTTCATCTGAGCCTGGGAAG / ACTGTAGACCCATGTTCTGATTAGG
D7Mit230	24,5	GGGTTAACTGCTTTTTAAAGTGC / ACTTCTGCATGTTGCCCTCT
D7Mit82	25,0	GGACACGGTGTCCATCA AG / CTGAGTAGAAAGCATGTGGGG
D7Mit194	26,9	GTGCAACACACAGAAAAGTTCC / AAAGGCTCACAACGGACTGT
D7Mit231	27,0	ATGCTCCAACCTGTGTGCAC / ATGCAATGCCCTCTGCTG
D7Mit249	27,8	TTCTCTTGACATACCTCAAACACC / AATGCTAGGTTGGGGTGTG
D7Mit91	28,1	TCTTGCTTGCATACACTCAGC / GAGACAAACCGCAGTCTCCT
D7Mit213	37,0	AGCACTTAGAGACCAACAGTAGC / ACCACTACAGTCATTTCCCTCC
D7Mit201	37,0	GCCTACCATGTACCTTTCTTGC / CCCTATTACACACTTGAAGATACA
D7Mit350	41,0	TCTGCATCTCACTGTCCCAG / ATCACAATGAGTTTCTAAGGACTGC
D7Mit31	44,0	TTCAAACCATCCAGTAAGTCCA / TTGGTGAAGTCTTCAATGC
D7Mit40	53,0	GTCAACAGTCAGGAAAGCTGG / CAGATGCTTGTATTTGCAAAGC
D7Mit332	65,6	TACCATCCCTAACTGGTTCTCT / CTGCACACTCACATACATACTCAT

Tab. 2: List of polymorphic microsatellite markers. Microsatellite markers used in section 2.3.7 that cover proximal chromosome 7 at an average density of 2-4 cM. All oligonucleotide primer sequences and locations (given in cM, genetic distance from the centromere) for the microsatellite markers were obtained from the Mouse Genome Database (MGD, <http://www.informatics.jax.org>). Only microsatellite markers, which exhibited a simple sequence repeat (CA-repeat) length polymorphism between C57BL/6 and C3H/He were used in the experiments.

Target gene	Oligonucleotide primers (forward/reverse)	length (Kb)
Dm15	CCCCTGAACCCTAAGACTCC / CAGGGCTGAGTAAAGCAAGG	0,3
Fosb	CAGGATCTTCAGTGGCGT / GGTGAGGACAAACGAGGAAG	2,4
Myod1	AAGCGCAAGACCACCAAC / TAGTAGGCGGTGTCGTAGCC	0,8
Ncx2	GATAGCAGAGATGGGCAAGC / ATCCTCATCCTCCTCCTCGT	4,5

Tab. 3: List of oligonucleotide primers used for PCR-amplification for intra-gene RFLP analysis. As described in section 2.3.8, primers were selected to span intronic segments or, if possible, amplify several kilobases amplicon. Dm15, Dystrophic myotonia kinase 15; Fosb, FBJ osteosarcoma oncogene B; Myod1, myogenic differentiation-1; Ncx2, Na⁺/Ca²⁺ exchanger NCX;

Target gene	Oligonucleotide primers (forward/reverse)	length (Kb)
Bax	TGGAGATGAACTGGACAGCA / TGTCCACGTCAACCAATCACT	0,8
Etfb	GGGTAAAGCCGGACAAGTCT / CCAGGAACAAAAGGTCCACT	0,6
Hrc-a	GGTGGGTGTGATGGAGGACT / CCTTGTGGCCAACTCAGTAG	0,7
Hrc-b	CATGGTTGCACACTTGTCT / ATCATCATCGTGGCCTTGGT	0,9
Myod1	TGTCCCGTAGCCTTGAGC / TCTGCTGTCTCAAAGGAGCA	0,7
Nfkbib	GATTTCTCTCTGGGCTTTTC / CCTCTTCGTTCTCTGGGTTG	0,4
Ryr1	GTGGATCCCAGCCGAGCGGCGCTGG / CAGAATTCTTCCAGGCCTGCTCCTC	1,6
SpiB-1	CTTGGCTTATGCTCCGTACC / GCCAACAACTCCTTGTGCTT	0,8
SpiB-2	TCTTCTACGACCTGGACAGC / GGCTGGTGAAGTCCTCTGG	0,5
Tgfb1-1	CACCTACCTTTCCTTGGGAGA / CTCCAGCCAGTTTCCTCTGA	0,5
Tgfb1-2	GTGGAATGCCAACCTGAGTT / TCGACTGTGCTGTACCCTCA	0,4
USF2	AGTGACCAAGCAGAGGCAGT / TGCCCAGTCATGTTGCTAAG	1.1

Tab. 4: List of oligonucleotide primers used to amplify PCR products for Radiation Hybrid analysis. Primers were selected to produce a positive PCR band signal in mouse, but not in hamster DNA as mentioned in section 2.3.9. Genes were selected to encode for proteins that play critical role in calcium homeostasis, apoptosis or inflammation. Bax, bcl2-associated x protein; Etfb, electron transferring protein-beta; Hrc, histidine-rich calcium binding protein; Nfkbib, nuclear factor of kappa light chain gene enhancer in B cells inhibitor beta; Ryr1, ryanodine receptor-1; SpiB, hematopoietic transcription factor; Tgfb1, transforming growth factor beta-1; USF2, upstream stimulator factor-2.

Target gene	Oligonucleotide primers (Forward / Reverse)
18S	TCAAGAACGAAAGTCGGAGG / GGACATCTAAGGGCATCACA
Bax	GACAGGGGCCTTTTTGCTAC / ACTCCAGCCACAAAGATGGT
Etfb-1	GGGTAAAGCCGGACAAGTCT / CCAGGAACAAAAGGTCCACT
Etfb-2	TGGCAGAGAAGGAGAAGGTG / CAGAGAGCTTGGAGGTCAGG
Hrc-a	CCATGGTTGCACACTTGTCT / ATCATCATCGTGGCCTTGGT
Hrc-b	GGTGGGTGTGATGGAGGACT / CCTTGTGGCCAAACTCAGTAG
Opn	ACACTTTCACTCCAATCGTCC / TGCCCTTCCGTTGTTGTCC
Osc	CCTAGCAGACACCATGAGGA / GCTGTGGAGAAGACACACGA
Osn	TGAGAAGCGCCTGGAGGCTG / TCCTTGATGCCAAAGCAGCCG
Tgfb1	CTGCTGACCCCACTGATAC / GTTGGACAACACTGCTCCACCT

Tab.5: List of oligonucleotide primers used to amplify PCR products for RT-PCR analysis. All primer sets were designed to produce a product length less than 500 bp and spanning if possible small introns. In addition to Bax, Etfb, Hrc and Tgfb1 genes, primers for Opn, Osteopontin; Osc, Osteocalcin; Osn, Osteonectin genes were also designed.

2. 2. Animal housing

C57BL/6, C3H/He inbred strains were purchased from Charles River (Sulzbach-Rosenberg, Germany). All animals had free access to water and food and were maintained with a 12-hr day/night cycle. Animals were fed a regular chow diet (Altromin 1324-pellet, Altromin, Lage, Germany) containing 19 % proteins, 4 % fat, 6 % fiber, 7 % ash, 13.5 % moisture, 0.9 % calcium, 0,7 % phosphorus, 15,000 IE vitamin A, 600 IE vitamin D3, 75 mg Vitamin E and 5 mg Copper.

2.3. Molecular biological methods

Procedures for DNA and RNA manipulation have been performed with standard molecular biological methods (Sambrook et al., 1989). Reagents and samples for enzymatic reactions were kept on ice before use. Buffer and solutions were prepared using bidestilled water and were sterilised by filtration or autoclaving.

2.3.1. Genomic DNA isolation from mouse tail.

DNA from C57BL/6 and C3H/He inbred strains was isolated from 2-3 mm mouse tail snips using a phenol/chloroform extraction method. 500 µl lysis-buffer was

added to the tail snip and digested at 55°C overnight. To the lysate, 550 µl phenol/chloroform/isoamyl (25:24:1) was added, mixed and centrifuged at 11000 x g for 3 min to achieve phase separation. The upper phase (400 µl) was transferred to a new tube and an equal volume of chloroform was added, mixed and centrifuged (11000 x g for 3 min). After transferring the upper phase to a new tube the DNA was precipitated by adding 60 µl of 3 M sodium acetate (pH 5.5) and 700 µl ethanol. After 10-12 tube inversions and centrifugation at 11000 x g for 5 min, DNA specimens were collected at the bottom of the tubes. DNA was washed using 70 % EtOH and finally 98 % EtOH. After evaporation of ethanol at room temperature for 8-10 min, the DNA was dissolved in TE-buffer.

2.3.2. Cytoplasmic RNA isolation from myocard

Samples of injured and healthy myocard of mouse hearts were excised quickly and separately homogenized on ice in 1 ml RNA-Clean solution employing an UltraTurrax Homogenizer. 0.1 ml chloroform was added to the monophasic solution, mixed and kept on ice for 10 min. Two phases were separated by centrifugation at 10000 x g at 4 °C. The upper aqueous phase was removed to a fresh tube and an equal volume of isopropanol was added to precipitate RNA for 15 min at 4°C. Then, samples were centrifuged again to collect a pellet of total RNA. After washing the RNA pellet twice with 70 % ethanol, total RNA (total RNA) was dissolved in 200 µl of 0.05 % Diethylpyrocarbonate (DEPC)-treated RNase free water. Approximately 60 µg total RNA was isolated from 40-60 mg myocardial tissue.

2.3.3. DNase treatment

To exclude DNA contamination, total RNA was treated with Dnase I using a DNA-free™ Kit according to the protocol supplied by the manufacturer. Briefly, 10 µl of 10x Dnase I buffer and 1 µl of Dnase I (2 U) was added to 100 µl total RNA (600 ng/µl). After mixing gently, specimens were incubated at 37°C for 20-30 min and then 10 µl DNase inactivation reagent was added. Thereafter, samples were incubated for 2 min at room temperature. To pellet the DNase inactivation reagent, the mixture was centrifuged at 7000 x g for 1 min. Finally, the DNA-free total RNA solutions were aliquoted and stored at -70°C until use.

2.3.4. Total RNA quality control

Before proceeding to the step involving RT-PCR we checked the quality of the total RNA by gel electrophoresis using 1 μ l of the total RNA (300 ng/ μ l) on a 1 % agarose gel with ethidium bromide.

2.3.5. Gel electrophoresis

DNA analysis was performed using standard agarose-gel electrophoresis with an agarose concentration varying from 0.8-2.5 %. To separate microsatellite markers which produced polymorphic PCR products differing at least 6 bp in length, 4 % high resolution metaphor agarose was employed. Identification of DNA was performed by adding 0,1 μ g/ml Ethidium bromide to 100 ml warm agarose gel solution before pouring and bands were characterised under UV light.

2.3.6. Determination of DNA and RNA concentrations

The concentration of DNA and RNA samples was determined by spectrophotometry at a wavelength of $\lambda=260$ nm as described by Sambrook, et al., 1989. For reference TE-buffer was used. The optic density of 1.0 corresponds to 50 ng/ μ l for double-stranded DNA or 40 ng/ μ l for RNA. A good quality of DNA or RNA samples was indicated by an OD₂₆₀/OD₂₈₀ ratio > 1.8.

2.3.7. Genotyping of polymorphic microsatellite markers in BXH-RI strains

The DNA from the set of the twelve recombinant inbred (RI) BXH strains of mice (BXH-2, -3, -4, -6, -7, -8, -9, -10, -11, -12, -14 and -19) was purchased from Jackson Laboratories (Bar Harbor, ME, USA).

Genotyping of the BXH-RI set, C57BL/6 and C3H/He strain of mice was carried with the technical assistance of Susanne B. Axtner in our laboratory using a panel of polymorphic microsatellite markers (Research Genetics, Huntsville, AL, USA) on chromosome 7 between D7Mit56 and D7Mit332 (Tab. 2). These markers were polymorphic between C57BL/6 and C3H/He strains and covered chromosome 7 at an average of 2-4 cM.

Microsatellite markers were amplified using 50-100 ng template DNA from BXH-RI, C57BL/6 or C3H/He strains in a 10 μ l PCR reaction containing

oligonucleotide primer pairs (1.0 μ M each), dNTP (0.2 mM each), 0.5 U Taq polymerase, 1x PCR buffer (supplied with the polymerase). For amplification a modified “touch down” program was employed. The thermal cycler was programmed to contain 3 stages: a first denaturation stage at 94 °C for 2 min; a 45 cycles amplification stage including 15 cycles (94 °C – 30 sec, 58°C – 30 sec, 72 °C – 30 sec) followed by 15 cycles (94 °C – 30 sec, 56°C – 30 sec, 72 °C – 30 sec), and another 15 cycles (94 °C – 30 sec, 54°C – 30 sec, 72 °C – 30 sec); and final extension stage for 72 °C at 10 min. Genotypes were determined analysing the PCR products after electrophoresis on 4 % Metaphor agarose and ethidium bromide staining.

2.3.8. Restriction fragment length polymorphism (RFLP) analysis

Intragenic RFLPs between strains C57BL/6 and C3H/He were identified subjecting PCR products of candidate genes to restriction endonuclease digestion. Employing the primer3 software (http://www-genome.wi.mit.edu/cgi-bin/primer/primer3_www.cgi; Dated from Jan. 2001 to Jul. 2002), oligonucleotide primers cited in Tab. 3 were designed to span, if possible, several kilobases of genomic template.

For the amplification of different potential candidate genes, 100 μ l PCR reactions were prepared using dNTPs (0.2 mM), 1x reaction buffer (provided by the manufacturer), 0.1 % Tween-20, 2 % dimethyl-sulfoxid (DMSO), 400 nM oligonucleotide primers, template DNA (10-100 ng), and 1 U Taq/Pwo polymerase mix as provided in a long-range PCR kit. If necessary, the PCR reactions were optimized by varying the concentrations of DMSO (2-10 % final concentration), $MgCl_2$ (0.25-5 mM final concentration) and/or adding formamide (up to 10 %). The PCR reactions were amplified in a thermal cycler as follows: The first stage for 2 min at 94°C, 35 amplification cycles of 3 steps: step1 at 94°C for 30 s, step2 for 30 s at the primers optimal annealing temperature, step3 at 72°C for 1 min per 1 kilobase of the expected size of the amplification product. The final extension time was programmed for 10 min at 72°C and finally, the temperature was held at 4°C. Aliquots of the PCR products were analyzed by ethidium bromide staining after gel electrophoresis.

The PCR products were then subjected to endonuclease digestion using a set of 26 restriction enzymes as cited in Tab. 1 to identify intragenic RFLPs. A 25 μ l restriction reaction containing 20 μ l of PCR product, 2.5 μ l restriction enzyme buffer and 4-8 U of enzyme(s) was digested over night. Restriction fragments were resolved by electrophoresis on 2 % agarose gel and ethidium bromide staining to determine allelic variations of the banding pattern.

2.3.9. Radiation Hybrid (RH) analysis

RH mapping involves screening of sequence tagged sites (STS) against cell lines from a RH panel created by fusing irradiated mouse cells with hamster cells which producing a random hybrid genome in these cells. STS that lie nearby in the genome tend to be retained in the same cell line. A T31 RH panel consisting of hybrid hamster/mouse DNA was purchased from Research Genetics (Huntsville, AL, U.S.A.). The panel contains 100 cell lines and two control samples: mouse genomic DNA from strain 129 and hamster genomic DNA from strain A23. Oligonucleotide primers (Tab. 3) were designed to obtain short PCR amplicons of murine candidate genes and did not produce a PCR product with hamster template. Amplification was successful, if a cell line retained the specific mouse chromosome fragment. Rarely, fragment length polymorphisms had to be used to distinguish mouse and hamster alleles. The 100 hybrids were amplified in triplicate or using two different oligonucleotide primers and the PCR results were scored 0, 1, or 2 if the target PCR product were negative, positive, or uncertain, respectively. The scores were submitted electronically to the Jackson Laboratory Mapping Panels to the automated Mouse RH database to evaluate pairwise linkage to markers already mapped. The submitted loci were published on the web (<http://www.jax.org/resources/documents/cmdata>; Dated from Sep. 2001 to Jul. 2002) (Rowe et al., 2000).

2.3.10. Reverse Transcription (RT)

RT reaction mix:

Display THERMO-RT 5x Buffer	4.0 μ l
5 mM dNTP mix	2.0 μ l
T ₂₅ V Primer (10 μ M)	2.0 μ l
RNase-free H ₂ O	7.0 μ l
Display Thermo-RT initiator mix	1.0 μ l

The cDNA was reverse-transcribed from total RNA after DNase treatment using the Display Thermo-RT™ kit. 2 μ l of the total RNA (300 ng/ μ l) was added to 18 μ l of the RT reaction mix and followed by an incubation at 65°C for 10 min. The temperature was decreased to 42°C and 2 μ l Display Thermo-RT Terminator Mix was added and incubated for 40 min to allow the synthesis of complementary DNA (cDNA) strand from the single stranded RNA genome upon binding free nucleotides to form DNA-RNA hybrid. A final incubation at 65°C was performed for 15 min and then cDNA was stored at -20°C until it was used for PCR.

2.3.11. One step RT-PCR

For more accuracy, real time RT-PCR was used to relatively quantify gene expression of candidate genes described in Tab. 5. Total RNA samples were reverse transcribed and subsequently amplified employing a Tth-polymerase-based 1-step RT-PCR kit for the LightCycler thermal cycler (RNA Master SYBR Green I, Roche, Germany). Approximately 100-150 ng total RNA were subjected to RT-PCR reactions in a mixture of 20 μ l containing 0,25 μ M of each primer, 1.3 μ l of a 50mM Mn(OAc)₂ stock solution, and 7.5 μ l of the 2.7x concentrated LightCycler-RNA Master SYBR Green I. Amplicon formation was followed by green fluorescence of the DNA double strand intercalating dye, SYBR Green I. Relative gene induction was calculated employing the $\Delta\Delta$ Ct method (Winer et al., 1999) comparing gene induction after freeze-thaw injury to baseline after normalisation to 18S rRNA concentration using a specific primer pair. Threshold cycle number (Ct) was obtained by “crossing point” analysis of

triplicate determinations using the second derivative maximum method as implemented in the LightCycler Software.

2.4. Freeze-thaw injury

Animal studies were performed in accordance with the German animal studies committee of Schleswig-Holstein (Reference Nr. 1/b/97). As previously described for mice by Brunnert et al. (1990) animals were received a median abdominal incision, in deep anaesthesia after an intra-peritoneal injection of 4-6 μ l/g mouse weight, tri-bromo-ethanol (Avertin™). The heart apex was reached through the diaphragm and freezed for 10 s using a steel rod (3 cm² in diameter) which was precooled in liquid nitrogen. For the sham operated animals a non-precooled steel rod was used. The abdominal incision was closed, and the animals were allowed to recover and then returned to their cages. After 0, 1, 2, 3, 5, 9 and 21 days, mice were sacrificed under anesthesia by cervical dislocation. The whole hearts were excised and quickly rinsed with phosphate-buffered saline (PBS). Samples of necrotic and healthy myocard were dissected and stored in liquid nitrogen until isolation of RNA.

For histological analysis, whole hearts were embedded in Jung tissue freezing medium (Leica Instruments) after removal of fat and aorta and were kept at -20°C until staining.

2.5. Immunohistological methods

2.5.1. Histological analysis

2.5.1.1. light microscopy

Hearts were examined by light microscopy as previously described (Ivandić et al., 1996 & 2001). Serial 6-8 μ m cryosections through the ventricles up to the aortic valves were prepared and sections containing necrotic lesions were collected on poly (D-Lysine)-coated slides.

For specific staining of calcium phosphate deposits, calcein staining, a calcium binding fluorochrome, and alizarin red S producing reddish stain with calcium were used. **For calcein staining**, slides were incubated in a solution containing 0.1 mM calcein in 0.05 M Tris-HCl buffer at pH 9 for 30 min in the dark. Slides were washed in Tris-HCl buffer at pH 9 and examined by fluorescence

microscopy with appropriate filters. For **alizarin red S staining**, we incubated slides in 0,5 % alizarin red S, Tris buffered solution at pH 9 for one h and Tris-buffered solution at pH 7 for 5 min. Sections were washed immediately in Tris-buffered solution at pH 9 and then at pH 7 for 5 s each. For dehydration, slides were then transferred into 60 % (v/v) and 100 % ethanol solutions for 3-5 s each. Finally, sections were embedded in XyloI for 10 min and mounted with Glycerol gelatine.

Sections were scored positive if calcified foci were seen at least three consecutive sections upon examination of the fibrotic lesions.

2.5.1.2. Transmission electron microscopy (TEM)

TEM analysis were performed in cooperation with PD Dr. M. Klinger (Anatomy Institute, Universitätsklinikum Schleswig Holstein, Campus Lübeck). The samples were fixed in 2,5 % glutaraldehyde (pH 7.4) and then postfixed in 2 % Osmium tetroxide solution. Samples were transferred into graded ethanol concentrations to eliminate water and then embedded in Araldit. 40-60 nm thick Ultra-thin sections were prepared and contrasted with Lead_citrate and Uranyl_acetate. The Ultrathin sections were then analysed using transmission electron microscope Philips EM 400 and scored positive for calcium phosphate deposits if electron dense granules were observed.

2.5.2. Immunological Analysis

Serial cryosections of injured myocard with a thickness of 4-6 μm were used for immunohistochemistry. To examine the involvement of different candidate proteins and cell composition of DCC, slides were left at room temperature for 30 min to adapt to room temperature after storage at $-20\text{ }^{\circ}\text{C}$ and were then fixed in acetone for 10 min. Endogenous peroxidases were blocked with 1-3 drops peroxidase block. Specimens were rinsed with PBS for 2 min and incubated for 20 min in 1-3 drops per slide of the specific serum block that was derived from the same species in which the secondary antibody was raised. The sections were incubated with primary antibodies at a concentration of 5 $\mu\text{g/ml}$ for MOMA-2, Tgfb1, Myod1 and osteopontin in a humid chamber for 2 h. For Bax, osteocalcin and osteonectin a dilution of 1/150 were used. Bound primary

antibodies were detected using biotinylated secondary antibodies which were visualized using a streptavidin-horseradish peroxidase complex. Controls were performed without primary antibodies or with non-specific IgG1 antibody. Hematoxylin or alizarin red S staining was used for counter staining. The sections were then examined by light microscopy.

For immunofluorescence staining, peroxidase block step was omitted and fluorescein or rhodamine-conjugated secondary antibodies were used instead of biotinylated secondary antibodies. Slides were prepared as described previously omitting the peroxidase block step and the final step involving treatment of sections with hydrogen peroxidase. For counter-staining, DAPI was used. Sections were examined using fluorescence microscope with appropriate filter settings.

2.5.3. Enzyme-linked immunosorbent assay (Elisa)

Solid-phase ELISA was used with the technical assistance of Alex Jurat (Department of Medicine I, Universitätsklinikum Schleswig Holstein, Campus Lübeck) for the specific detection of osteopontin in heparinated plasma. 0, 1, 2, 3, 5, 9 and 21 days after freeze-thaw injury, whole blood was collected in tubes with lithium heparin from C57BL/6 and C3H/He mice by retro-orbital puncture under anesthesia. Samples were then centrifuged at 7000 x g for 3 min to separate plasma. Mouse osteopontin enzyme immuno-assay (EIA) kit was used and the detection of osteopontin was performed following the manufacturer's instructions. 100 µl of samples at a dilution of 1/50, diluted standards and sample blanks (0.9 % (w/v) NaCl) were pipetted into the 96 wells plate containing anti-mouse osteopontin antibody followed by an incubation for 1 h at 37°C. For staining, HRP-conjugated anti-mouse osteopontin was used as secondary antibody and tetra methyl benzidine (TMB) as colour agent. The staining intensity was determined using an ELISA plate reader with a 450 nm filter.

2.6. Clinical Chemistry

Heparinized plasma was obtained from mice as described above. Calcium, phosphate and magnesium plasma concentrations were determined in blood samples from C57BL/6 and C3H/He animals, sham operated or after freeze-

thaw injury, employing standard atom absorption spectrometry (Institute of Clinical Chemistry, Universitätsklinikum Schleswig Holstein, Campus Lübeck). For Troponin T, an established marker of myocardial necrosis (Wu et al., 1998), the concentration was determined in 150 µl whole blood drawn 0, 1, 2, 3 and 5 days after myocardial injury using quantitative troponin T strip tests designed for clinical use and the Cardiac Reader™ System.

3. Results

3.1. Mapping *Dyscalc1* in BXH RI strains

Densely-spaced polymorphic microsatellite markers were typed on proximal chromosome 7 in the BXH RI strains to obtain information about the extension of the chromosomal interval likely to contain *Dyscalc1*. Typed polymorphic microsatellite markers are shown in Tab. 6. Markers D7Mit309, D7Mit227, D7Mit247, D7Mit270, D7Mit229 and D7Mit82 spanned the entire *Dyscalc1* interval. In previous quantitative trait locus (QTL) analysis this chromosomal region exhibited highly significant LOD scores with a maximal peak of 14.8 at D7Mit229 (Ivandić et al., 2001). Moreover, in this interval, microsatellite marker alleles (in Tab. 6 genotypes 'B' and 'H' designate alleles conferring resistance and susceptibility to DCC, respectively) exhibited complete co-segregation with the DCC phenotype in BXH-7, BXH-8 and BXH-9 (resistant to DCC), BXH-10 (susceptible to DCC), and in the remaining members of the BXH set. Now more polymorphic markers in strain BXH-8 were analysed between markers D7Mit229 and D7Mit82, which are separated only by about 2 cM according to the CCR 2000 map employing markers D7Mit158 and D7Mit230. D7Mit230 marker exhibited 'H' alleles in strain BXH-8. On this basis a 1.5 cM region between D7Mit158 and D7Mit82 could be excluded. In contrast, the centromic boundary of the *Dyscalc1* interval was defined by a recombination in BXH-7, which had occurred in a 2-cM interval between markers D7Mit224 and D7Mit247. No polymorphic microsatellite markers were found to further narrow down this interval.

3.2. Identification of candidate genes

Candidate genes were selected from genes already identified on proximal chromosome 7 which are involved in apoptosis, calcium homeostasis, or inflammation.

To confirm or exclude as potential candidate genes the myotonic dystrophy kinase gene (Dm15), the muscle creatine phosphokinase (Ckmm), the Na⁺ /Ca²⁺ exchanger (Ncx2), the transforming factor beta 1-subunit (Tgfb1), the ryanodine receptor (Ryr1), the FBJ osteosarcoma oncogene (Fosb) the upstream

Locus	cM	BXH RI Strains											
		2	3	4	6	7	8	9	10	11	12	14	19
D7Mit56	2.2	BB	HH	HH	BB	BB	BB	BB	BB	HH	HH	BB	BB
Dm15	4	BB	HH		BB	BB	BB	BB	BB	HH	HH		BB
Slc8a2	4	BB	HH	HH	BB	BB	BB	BB	BB	HH	HH	BB	BB
Calm	4.5												
Fosb	5	BB	HH	HH	BB	BB	BB	BB	BB	HH	HH	BB	BB
Tgfb1	8												
lap3ra3	9	BB	BB	HH	HH	HH	BB	BB	BB	HH	HH	BB	BB
Tnni3	9	BB	BB	HH	HH	HH	BB	BB	BB	HH	HH	BB	BB
Ryr1	11												
NfKbib													
D7Mit309	13.1	HH	HH	HH	HH	HH	BB	BB	HH	HH	HH	HH	HH
D7Mit227	13.1	HH	HH	HH	HH	HH	BB	BB	HH	HH	HH	HH	HH
D7Mit247	13.1	HH	HH	HH	HH	HH	BB	BB	HH	HH	HH	HH	HH
D7Mit224	15	HH	HH	HH	BB	BB	BB	BB	HH	HH	HH	HH	HH
D7Mit310	15.3	HH	HH	HH	HH	BB	BB	BB	HH	HH	HH	HH	HH
D7Mit270	15.3	HH	HH	HH	HH	BB	BB	BB	HH	HH	HH	HH	HH
D7Mit228	16.4	HH	HH	HH	HH	BB	BB	BB	HH	HH	HH	HH	HH
Hrc	23												
Bax	23												
D7Mit81	23												
SpiB	23												
D7Mit229	23	HH	HH	HH	HH	BB	BB	BB	HH	HH	HH	HH	HH
D7Mit158	23	HH	HH	HH	HH	BB	BB	BB	HH	HH	HH	HH	HH
Myod 1	23.5	HH	HH	HH	HH	BB	BB	BB	HH	HH	HH	HH	HH
D7Mit230	24.5	HH	HH	HH	HH	BB	HH	BB	HH	HH	HH	HH	HH
D7Mit82	25	HH	HH	HH	HH	BB	HH	BB	HH	HH	HH	HH	HH
D7Mit194	26.9	HH	HH	HH	HH	BB	HH	HH	HH	HH	HH	HH	HH
D7Mit249	27	HH	HH	HH	HH	BB	HH	BB	HH	HH	HH	HH	HH
D7Mit231	27.8	HH	HH	HH		BB	HH	BB	HH	HH	HH	HH	HH
D7Mit91	28.1	HH	HH	HH		BB	HH	BB	HH	HH	HH	HH	HH
D7Mit213	37	HH	HH	HH	HH	BB	HH	HH	HH	HH	HH	HH	HH
D7Mit201	37	HH	HH	HH	HH	BB	HH	HH		HH	HH	HH	HH
D7Mit350	41	HH	HH	HH		BB	HH	HH	HH	HH	HH	BB	HH
D7Mit31	44	HH	HH	HH	HH	BB	HH	HH	HH	HH	HH	BB	HH
D7Mit40	53	BB	BB	HH	HH	BB	HH	BB	HH	HH	BB	HH	BB
D7Mit332	65.6	BB	BB	BB	HH	BB	HH	BB	HH	HH	HH	BB	BB

DCC Phenotype (%)

High fat diet	78	50	75	25	0	0	0	0	100	19	29	14
Freeze thaw injury					0	0	0	100				

Tab. 6: Genotype and DCC phenotype determination in BXH RI strains. Position map of the markers were given in cM according to the <http://www.informatics.jax.org>, Dated from Jan. 2001 to Jul. 2002. ``B`` and ``H`` denote alleles inherited from C57BL/6 and C3H/He respectively. ``DCC phenotype`` is expressed in percentage after high-fat diet and freeze-thaw injury (Ivancic et al., 2001). In blue color, loci were re-mapped using RH panel according to their map position in cM. In red, genotype of loci re-mapped by RFLPs were replaced after finding linkage to a marker.

transcription factor 2 (Usf-2), the histidine-rich calcium binding protein (Hrc), the myogenic differentiation 1 (Myod1), the nuclear factor of kappa light chain gene enhancer in B-cells inhibitor (Nfkbib) the hematopoietic transcription factor (SpiB) and the electron-transferring flavoprotein-beta (Etfb) were remapped exactly by radiation hybrid mapping and, if possible, intragenic RFLPs were also genotyped to analyse allelic segregation in DCC-susceptible and resistant RI BXH strains. The data are outlined in the following sections.

3.2.1. Typing of intragenic RFLPs in BXH RI strains

Informative intragenic RFLPs were found for Dm15, Ncx2, Fosb, Ckmm and Myod1.

Dm15 is the disease locus of myotonic dystrophy. It was tested, because a targeted disruption of the Myotonic dystrophy protein kinase was associated with increased fibre degeneration and fibrosis in a mouse model (Reddy et al., 1996). RFLPs produced by MbolI excluded Dm15 as candidate gene (Fig. 3A). Interestingly, no PCR product was consistently obtained in BXH-4, -6 and -14 mice in 3 repeated assays with the primers listed in Tab. 3. Slc8a2 is the locus of a member of the $\text{Na}^+/\text{Ca}^{2+}$ exchanger Ncx2. Polymorphic fragments generated by EcoRI and MbolI (Fig. 3B) did not cosegregate with DCC in BXH-8 and BXH-10 excluding Ncx2 as candidate gene. As part of the AP-1 transcription complex Fosb plays a critical role in Tgf-beta-dependent apoptosis (Yamamura et al., 2000). RFLPs were found in Fosb using restriction enzymes MspI and BamHI excluding it as candidate gene (Fig. 3C and D). Ckmm catalyses the synthesis from ATP and creatine of the major energy reserve in muscle, creatine phosphate. Located in the mitochondrial intermembrane space Ckmm is also associated with the permeability transition pore complex, PTPC, which plays a central role in apoptosis (Zamzami and Kroemer, 2001). Ckmm is located at Fosb, because both genes are separated only by 64 Kb of sequence (clone containing both sequences has GenBank accession number AC073787). All these genes were excluded as candidate genes, because they exhibited resistant parental C57BL/6 genotypes in DCC-susceptible strains BXH-2 and -10 as well as in BXH-14 and -19. For myogenic differentiation 1 (Myod1) involved in muscle regeneration by formation of myotubules from muscle satellite cells, informative intragenic RFLPs were found employing endonuclease restriction enzymes MnlI (Fig. 3E) that

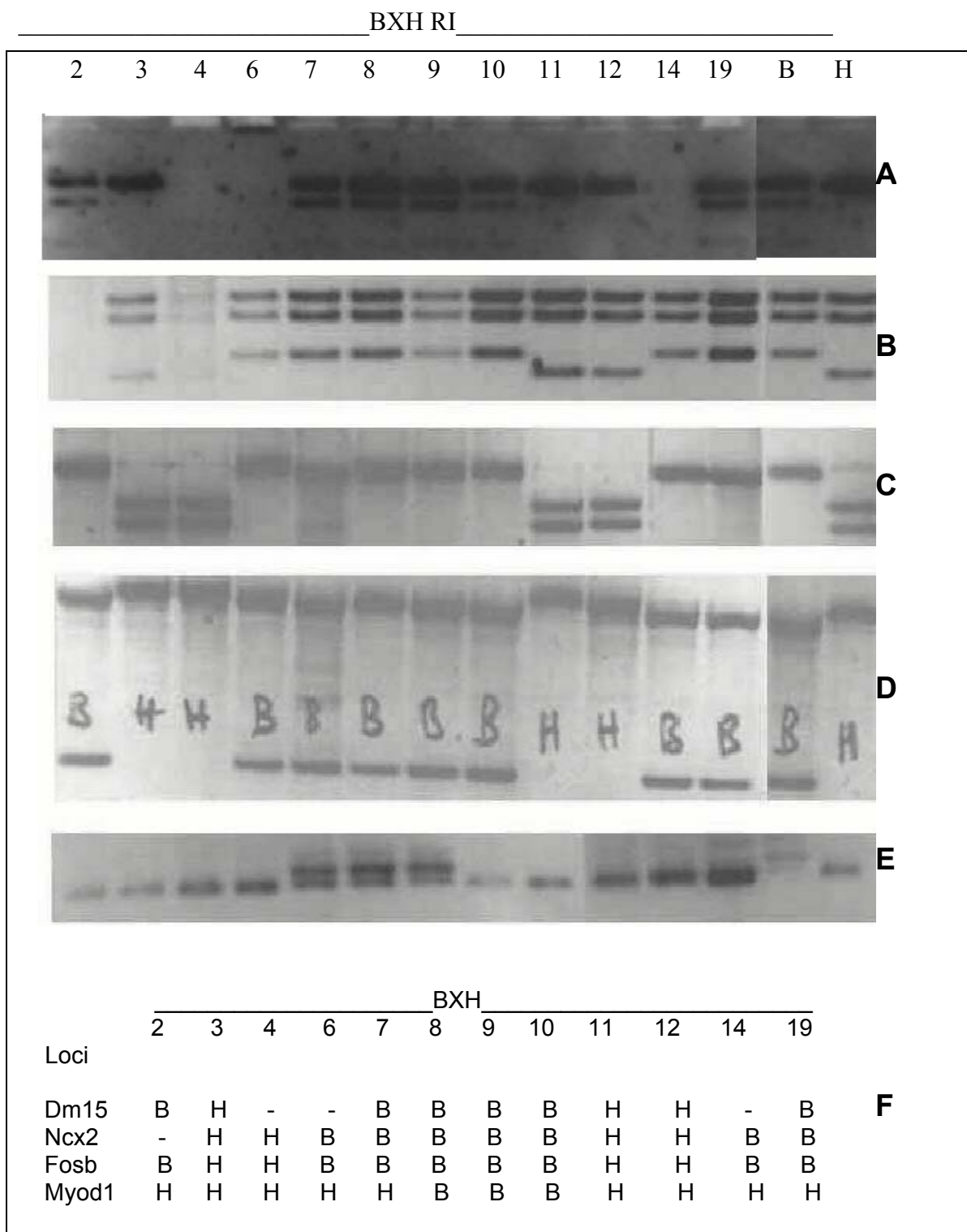


Fig. 3: RFLPs obtained from different BXH RI strains. Genotype of the parental inbred strains C57BL/6J and C3H/He were designated "B" and "H", respectively. Enzymatic digestion was carried as described in Material and Methods. Intragenic RFLPs were found for Dm15 using MboII endonuclease enzyme, (A), for Ncx2 using EcoRI endonuclease enzyme, (B), for Fosb using MspI and BamHI, (C and D) and for Myod1 using MnlI endonuclease enzyme, (E). The genotype of BXH RI strains at loci examined by RFLP method are summarised in (F).

recognize sequence described in Tab. 1. Analysis revealed full co-segregation of resistant C57BL/6 genotypes in resistant strains BXH-7, -8 and -9. Consistently,

the remaining susceptible strains BXH-2, -3, -4, -6,-10, -11, -12, -14 and -19 revealed C3H/He genotypes placing *Myod1* in the interval containing *Dyscalc1*. On the basis of these data *Myod1* must be considered as candidate gene.

3.2.2. Radiation Hybrid mapping of potential candidate genes

Potential candidate genes which could not be excluded by RFLPs analysis were mapped employing Radiation Hybrid (RH) panel. Thus, loci of the transforming growth factor-beta1, *Tgfb1*, the beta-subunit of NfKB inhibitor Ikb-beta, *Nfkbib*, the ryanodine receptor, *Ryr1*, the histidine-rich calcium binding protein, *Hrc*, the Bcl2-associated X protein, *Bax*, the hematopoietic transcription factor, *SpiB*, and the electron-transferring flavoprotein-beta, *Etfb*, were analysed for close linkage with *Dyscalc1*.

Tab. 7 shows the data obtained by amplifying fragments of target genes from 100 hybrid hamster/mouse DNA containing in the RH panel as described in Materials and Methods. After submitting RH mapping data for these candidate gene loci they were placed into the RH map maintained at the Mouse Genome Database and published ("<http://www.jax.org/resources/documents/cmdata/rhmap/rh.html>").

Based on the data obtained by RH mapping, *Tgfb1* was mapped between D7Mit144 and D7Mit265, which is consistent with the published location, but also ruled it out as candidate gene. *Nfkbib* was previously mapped to proximal chromosome 7 by in-situ hybridisation (Klein et al., 1999). Although *Nfkbib* is now mapped with more accuracy, its placement just proximal to D7Mit266 exclude it as candidate gene. RH mapping placed *Ryr1* between D7Mit72 and D7Mit210. This location is still proximal to D7Mit267 marking the proximal boundary of the interval likely to contain *Dyscalc1*. The histidine-rich calcium binding protein (*Hrc*) is a sarcoplasmic calcium binding protein. Different from the location (20.4 cM) reported in the CCR map, the RH data obtained here placed *Hrc* further distal between D7Mit26 and D7Mit81, close to D7Mit229 at 23.0 cM suggesting *Hrc* as a relevant candidate gene for *Dyscalc1*. In addition to *Hrc*, *Bax*, the locus of the proapoptotic Bcl2-associated X protein; *Etfb*, the locus of electron transferring protein-beta and *SpiB*, a hematopoietic transcription factor showed evidence of close linkage with D7Mit229 (Tab. 6).

Loci	Cell lines(1-100)
Nfkbib D7Mit265	10000000100010101000000000101000000000000000010001000101010000010001010000100100100000000100000110
Tgfb1 D7Mit267	000000001000101010000102100101000000100000100000100110120100010001010000101100000000000100001100
Ryr1 D7Mit155	0000000110001010100001020101210000000000000001000100010101000001000000000100100100000000100001111
USF2	000000211010100010000101000101000001001010100000000100010101102200000010002100100120000000100001111
D7Mit309	00000000111020001001000000011000200000201000001001000101000010000110021111000010000000100102110
D7Mit26 D7Mit311	00010000011001000000011000000100000001000100000000100010101000000000100011111011010000000000110
Bax	200100001110000000001210000110000000110101000000010000011100000000002000001110000100000000200120
Hrc	20010000121000000000110000011000000011010100200100100000111000000100010001111101001000000110100110
D7Mit81	10010000111010000000110000011000000011010100000100100000111000000100010001111001001000000100100110
SpiB	1001000011111000000011000001100000001101010000020010000010100000010001000111110100100000000100110
Etfb	0001201011101100000001110000110001000101010100000101100010101000010010011000011110110100000000100110
D7Mit229	000100001112200000000110000011002000011012100000100100000111000000010001000111110100100000010110000
D7Mit158 Myod1	0001000010001200000001100020110002000110100200021001002101110002000100110001111101001000000101120000 000100001000101000000110000011000200011010000200100100210111000000100110001111101001000000101120000
D7Mit230	10110001100212001002010201011000111010100002211011000101112200000100010101100100011002000101222222
D7Mit82	0011000100001000100001100000110001100101010000011001000101001000000100110001100000001000000101100111

Tab. 7: Data obtained by genotyping various loci on chromosome 7 using template DNA from cell lines 1-100 of the Radiation hybrid panel. The PCR product of the 100 hybrids were scored 0, 1, or 2 if the target amplicon is negative, positive or uncertain, respectively.

3.2.3. Candidate gene expression analysis

The cardiac expression of genes mapped to the *Dyscalc1* interval were examined by relative RT-PCR to obtain additional evidence to support their putative association with DCC. Initially, we employed the QuantumRNA kit for relative RT-PCR analysis by densitometry of ethidiumbromide-stained bands. In this setting, log-linear amplification ranges, which are considered optimal for quantification, proved to be rather narrow. For this reason fluorescence-based quantification of RT-PCR products which offered a broader dynamic range of detection was employed for this study. In all cases the sensitivity of quantitative RT-PCR using SYBR Green I detection was critical and was achieved only by following closely the procedures described in Materials and Methods.

Starting from total RNA isolation, DEPC-treated glassware and instruments were used to avoid RNA degradation. Samples were aliquoted after total RNA isolation to minimise degradations that might be caused by repeated freeze-thawing and handling. Fig. 4 shows the quality control of the total RNA isolated and separated by electrophoresis. Samples from C57BL/6 and C3H/He myocardium tissue following a time course after freeze-thaw injury, demonstrated the typical 18S and 28S bands after staining with ethidium bromide.

For the accuracy of the results obtained by quantitative RT-PCR, 3 animals at each time point were analysed in duplicate. As described by Thellin et al. (1999), 18S was chosen as internal standard for normalisation of the RNA sample concentrations. Prior to quantification of the samples, experiments were performed to optimise primer annealing temperature and concentration as well as total RNA concentrations in the reaction mixture containing polymerase and

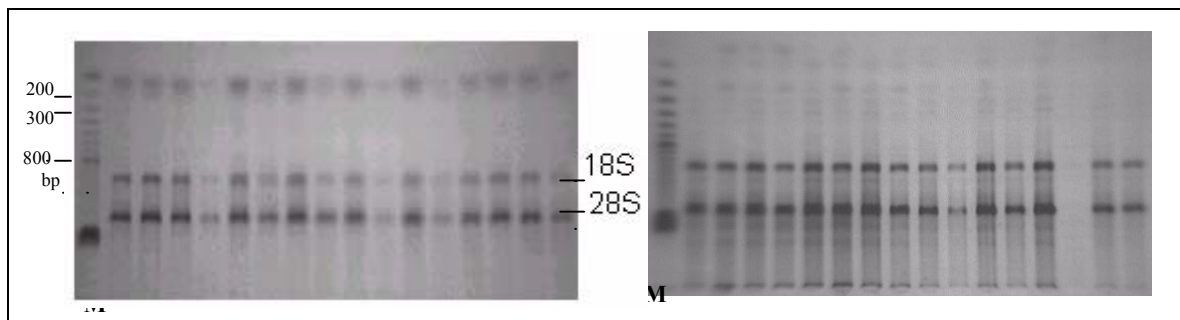


Fig. 4: Quality control of RNA degradation. Electrophoresis of total RNA isolated by RNA Clean solution for C57BL/6 and C3H/He samples 0, 1, 2, 3, 5, and 9 days after freeze-thaw injury. RNA preparations (1 μ g) were electrophoresed in agarose gel (1%) and stained with ethidium bromide. Bands correspond to the typical 18S, 28S and mRNA smear bands. M, for 100bp leader DNA marker.

SYBR Green I dye as described by the manufacturer. For each gene, serial dilutions of total RNA with a factor of 5 (1, 1/5, 1/25 and 1/125) were analysed to determine the optimal total RNA concentration with respect to the expected copy number of the gene under study. Standard curves for 18S (Fig. 5-1A), Hrc (Fig. 5-2A), Etfb (Fig. 5-2B), and Bax (Fig. 5-3) mRNA levels were established to determine the threshold of cycle number (Ct), obtained by crossing point analysis using the second derivative maximum method implemented in the LightCycler, versus fluorescence changes (upper curves). Bottom curves represent the corresponding linear regression of the threshold cycle number where the fluorescence signal first exceeds the level of background noise, versus the logarithm of the sample concentration with a regression coefficient (r^2) of all genes ranging from 0,99 to 1,00. For the specificity of RT-PCR amplicons, end PCR products were analysed by melting temperature curves, a typical melting curve is shown in Fig. 5-1B for 18S, and gel electrophoresis after ethidium bromide staining (data not shown).

The results obtained by relative real-time RT-PCR from cardiac expression of candidate genes identified as described under section 3.2. by RFLP and RH mapping such as Hrc, Etfb and Bax in both calcified lesions and healthy myocard are illustrated in Fig. 6. To obtain relative gene expression data, the deltadelta Ct method with 18S RNA as internal standard for normalisation of varying RNA concentrations was used (Winer et al., 1999; Yin et al., 2001). In healthy myocard of C57BL/6 strain, an upregulation by a factor of 3 of Hrc and Etfb was noticed

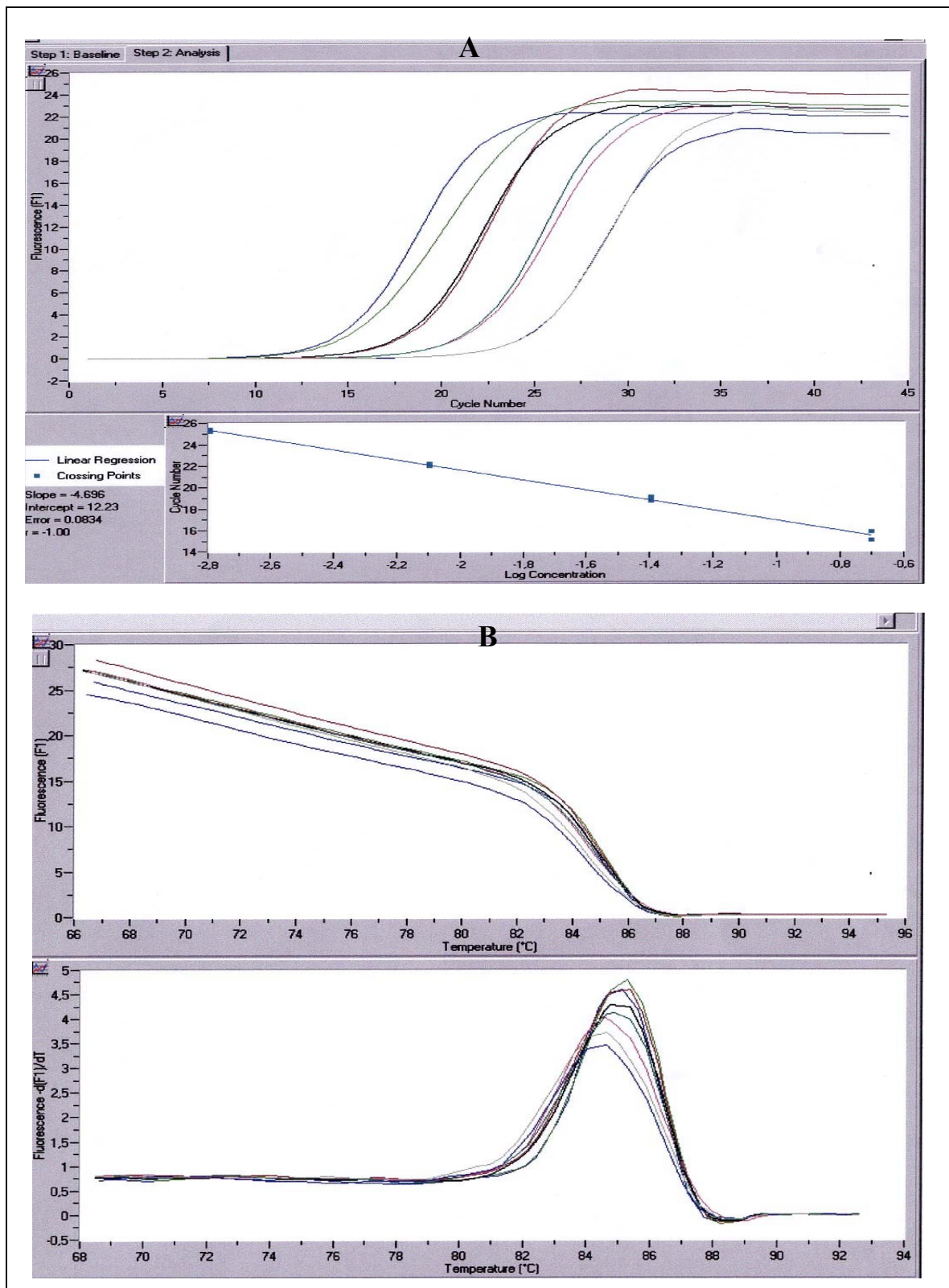


Fig. 5-1: Determination of the standard curve and melting temperature for 18S. Serial 5-fold dilutions of mouse heart total RNA were used to amplify RT-PCR products that are detected by SYBR Green I dye. (A) illustrates two types of curves: the upper curve corresponds to the threshold cycle number (C_t) versus fluorescence changes (F) and the corresponding bottom curve representing the linear regression of the threshold cycle versus the logarithm of the sample concentrations. The C_t was obtained by crossing point analysis using the second derivative maximum method implemented in the LightCycler. (B) represent one of the typical melting temperature curves obtained for 18S to show the specificity of the RT-PCR reaction. The regression coefficient ($r^2=1$) shows high reproducibility ($r^2=1$).

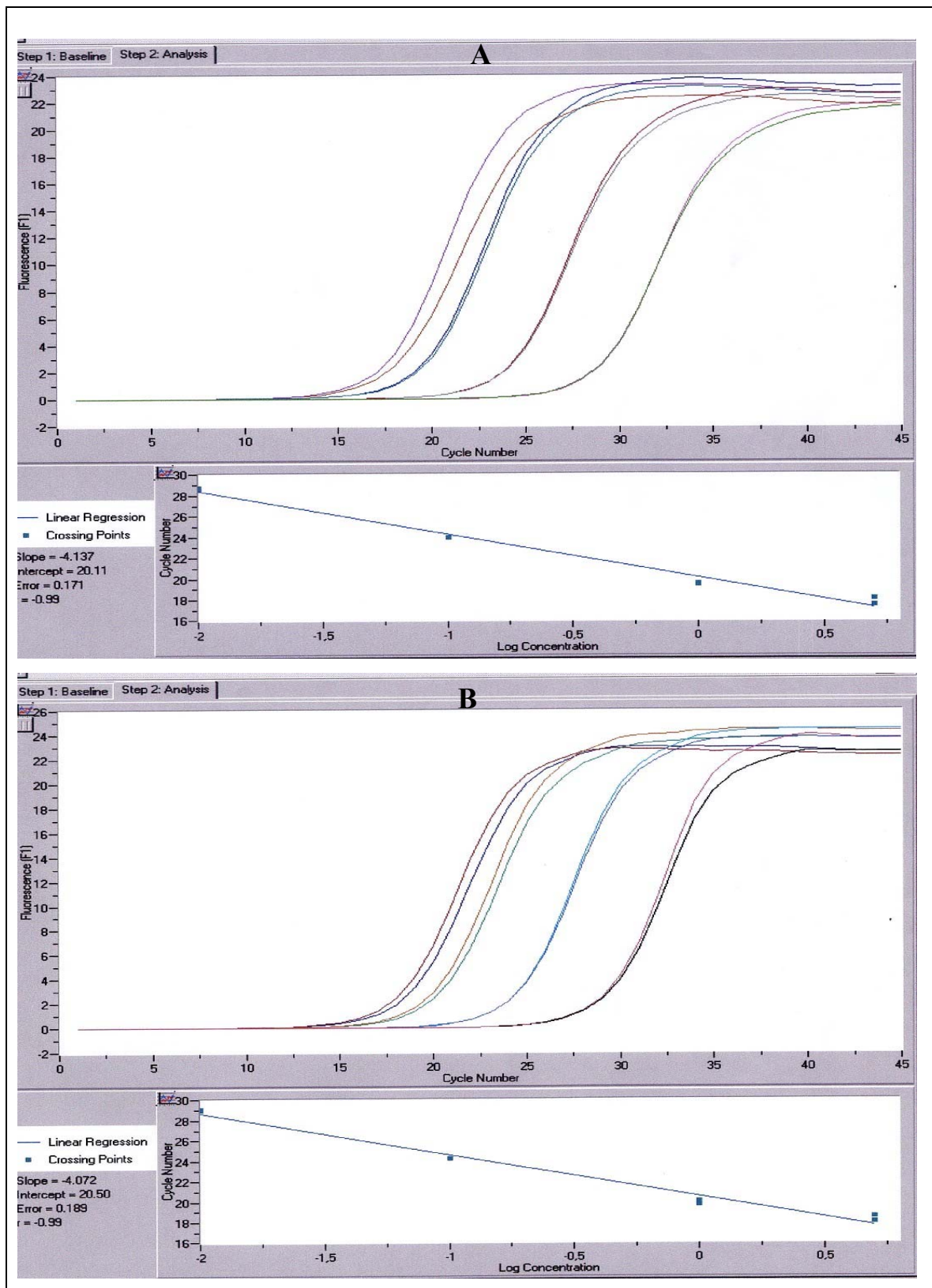


Fig. 5-2: Determination of the standard curve for Hrc and Etfb. Serial 5-fold dilutions of mouse heart total RNA were used to amplify RT-PCR products for Hrc (A) and Etfb (B). SYBR Green I dye was employed to detect PCR products. For each gene, two types of curves are illustrated: the upper curve corresponding to the threshold cycle number (Ct) versus fluorescence changes (F) and the corresponding bottom curve representing the linear regression of the threshold cycle versus the logarithm of the sample concentrations. The Ct was obtained by crossing point analysis using the second derivative maximum method implemented in the LightCycler. The regression coefficient (r^2) shows high reproducibility ($r^2 > 0.99$).

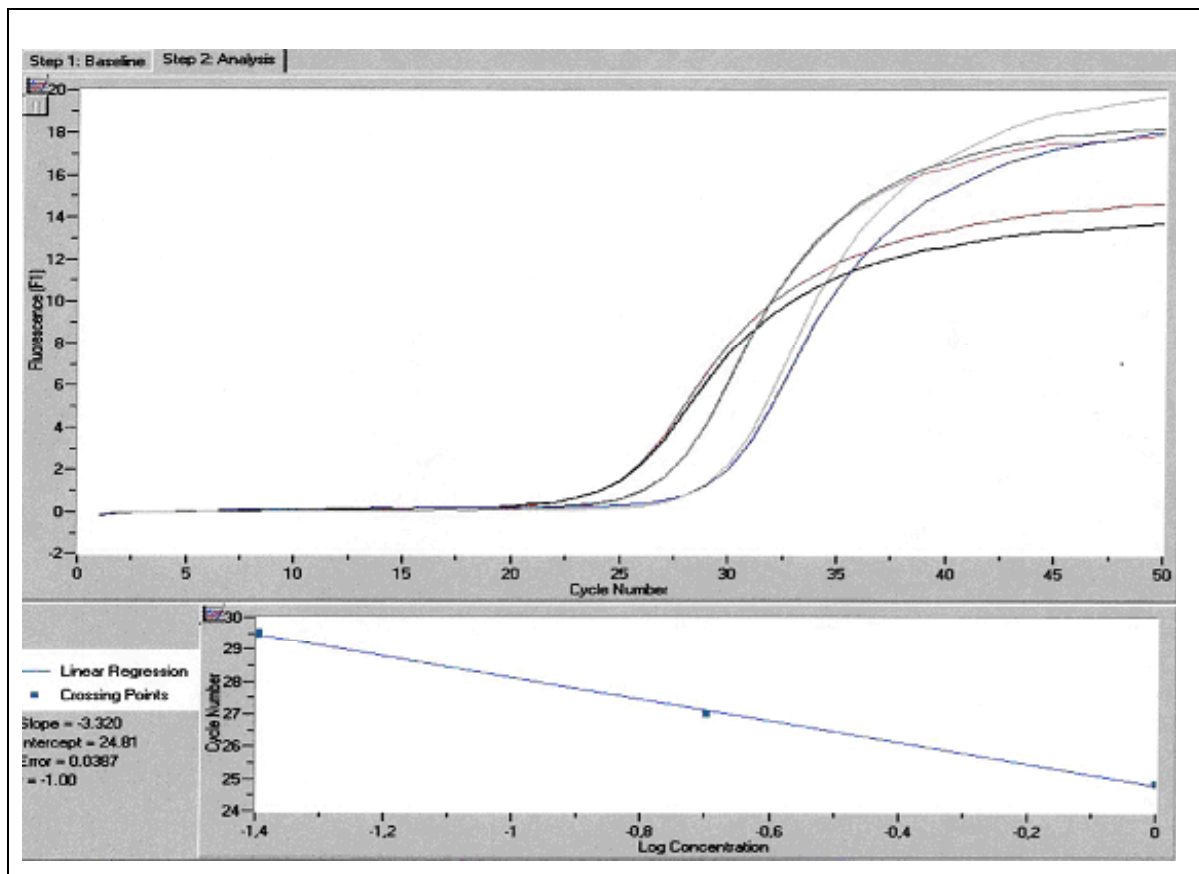


Fig. 5-3: Determination of the standard curve for Bax. Serial 5-fold dilutions of mouse heart total RNA were used to amplify RT-PCR products that are detected by SYBR Green I dye. Two types of curves are illustrated: the upper curve corresponding to the threshold cycle number (Ct) versus fluorescence changes (F) and the corresponding bottom curve representing the linear regression of the threshold cycle versus the logarithm of the sample concentrations. The Ct was obtained by crossing point analysis using the second derivative maximum method implemented in the LightCycler. The regression coefficient (r^2) shows high reproducibility ($r^2=1$).

one day after freeze-thaw injury (Fig. 6A-B). This increase expression remain constant thereafter for Hrc and decrease slightly for Etfb at day 3. In C3H/He mice the expression of Hrc and Etfb in healthy myocardium peaked at day 1 with a maximal of 1.5- and 2.5-fold, respectively, and become comparable to base line thereafter.

Contrary, Bax didn't reveal any significant upregulation in healthy myocardium of both inbred strains (Fig. 6C). In the calcified lesion, however, Hrc and Etfb were downregulated in C3H/He after day 1 and late in C57BL/6 mice after day 3 (Fig. 6D-E). In contrast, we noticed a marked upregulation of Bax reaching a plateau of 8-fold-induction early at day 2 in C3H/He animals, but only a maximum of 4.5-fold in C57BL/6 late at day 3 declining slowly thereafter (Fig. 6F).

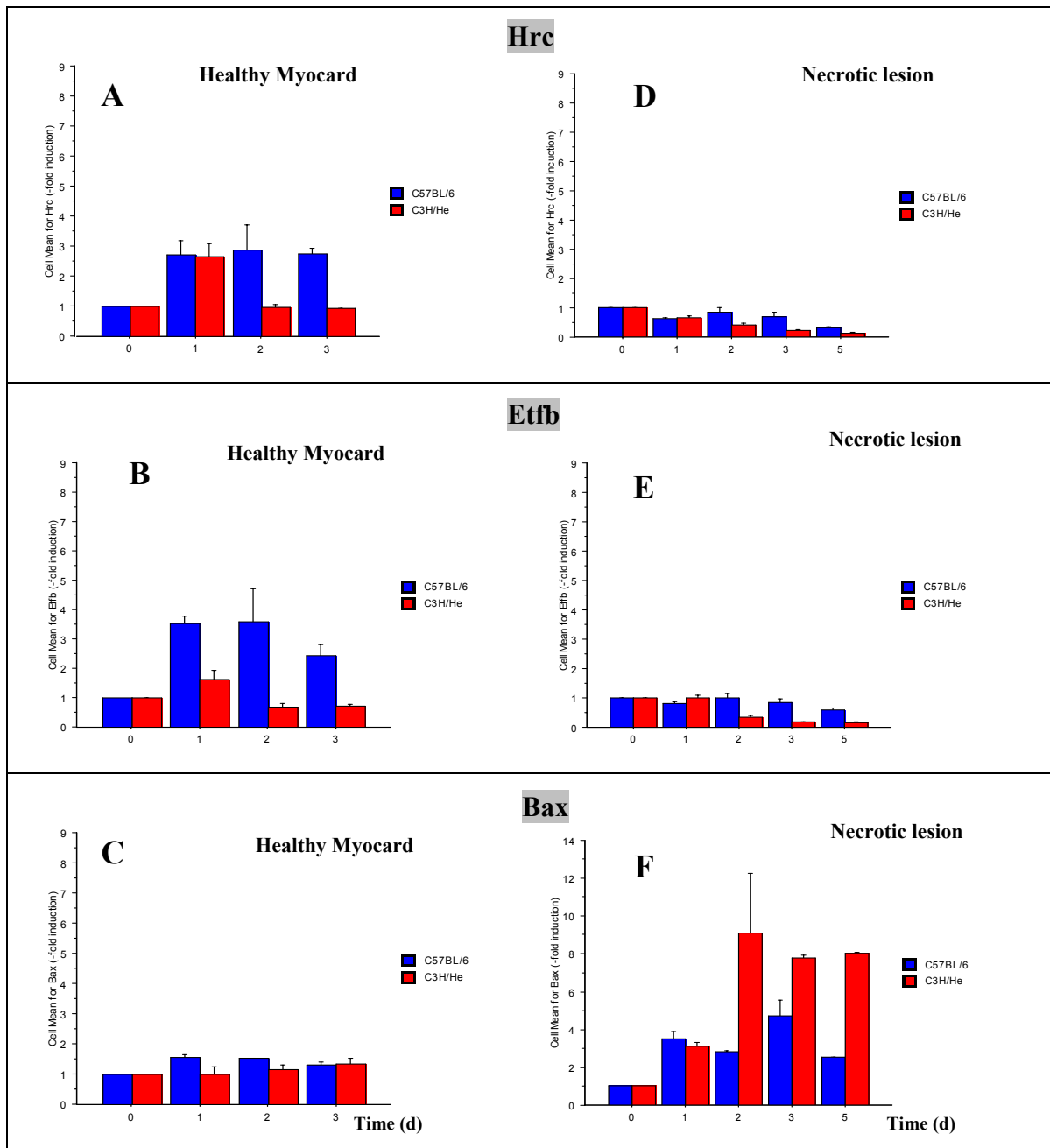


Fig. 6 : Candidate gene expression analysis after injury. Relative fold induction of Hrc (A and D), Etfb (B and E) and Bax (C and F) in healthy myocardium (left) and injury lesions (right) in C57BL/6 (blue) and C3H/He (red) inbred strain of mice. Myocardial infarct was promoted using the freeze-thaw injury method. The total RNA samples from different animals at various time points after injury were isolated as described in Materials and Methods. For statistical analysis three animals per group were analyzed by RT-PCR in duplicate and detected by SYBR Green I using a LightCycler. Relative fold induction was calculated using delta-delta Ct method. The mean of each sample is plotted and the error bars represent standard errors (SE).

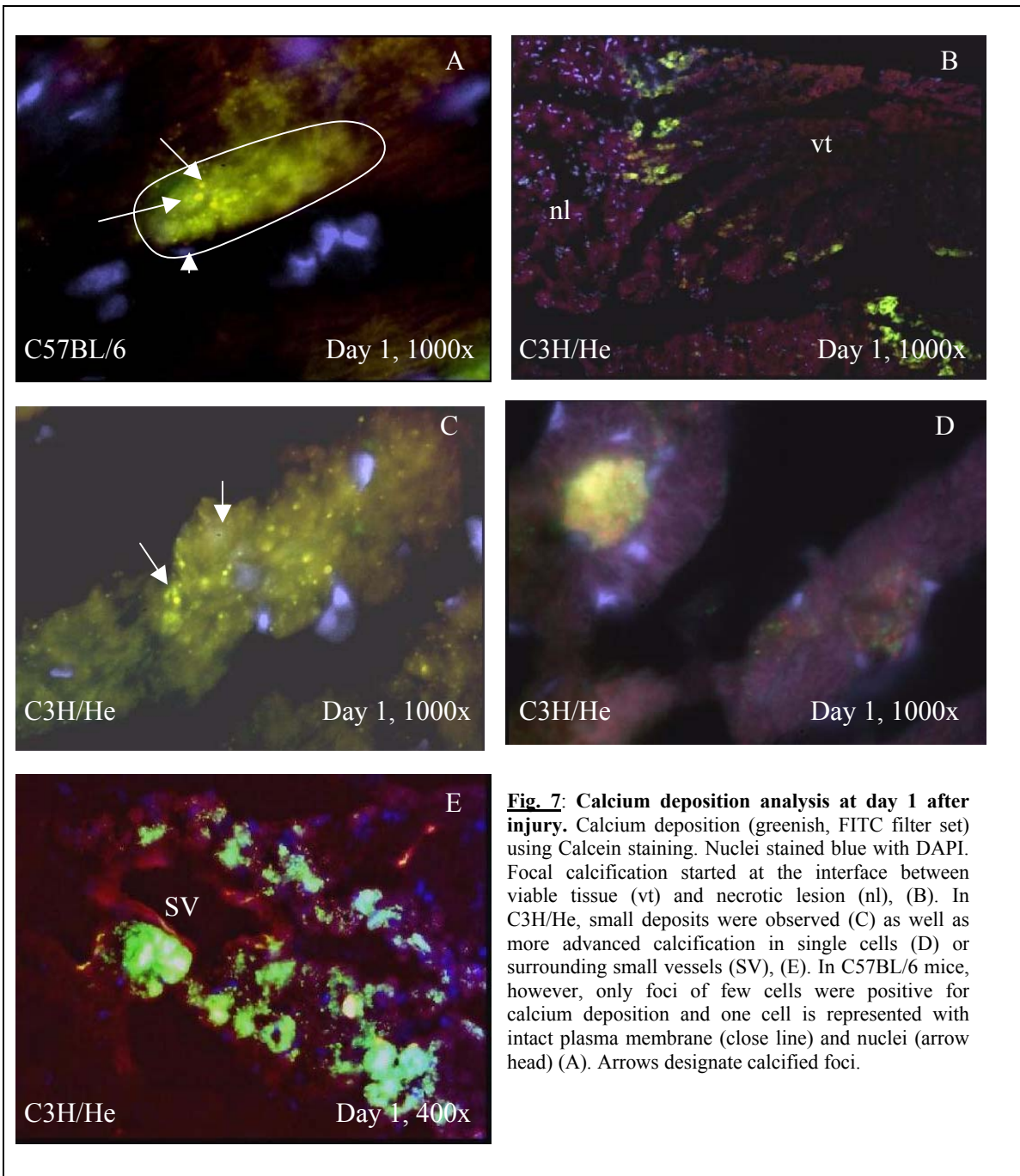
3.3. Histopathological investigations

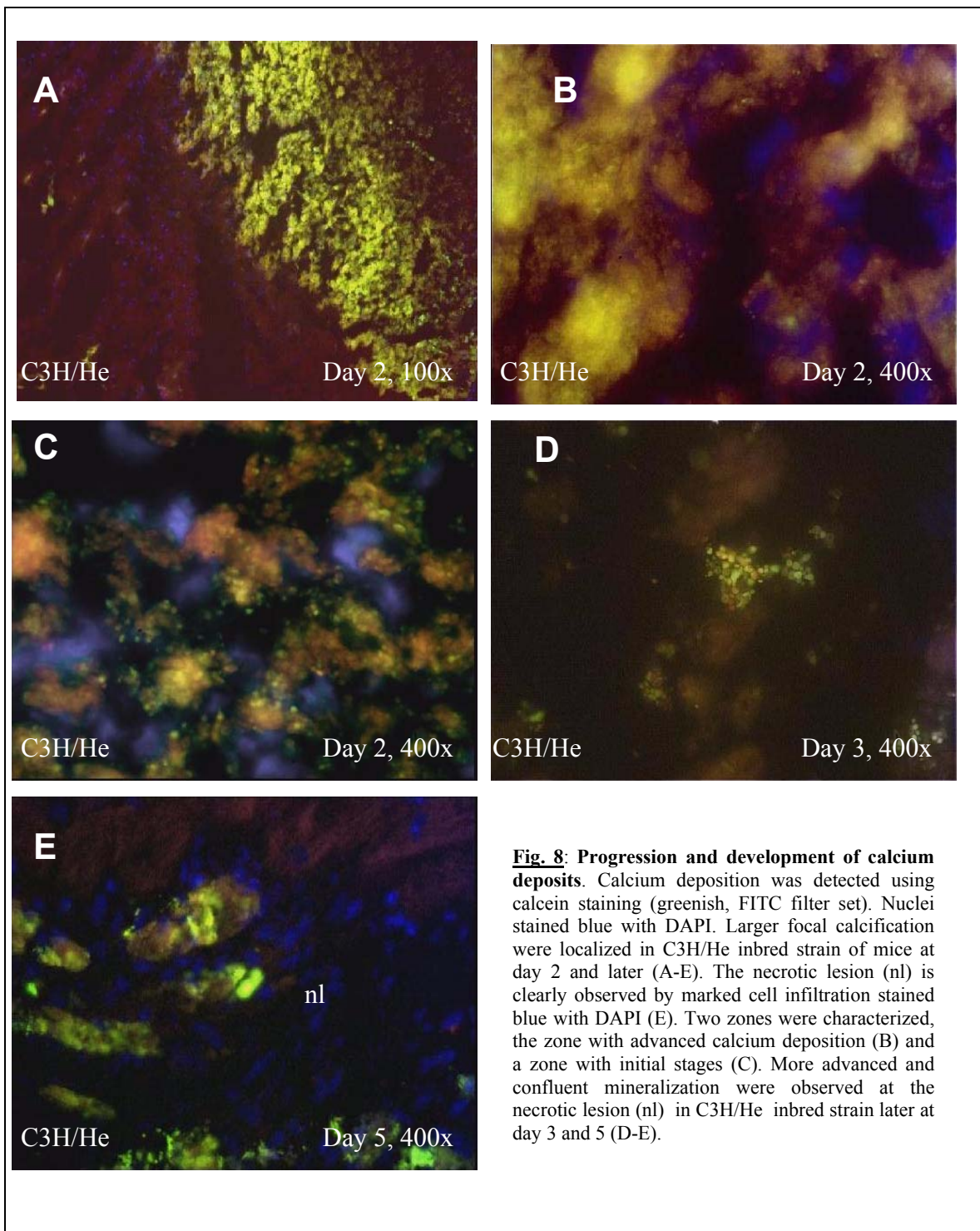
3.3.1. Calcein staining

Calcein staining is based on the visualisation of insoluble calcium phosphate deposits with the use of calcium binding fluorochromes. The necrotic areas could be easily differentiated from the healthy zone by the marked infiltration of polymorph nuclear cells in the necrotic tissue using DAPI that stain nuclei. In C57BL/6 mice (control strain), only few calcein positive stained cells were observed in the necrotic tissue at day 1 after injury (data not shown). Fig. 7A shows an example at a 1000 x magnification (C57BL/6, day1) of one cell that exhibited staining with calcein in intracellular vesicles (arrows) within an intact plasma membrane and nucleus. By day 2 post injury and later, no calcein-positive cells were detected within the necrotic area of DCC-resistant C57BL/6 mice (data not shown). In contrast, many morphological changes were observed in susceptible C3H/He mice during myocardial calcium deposition. Fig. 7B-E illustrate the localisation of calcium deposition in C3H/He mice, which is markedly observed at the interface between healthy and necrotic tissue at day 1 (Fig. 7B). Some cells present small deposits (Fig. 7C) and were morphologically similar to thus observed in DCC-resistant C57BL/6 (Fig. 7A), whereas others were in more advanced stage and calcium deposits were larger (Fig. 7D). Many calcein positive stained cells were also noticed surrounding a small vessel (Fig. 7E).

By day 2, we could differentiate two zones in the necrotic lesion of C3H/He mice: (1) a zone close to healthy myocard, where calcium deposition is already advanced, showing very condensed, “hard” mineral deposits (Fig. 8B), and (2) a zone in the core of the necrotic area, relatively remote from the interface, where calcium deposits appear to be still in an initial stage (Fig. 8C).

Later at day 3 and 5, we observed more advanced, confluent mineralization in the necrotic lesion (Fig. 8D-E).





3.3.2. Alizarin Red S staining

Employing Alizarin Red S, calcium deposits were detected by light microscopy first after 3 days (data not shown) and gave very strong staining at 5 days after freeze-thaw injury in C3H/He inbred strain of mice (Fig. 9). In C57BL/6 strains,

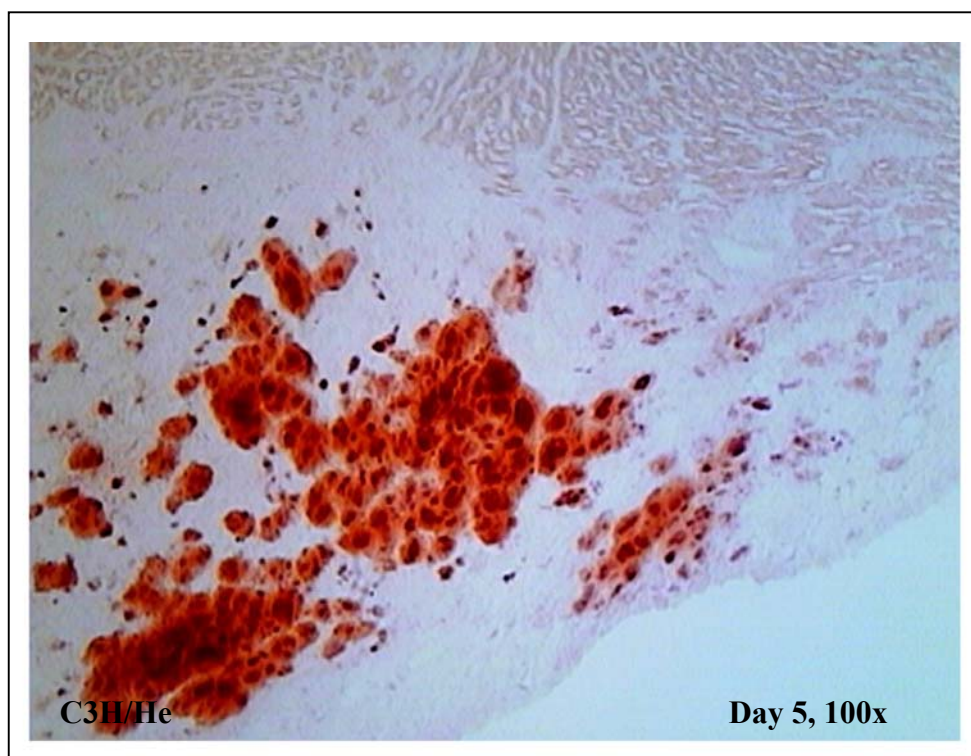


Fig. 9: Calcium deposition using Alizarin red S staining. Alizarin red S stains calcium deposits in red. Focal calcification were observed at the necrotic lesion of C3H/He inbred strain 5 days after freeze-thaw injury.

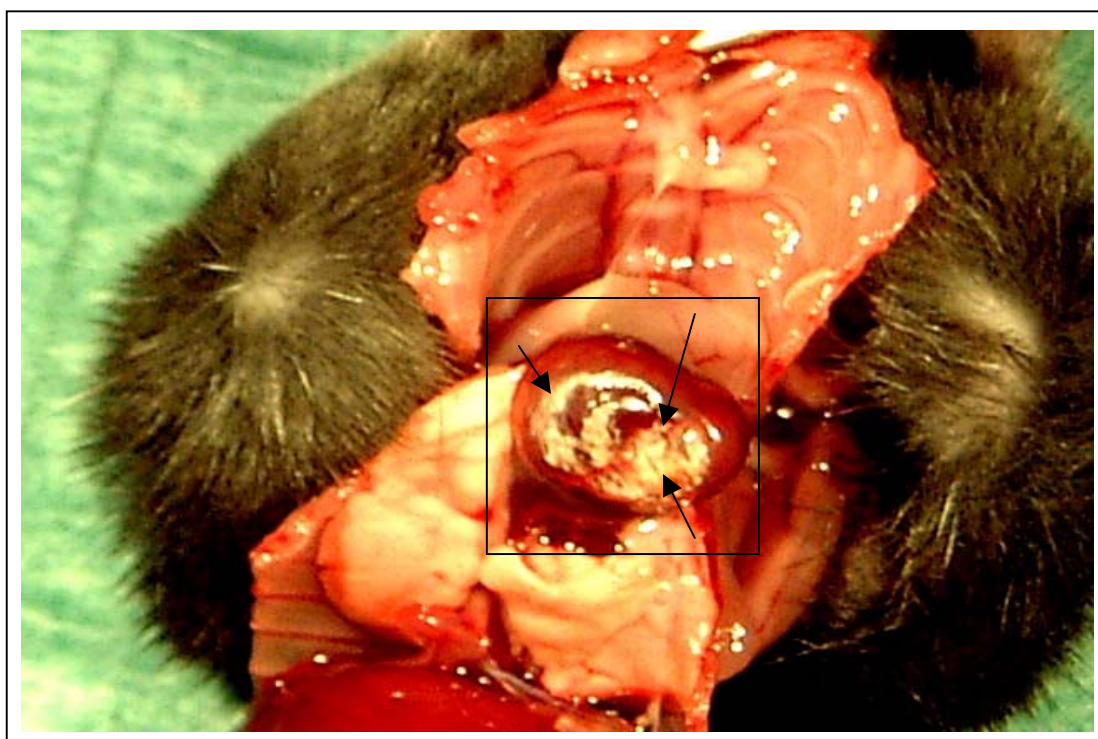


Fig. 10: Macroscopic observation of calcium depositions. Hearts of DCC-predisposing inbred strain of mice C3H/He, 15 days after myocardial infarct promoted by freeze-thaw injury, as shown within the square field. Arrows revealed well observed grey-white streaks.

however, no positive staining was observed (Data not shown). Late, after day 5, the calcification formed larger, very condensed structures that could be clearly visible by naked eye as grey-white streaks in the necrotic myocardium of DCC-susceptible C3H/He inbred strain of mice (Fig. 10).

3.3.2. Transmission Electron Microscopy (TEM)

Samples from DCC-resistant C57BL/6 and DCC-susceptible C3H/He mice were subjected to TEM analysis to confirm intracellular calcium deposits observed employing calcein staining and results already published by Brunnert, 1997. In cooperation with PD Dr. Klinger M (Institut für Anatomie, Universität Lübeck), hearts were collected from C57BL/6 and C3H/He inbred strains after day 1, 3 and 4 -freeze-thaw injury and investigated morphological changes in myocardium tissue of these strains. By day 1 calcium phosphate deposits were observed as electron dense granules in mitochondria of both C57BL/6 and C3H/He strains within larger necrotic tissue zones as shown in transmission electron micrographs, Fig. 11-1. By day 3 some mitochondria contain already large calcification deposits however others become swollen and present cristea with distortion as noted in the necrotic area of only C3H/He mice, Fig. 11-2. However, C57BL/6 inbred strain of mice presented no calcification at this time point and thereafter (data not shown). By day 4 we could identify the needle-like structures that characterise hydroxyapatite crystal deposits during the biological bone mineralisation, Fig. 11-3.

3.4. Bone related proteins expression analysis

3.4.1. Osteopontin

3.4.1.1. Myocardial osteopontin expression

Osteopontin (Opn) is an acidic phosphoprotein with an RGD (arginine-glycine-aspartate) motif. It is synthesized by macrophage, smooth muscle and endothelial cells (O'Brien et al., 1994). It is expressed during embryogenesis, wound healing and tumorigenesis. Until now the exact molecular function of osteopontin is unclear but many authors suggested a regulatory role of Opn in the pathological cardiovascular calcification. Murry et al. (1994) reported a transitory expression of

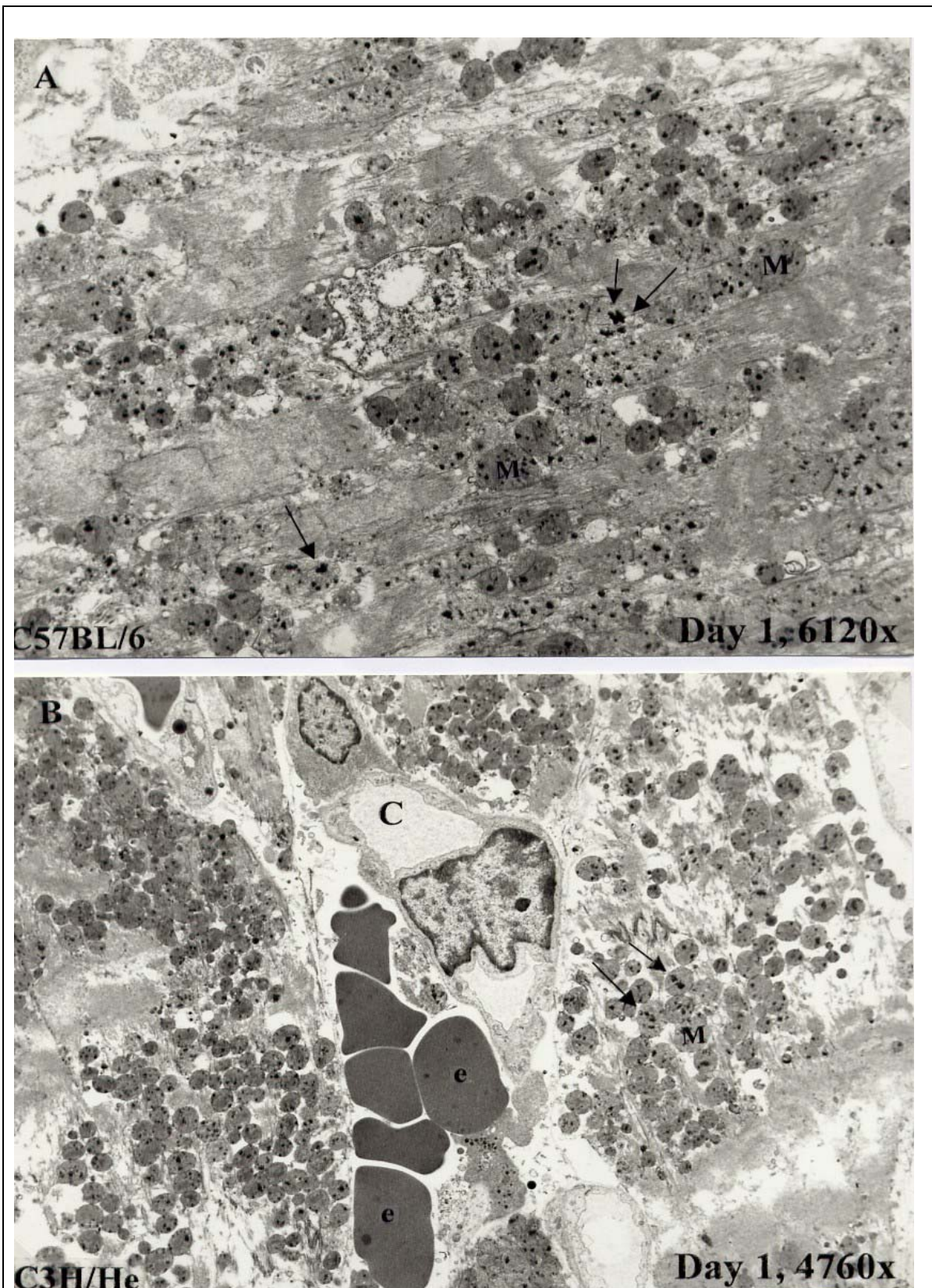


Fig. 11-1: Transmission electron micrographs of C3H/He and C57BL/6 myocardium 1 day after freeze-thaw injury. Early amorphous calcium deposits were seen as electron dense particles (arrows) in mitochondria of both injured myocardium of C57BL/6 (A) and C3H/He mice (B). At this early stage of cell alteration, mitochondria present moderate round forms but still indistinguishable from mitochondria of non altered cells. Notice the disorganized structure and myofibrillosis of the myocardium tissue after injury. "M", mitochondrion; "e", erythrocytes; C, capillary.

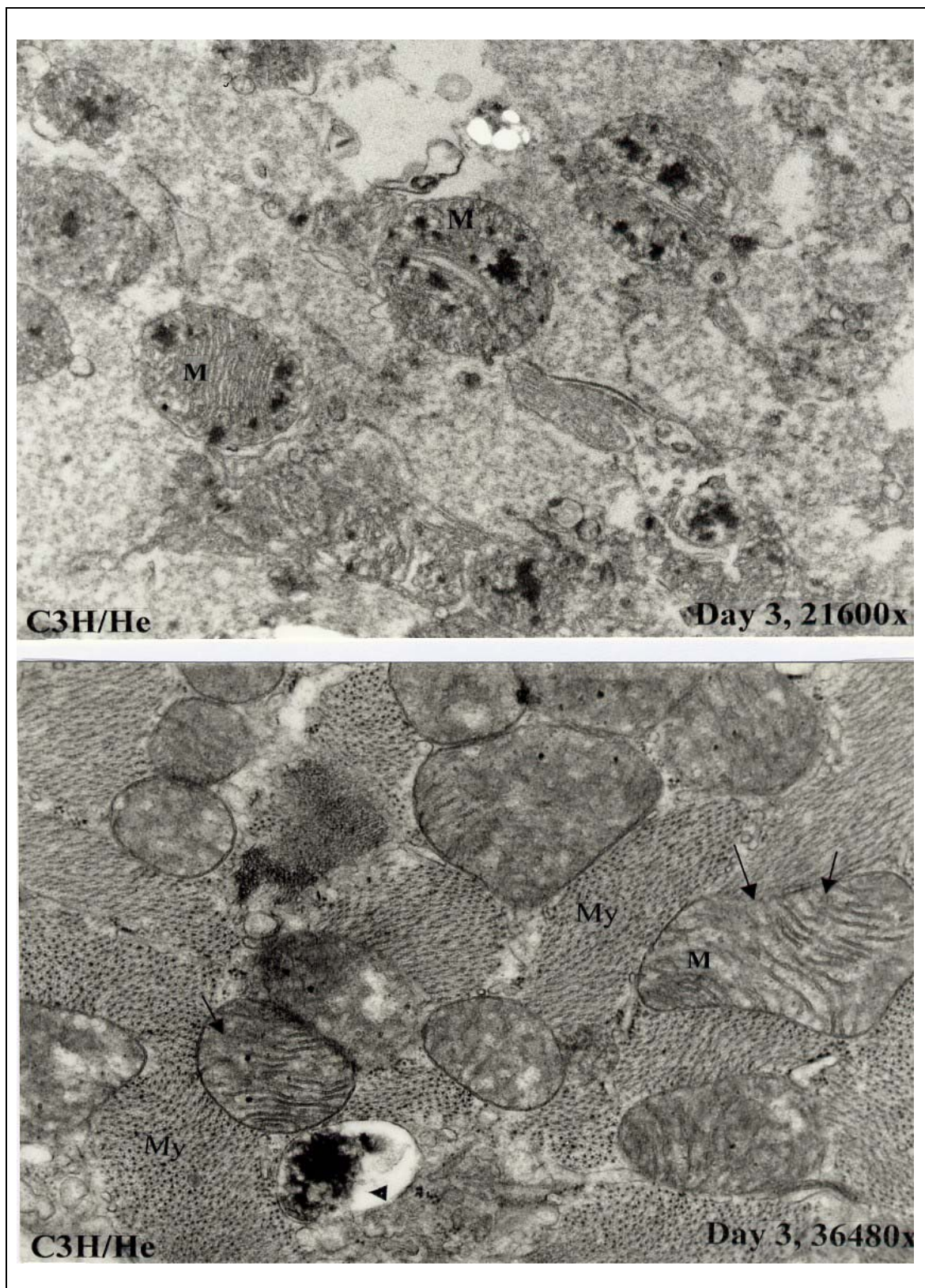


Fig. 11-2: Transmission electron micrographs of C3H/He myocardium 3 days after freeze-thaw injury. A, at this stage of alteration, advanced amorphous calcium deposits were noted in mitochondria of some injured myocardium area of C3H/He mice (seen as electron dense particles) with various sizes that are clumped or scattered between intact cristea. B, Other injured area present moderate swelling of the mitochondria with distortion of the cristae (arrows) and intact myofibril (My). Arrow head shows large phosphate calcium deposits within a disintegrated Mitochondrion. M, designate mitochondrion.

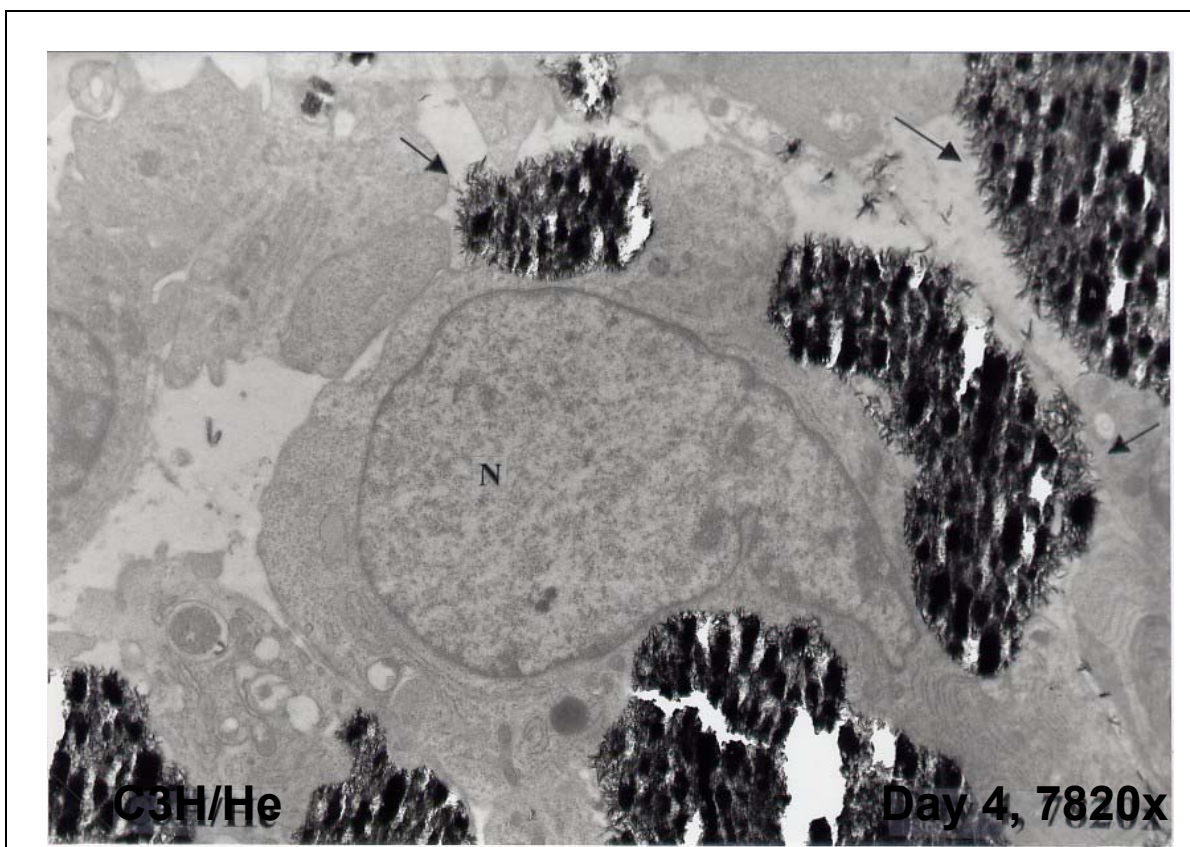


Fig. 11-3: Transmission electron micrographs of C3H/He myocardium 4 days after freeze-thaw injury. Micrograph present advanced calcified plaques within the cytoplasm of a giant cell, possibly a macrophage, with well observed nucleus (N). Deposits were in the form of generally various sizes composed of randomly oriented individual needle-like crystals, easily observed at the border of the deposits (Arrows). This needle-like crystal form is a characteristic of hydroxyapatite composition of biological mineralisation.

Opn in a subpopulation of macrophages after myocardial freeze-thaw injury in rats. This prompted us to examine a potential role of Opn in the development of DCC in resistant C57BL/6 and susceptible C3H/He mice. Macrophage infiltration and osteopontin expression were determined by immunohistochemistry to analyse the induction and the localisation of Opn expression in physiological and pathological conditions. The infiltration of macrophages appeared to be comparable in C57BL/6 and C3H/He following a similar spatial and temporal distribution. At day 1 after injury increased densities of polymorphnuclear cells were observed in the necrotic lesions of myocardium of both C3H/He and C57BL/6 mice, the majority of which stained positive for the macrophage antigen MOMA. At day 3 the infiltration of macrophages progresses covering the entire necrotic area, Fig. 12.

In contrast, osteopontin expression showed a very significant difference between C57BL/6 and C3H/He inbred strains as illustrated in Fig. 13. Specific anti-Opn antibody staining was noted already at day 1 after injury in the border zone

separating necrotic and healthy tissue of C3H/He inbred strain of mice. Opn expression increased at day 3 and much stronger was clearly seen in C3H/He than C57BL/6 mice. At day 5, no positive cells were found in C57BL/6. In C3H/He inbred strains, however, the expression of Opn was still maintained at a very high level comparable to day 3 in the necrotic area. Opn staining was limited to areas of calcification. Fig. 13 (C3H/He, day5) shows a colocalization of osteopontin (brownish) and calcium deposits (coloured in blue-violet), arrows.

RT-PCR was performed to examine the time course of the mRNA induction in response to injury. Before proceeding to gene analysis, the sensitivity of the PCR was first determined. Therefore a correlation between concentration changes and cycle number was analysed using SYBR Green I detection in LightCycler PCR machine. A serial 5 -fold dilution was performed to determine the standard curve of Opn mRNA. Fig. 14 shows the linearity of the relationship between the Ct value and the logarithm of concentration with a correlation coefficient of 1.00.

Osteopontin mRNA expression was comparable to the results of protein expression assessed by immunostaining with respect to intensity and kinetics in both C57BL/6 and C3H/He inbred strains. Gene expression changes in a time course series 1, 2, 3 and 5 days after freeze thaw-injury in both calcified lesions and healthy myocard of both C57BL/6 and C3H/He inbred strains are illustrated in Fig. 15. In the healthy myocardium the expression of Opn increased and peaked at day 2 reaching a maximum of 3.6 ± 1.68 (means \pm SE) in C57BL/6 mice and varied between 1 and 2 -fold induction in C3H/He mice. In the calcified lesions, however, it was increased reaching a maximum at day 3 of 65.27 ± 21.93 -fold induction and 1364.29 ± 141.30 -fold in C57BL/6 and C3H/He mice, respectively.

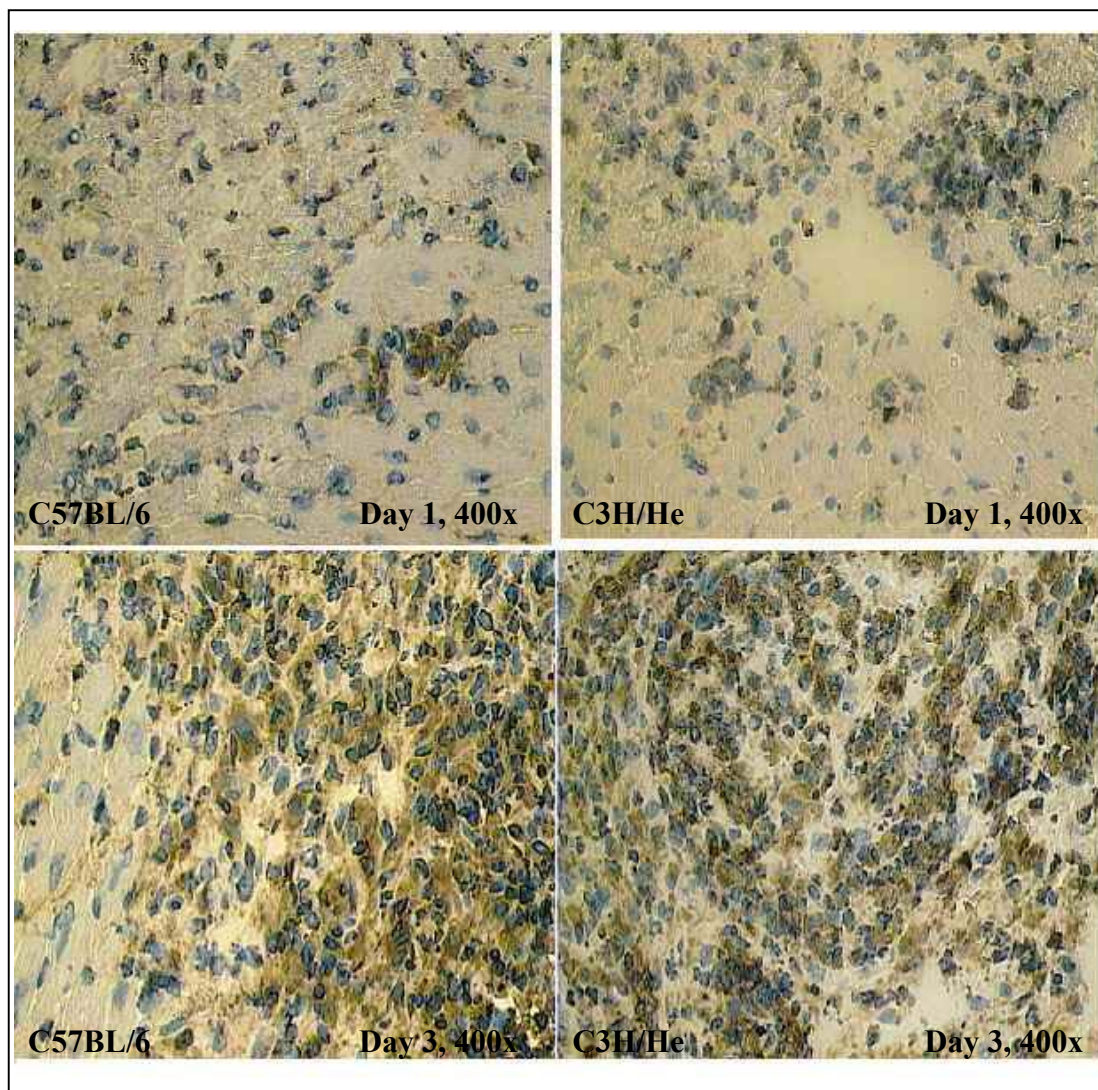


Fig. 12: Detection of macrophages infiltration. Macrophages determination was performed employing rat anti-macrophage monoclonal antibody (MOMA-2) and visualized by Diaminobenzidine (brownish staining). Macrophages infiltration was observed in both C3H/He and C57BL/6 inbred strain of mice with marked staining at day 3 post injury. As counter staining we used Hematoxylin (stain nuclei in blue).

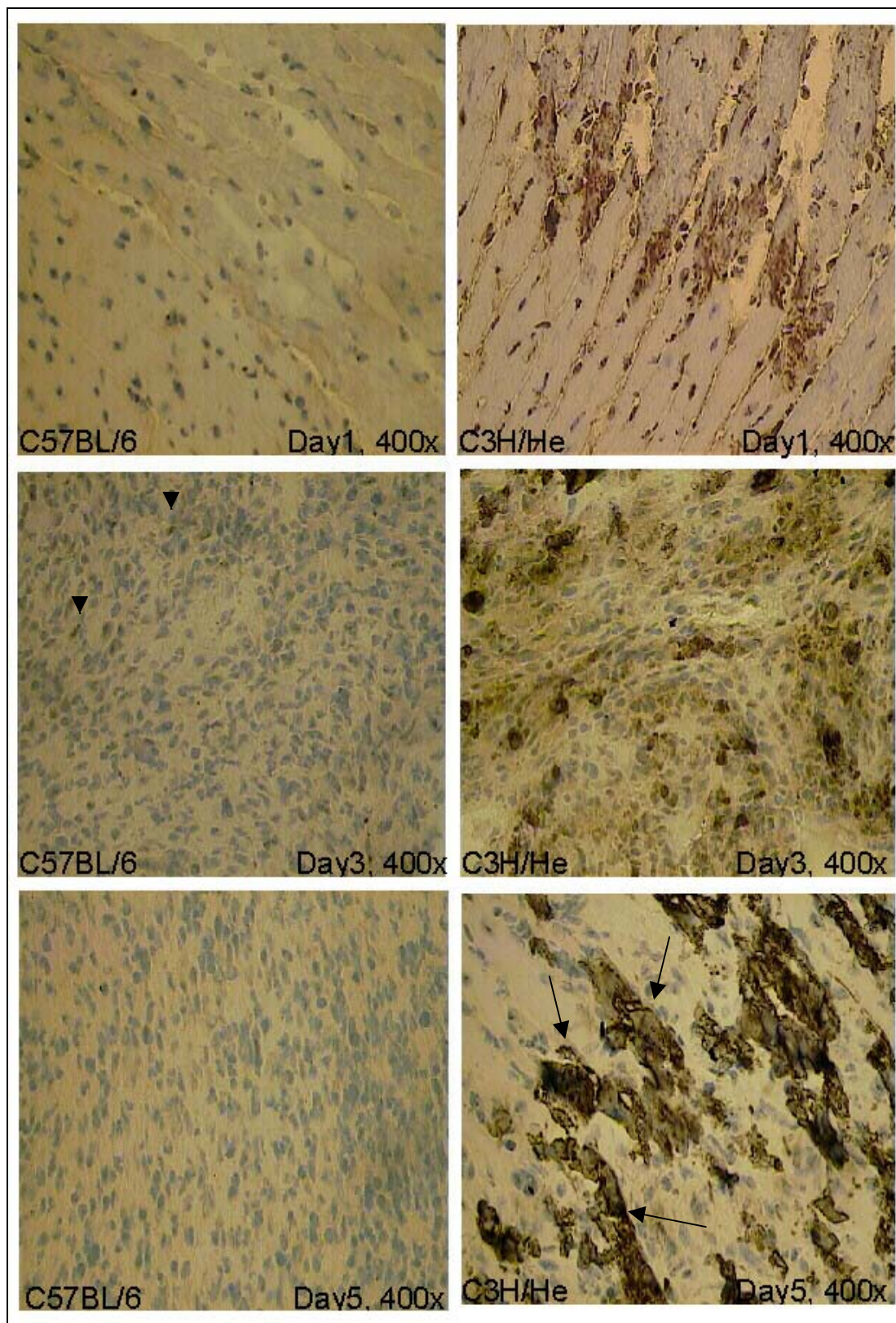


Fig. 13: Osteopontin protein expression (brownish). A polyclonal goat anti-osteopontin antibody was used as described in Materials and Methods. Extensive Opn immunostaining was noted already at day 1 and peaked at day 3 in C3H/He inbred strains. In C57BL/6 mice, however, Opn staining was hardly detected 3 days after injury (Arrow heads). By day 5, staining of Opn remained stronger and was co-localized with calcium deposition (seen as plaques, arrows) in C3H/He mice whereas it was no longer detectable in C57BL/6 mice by day 5. Hematoxylin was used to stain nuclei.

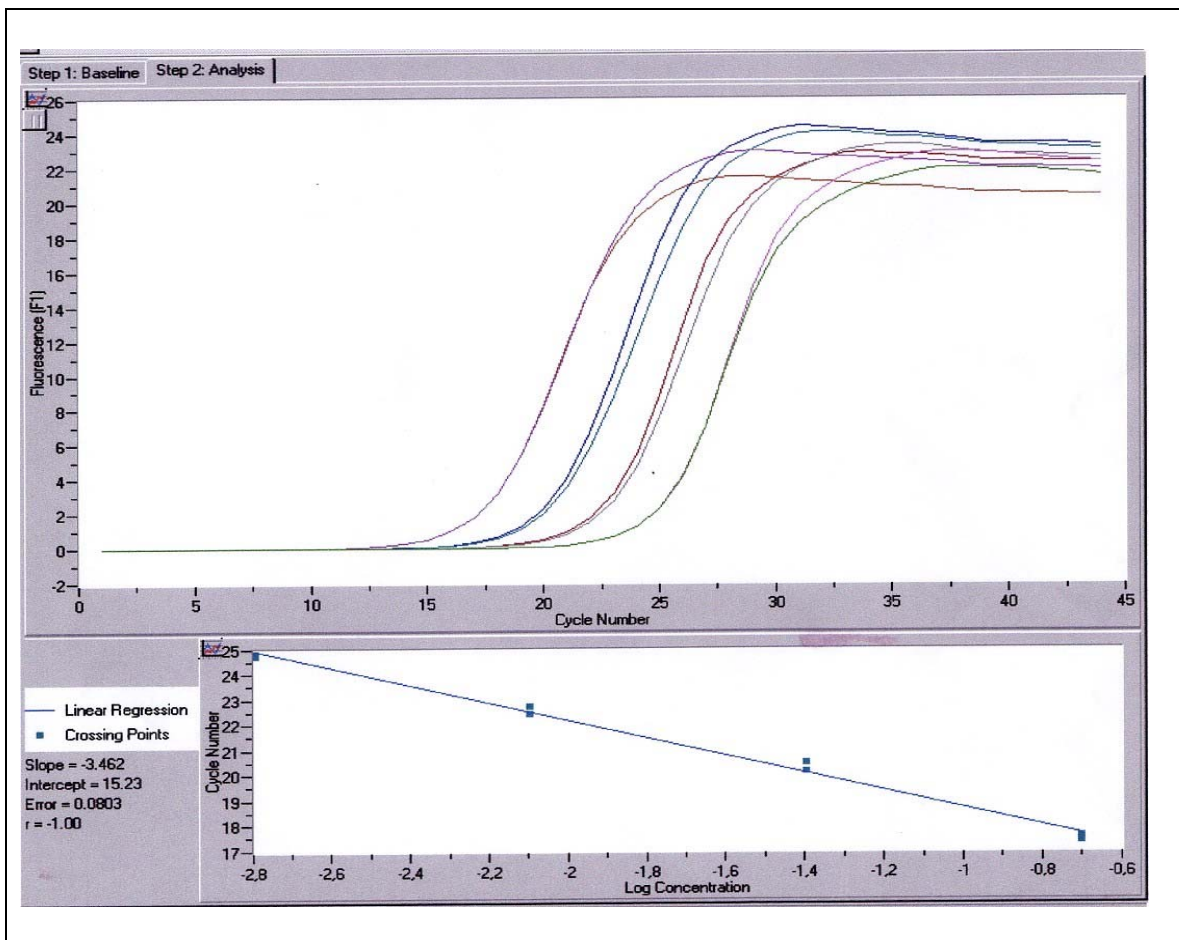


Fig. 14: Standard curves for Opn mRNA. Serial dilutions of mouse heart total RNA were analyzed by RT-PCR for osteopontin. The standard curves show plot of cycle number (Ct) versus fluorescence changes (F1) and the relating Ct in function of the logarithm concentration. The Ct was obtained by crossing point analysis using the second derivative maximum method implemented in the LightCycler. The regression coefficient shows high reproducibility ($r^2=1.00$).

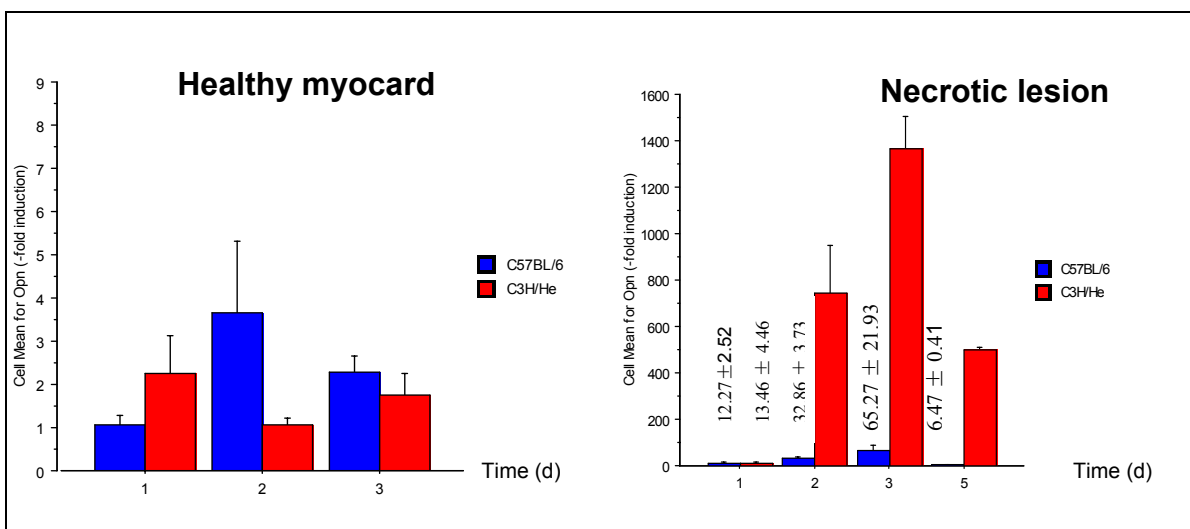


Fig. 15: Opn mRNA induction in C57BL/6 and C3H/He mice. Osteopontin mRNA expression changes after freeze-thaw injury following a time course. The PCR product amplification was followed by LightCycler using SYBR Green I detection in healthy myocardium and injured area. Three animals per group were analysed for RT-PCR in replicate. Relative fold induction was calculated using delta-delta Ct method. The mean of group is plotted and the error bars represent SE.

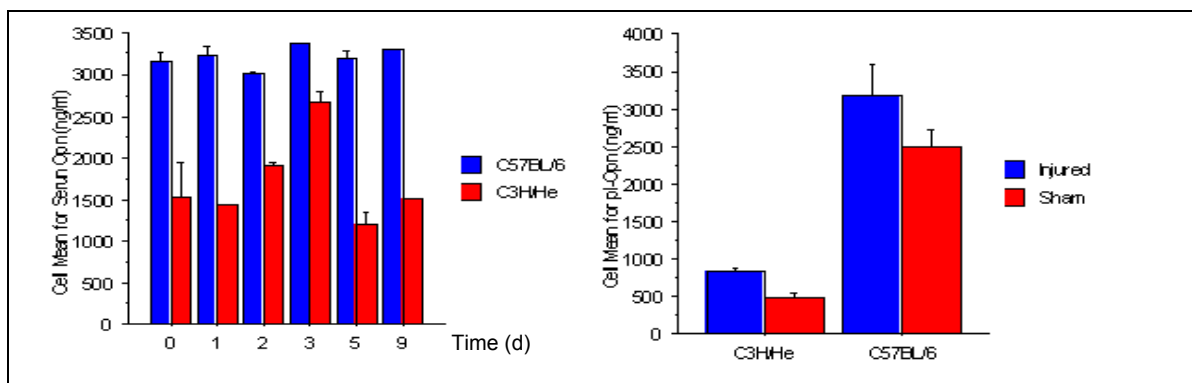


Fig. 16: Opn plasma concentration. Osteopontin concentration (ng/ml) was determined in plasma of C57BL/6 and C3H/He mice using ELISA kit as described in Materials and Methods. To the left, a number of two animals per group of each strain were screened after 0, 1, 2, 3, 5 and 9 days after freeze thaw injury. For statistical analysis (Right) the number of animals was raised to five per group for each strain and determined the concentration of Opn in plasma after day 3 post freeze in comparison to the sham operated animals. The mean of each sample is plotted and the error bars represent SE.

3.4.1.2. Osteopontin concentrations in plasma

The striking strain differences in Opn expression at the protein and RNA level prompted to examine plasma concentrations of this secreted protein to determine if the increase of Opn expression is a systemic or a local response to myocardial damage after freeze-thaw injury. The concentrations of Opn in plasma was measured employing enzyme immuno-assay using an ELISA kit as described in section 2.5.3.

After screening all animals at different time points myocardial injury, an increase of plasma concentrations of Opn was observed in C3H/He peaking at day 3 (Fig. 16, left). In C57BL/6 mice, however, the Opn concentrations remained stable at different time points in C57BL/6 mice compared to the sham operated C57BL/6 animals. The concentration of Opn in C57BL/6 was two times greater than C3H/He plasma Opn in all these time points post freeze including sham operated myocard tissue. For statistical analysis, we repeated this experiment and examined ten animals from each strain. Each strain of mice is divided into two groups of five animals. Changes of Opn plasma concentrations were measured at day 3 after freeze-thaw injury in comparison to sham operated animals (Fig. 16, right). Thus an increase of the concentration was revealed in both C57BL/6 and C3H/He inbred strain after injury compared to the baseline values of sham operated animals. The mean concentration of Opn after myocardial infarction reached a maximum of 3289 ± 403.25 (mean \pm SE) ng/ml in C57BL/6 mice in comparison to 2503 ± 226 of the sham operated and 839 ± 31.18 ng/ml in injured

C3H/He mice versus 481 ± 55.55 of the sham operated mice. Our observations suggested that, in general, myocardial injury lead to a systemic increase of Opn plasma levels in response to injury, rather than being a strictly local paracrine response of tissue macrophages.

3.4.2. Transforming growth factor- β 1, Tgf β 1

Tgf β 1, a multifunctional cytokine, plays a major role in tissue remodeling during wound repair and inflammation. Immunohistochemistry and RT-PCR were performed to examine Tgf β 1 protein and mRNA expression. Fig. 17 illustrates the time course of Tgf β 1 protein expression. In both C57BL/6 and C3H/He, Tgf β 1 staining was detected already at the first day after freeze thaw-injury, with particular concentrations in the border zone between necrotic and healthy zones. The secretion of Tgf β 1 increased progressively within the whole necrotic area at day 3 after injury. 5 days after injury, Tgf β 1-positive cells began to decrease and were more predominant in the periphery of the necrotic lesion. After day 9 no staining for Tgf β 1 could be detected anymore (data not shown).

Tgf β 1 mRNA expression was examined using real time RT-PCR by SYBR Green I detection. First, the linearity of the relationship between the Ct values and the logarithm of concentrations was determined (Fig. 18). The results illustrated in Fig. 19 showed the expression of Tgf β 1 mRNA following a time course. Significant increase of Tgf β 1 messenger RNA in calcified myocardial lesions was noticed in the C3H/He strain peaking at day 3 reaching a maximum of 7.5 –fold induction. This increase was also observed in the healthy myocard of C3H/He mice already at day 1 with a maximum of 2.5 –fold induction.

In contrast, however, mRNA expression remained stable and no significant increases were noticed in C57BL/6 mice in both healthy and necrotic myocard tissue in comparison to the baseline.

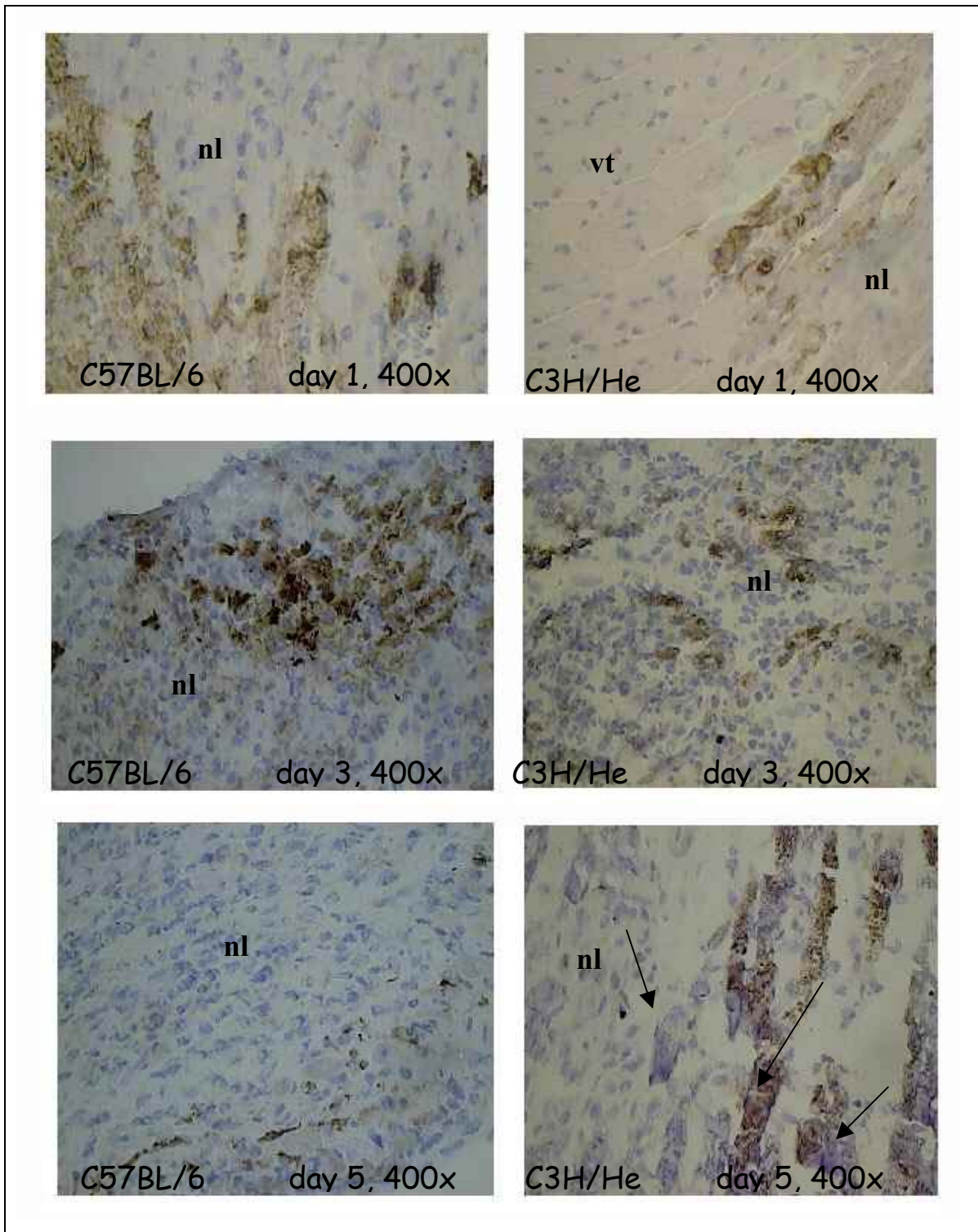


Fig. 17: Tgfb1 protein expression. Immunohistochemical detection (brownish) of transforming growth factor-beta 1 (Tgfb1) in mouse myocardium after freeze-thaw injury using a polyclonal rabbit anti-Tgfb1 antibody. For counterstaining Hematoxylin was used to detect nuclei (blue). Tgfb1 was detected in injured myocardium (nl) of both C3H/He and C57BL/6 mice 1, 3, and 5 days post injury. Arrows show visible calcification plaques (blue-violet). vt, designates vital tissue shown by its intact structure.

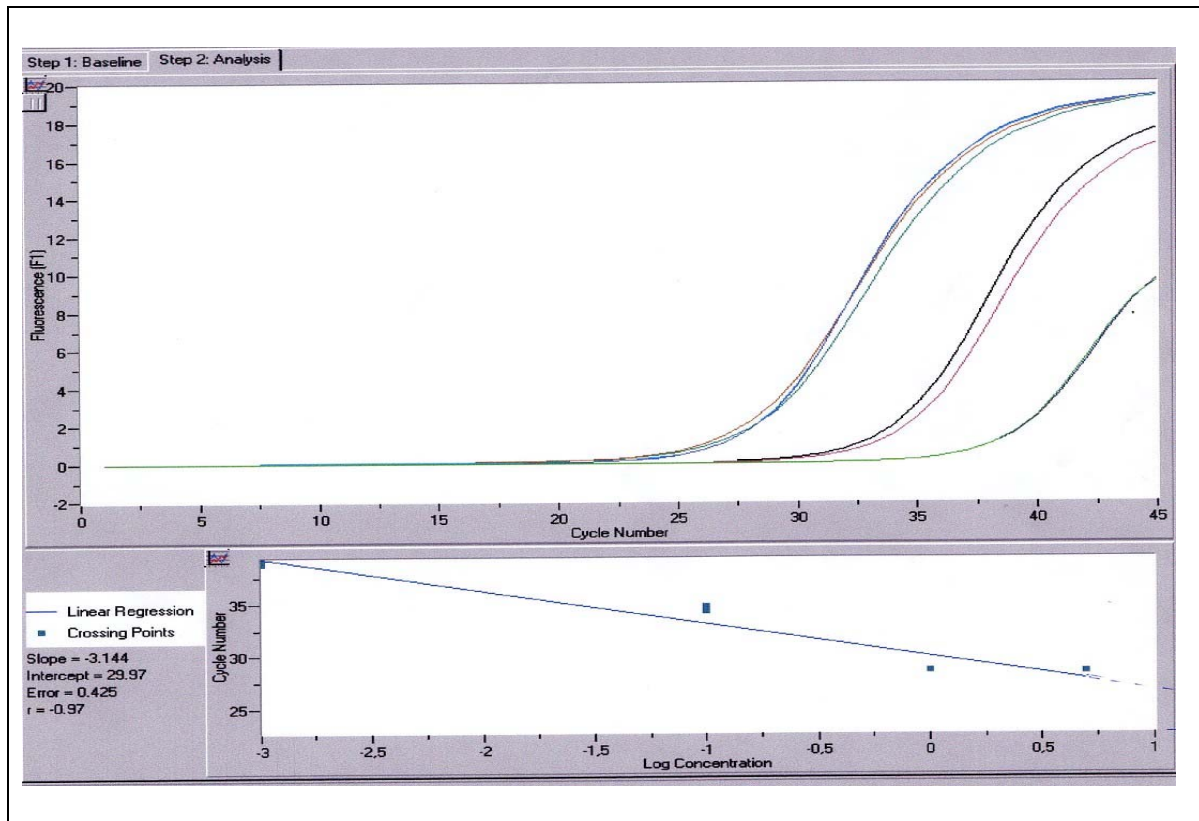


Fig. 18: Standard curves for Tgfb1 mRNA. Serial dilutions of mouse heart total RNA were analyzed by RT-PCR for Tgfb1. The standard curves show threshold cycle number (Ct) versus fluorescence changes (upper curve) and the relating Ct in function of the logarithm concentration (bottom). The Ct was obtained by crossing point analysis using the second derivative maximum method implemented in the LightCycler. The regression coefficient shows high reproducibility ($r^2=0.97$).

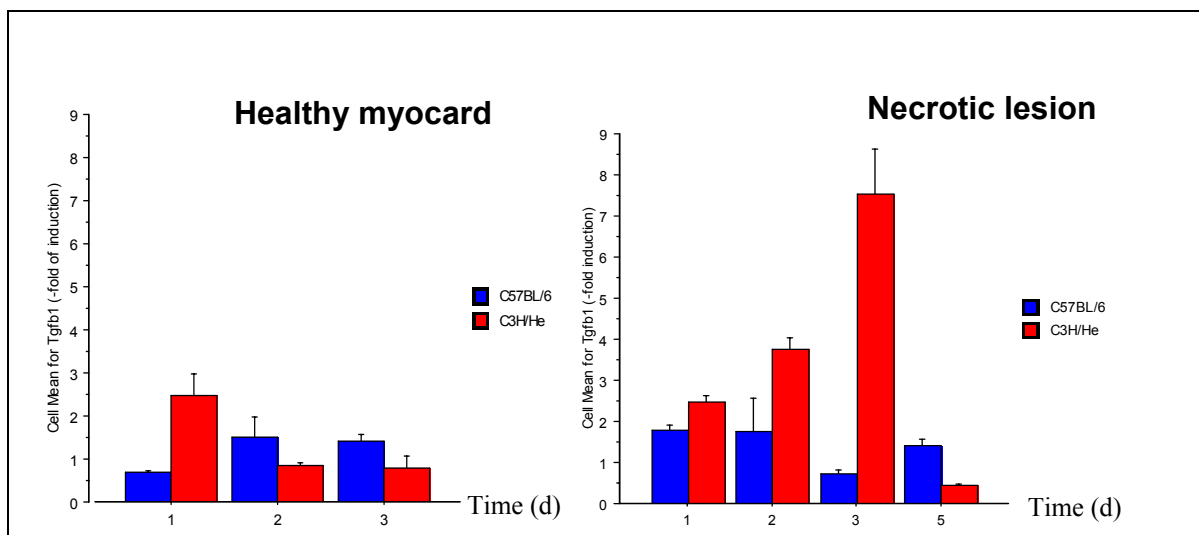


Fig. 19: Tgfb1 mRNA expression. Relative fold induction of Tgfb1 in healthy myocard (left) and injury lesions (right) in C57BL/6 (blue) and C3H/He (red) inbred strain of mice. Myocardial infarct was enhanced using freeze-thaw injury method. The total RNA samples from different animals at various period of time were isolated as described in Materials and Methods. For statistical analysis three animals per group were analyzed for RT-PCR in replicate and detected by SYBR Green I using LightCycler. Relative fold induction was calculated using deltadelta Ct method. The mean of each sample is plotted and the error bars represent SE.

3.4.3. Osteocalcin

Osteocalcin (Osc) is the most abundant non-collagenous bone-related protein that is expressed only in osteoblasts and in non other extracellular matrix (ECM) producing cell (Weinreb et al., 1990; Ducy and Karsenty, 1995). Similar to other non-collagenous proteins, such as osteonectin, Osc possesses gamma-carboxyglutamic acid residues which exhibit a high affinity for hydroxyapatite and collagen (Fujisawa et al., 1996) and are considered inhibitors of crystal growth (Hunter et al., 1996). Gene expression of Osc was studied at mRNA and protein level in healthy and necrotic tissue following myocardial freeze-thaw injury. With regard to mRNA, Osc appeared to be expressed at a very low level that RT-PCR analysis by SYBR Green I was not able to quantify differential changes in Osc gene expression because of high signal noise caused by primer dimers after high amplification rate. Similar results were obtained even a new primer redesign. To semiquantify Osc mRNA expression, analysis were carried after RT-PCR amplification on agarose gel by electrophoresis using Gel-Pro-Analyser software. 18S RNA was used as internal standard. Fig. 20 shows evidence of an increase of Osc mRNA expression after injury in the necrotic lesions of C3H/He myocardium, reaching a maximum at day 3 and 5 and declining thereafter. To support these results immunohistological investigations were carried employing a specific murine anti-osteocalcin antibody. None of the cryosections obtained from C57BL/6 mice showed positive staining for Osc at any time point after freeze-thaw injury. However, in the C3H/He strain sections of day 3 and 5 after injury exhibited positive staining in the necrotic lesions of myocardial tissue (Fig. 21). After day 5 Osc positive cells were co-localized to the calcified lesions. Thus, Osc seems to be increased by day 3 after freeze-thaw injury at both transcriptional and protein levels. The failure to mirror these changes by real time RT-PCR analysis using SYBR Green I detection may be attributed to a lack of sensitivity.

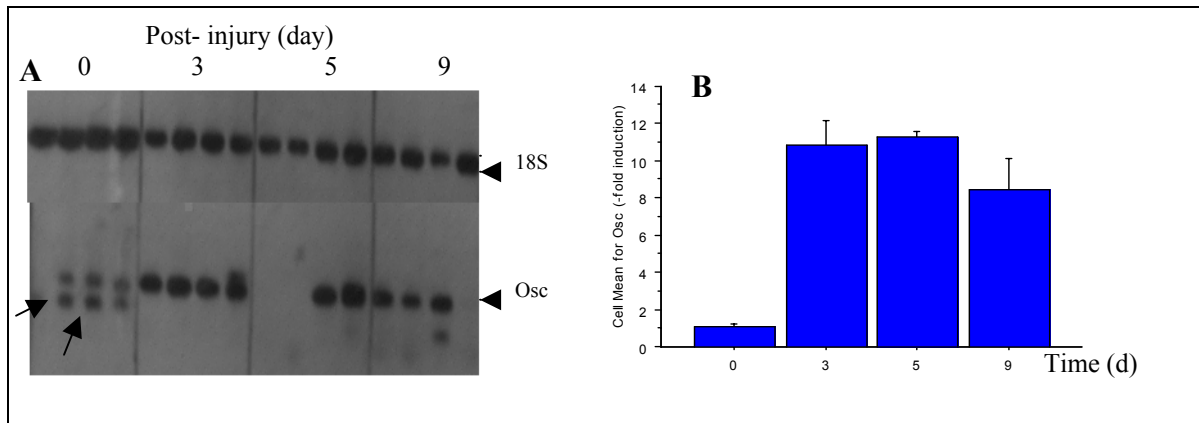


Fig. 20: Osc mRNA induction in C3H/He mice. Semi quantitative determination of Osteocalcin mRNA expression (Osc) using 18S as internal standard. Amplicons were determined after a high amplification rate (45 PCR cycles) by agarose gel electrophoresis employing ethidium bromide staining (A). Semiquantitative analysis were carried employing Gel-Pro Analyzer software that quantify the density of bands (B). By day 1 unspecific PCR products were observed (arrows). However, an increase of Osteocalcin mRNA expression was detected after day 3 and declining by day 9 after injury (B). Four assays were used at each time points.

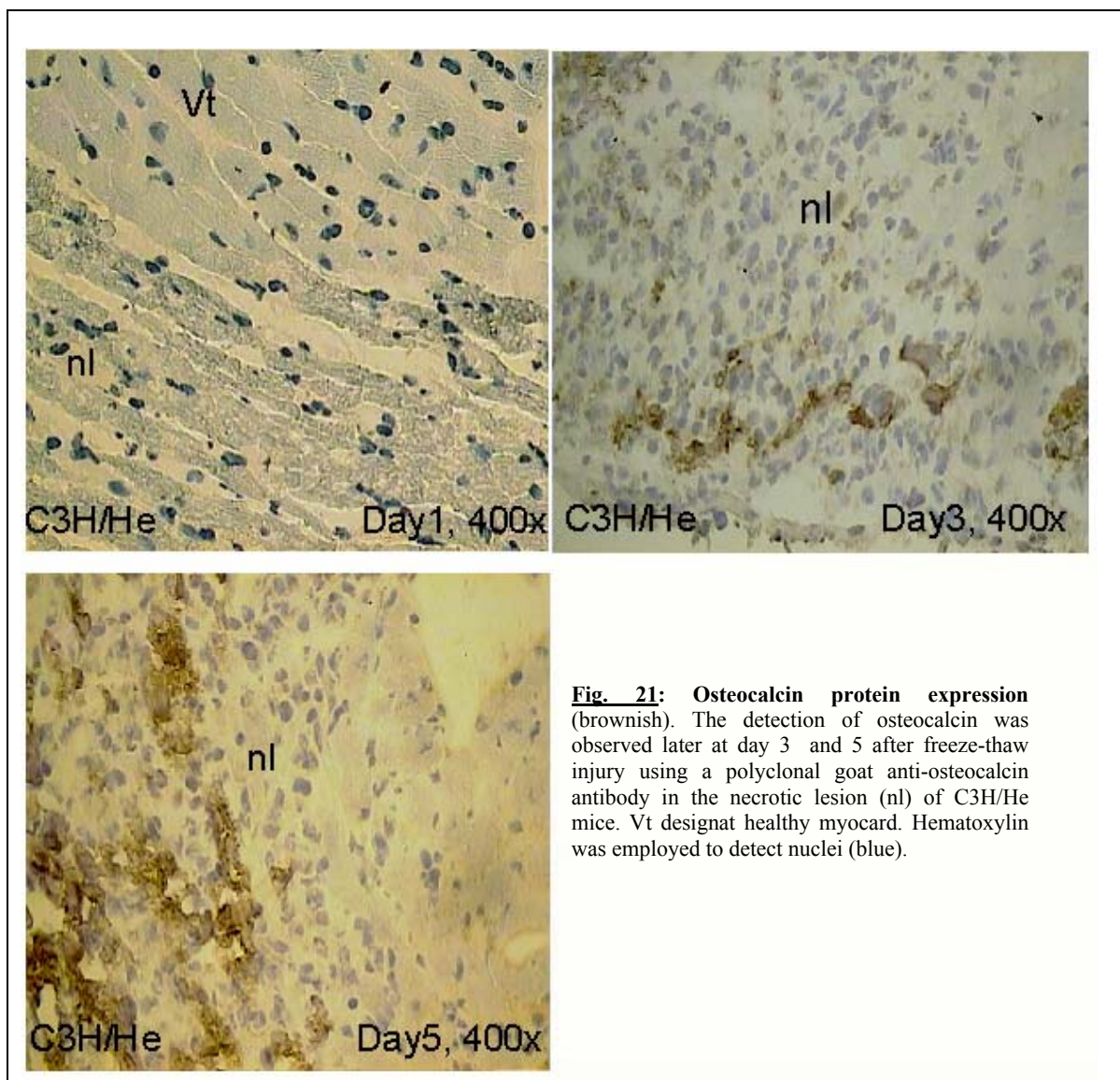


Fig. 21: Osteocalcin protein expression (brownish). The detection of osteocalcin was observed later at day 3 and 5 after freeze-thaw injury using a polyclonal goat anti-osteocalcin antibody in the necrotic lesion (nl) of C3H/He mice. Vt designat healthy myocard. Hematoxylin was employed to detect nuclei (blue).

3.4.4. Osteonectin.

Osteonectin (Osn), also known as SPARC or BM40, is a calcium binding matricellular glycoprotein mediating cell-matrix interaction. Differential Osteonectin mRNA and protein induction was examined in strains C57BL/6 and C3H/He in healthy and necrotic myocard at different time points after myocardial injury. As mentioned for previous genes under study, the standard curve for osteonectin mRNA was first determined (Fig. 22). Then changes in osteonectin mRNA after freeze-thaw injury were analysed (Fig. 23). In the necrotic lesions of C3H/He a significant increase of osteonectin mRNA was observed at day 2 peaking at day 3 with a maximum of 3.82 ± 1.03 (means \pm SE) and rest constant thereafter. In C57BL/6 mice, an increase of gene expression was observed at day 1 within injured area reaching a maximum of 3.41 ± 0.51 -fold of induction at day 3 and decreased at day 5. In healthy myocardium significant increase in Osn expression was observed in C3H/He at day 1.

Taking in consideration that osteonectin is secreted by many different types of cells and was highly conserved among species (Termine et al. 1981, Damjanovski et al 1992), immunohistological analysis performed using a polyclonal anti-osteonectin antibody which was raised against human and was shown to cross-react with rat but was not tested for mouse. Specific antibodies against mouse were not available when this investigation was carried. No positive cell staining was detected in sections of both strains at different time points after freeze-thaw injury. With this result we could not confirm whether or not osteonectin is also expressed in the murine heart at protein level.

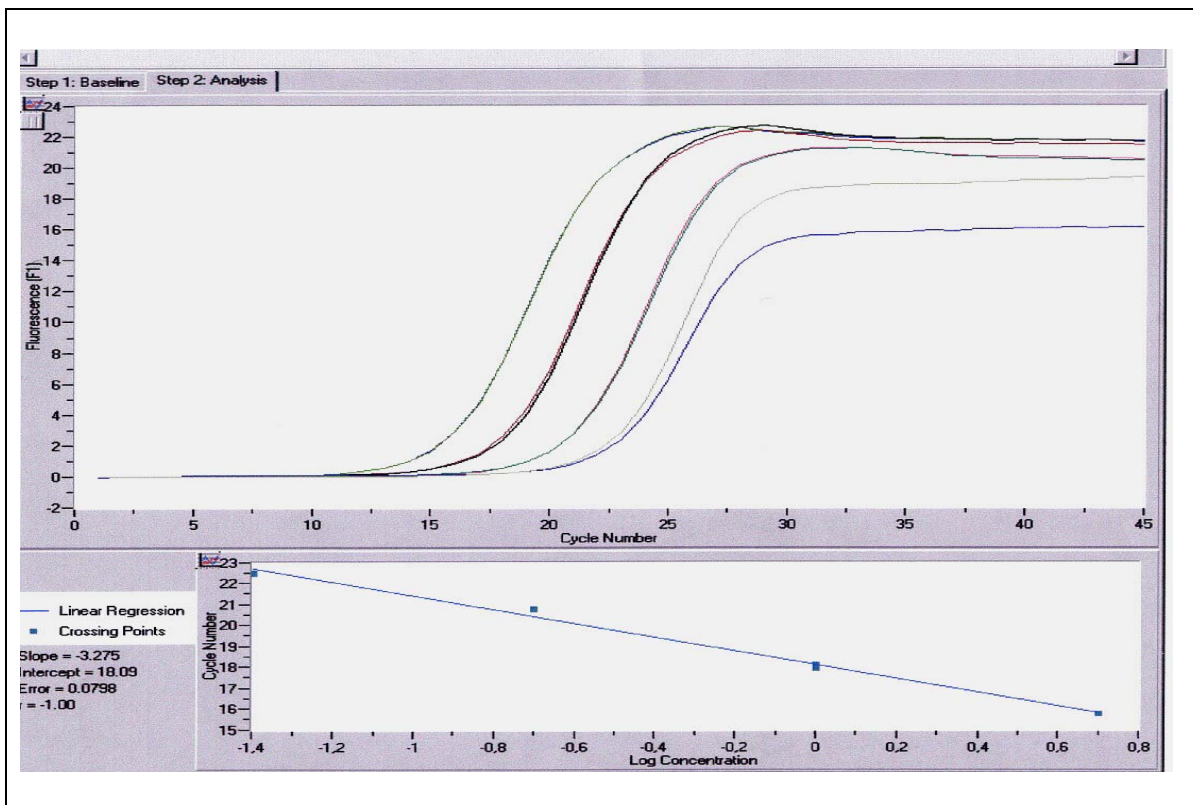


Fig 22: Standard curve for osteonectin mRNA. Serial factor 5 dilutions of mouse heart total RNA were analysed by RT-PCR for osteonectin. The standard curves show plot of cycle number (Ct) versus fluorescence changes (upper curve) and the relating Ct in function of the logarithm concentration (bottom). The Ct was obtained by crossing point analysis using the second derivative maximum method implemented in the LightCycler. The regression coefficient shows high reproducibility ($r^2=1.00$).

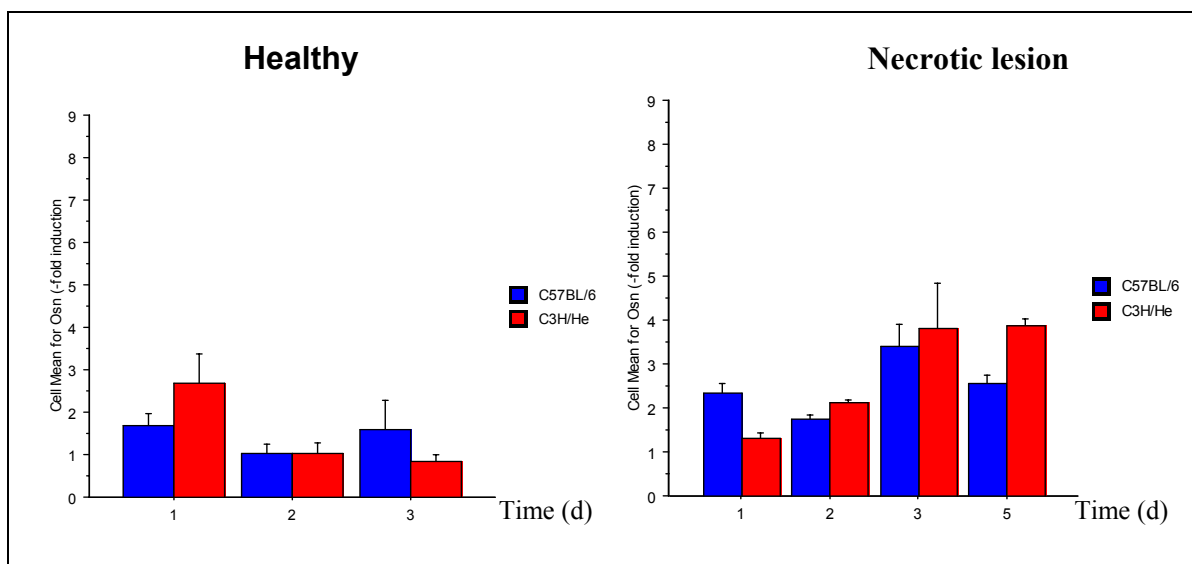


Fig. 23: Osteonectin mRNA expression in C57BL/6 and C3H/He mice. Osn mRNA expression was examined following a time course after freeze-thaw injury. The PCR product amplification was followed by LightCycler using SYBR Green I detection in healthy myocardium (left) and injured area (right). Three animals per group were analysed for RT-PCR in replicate. Relative fold induction was calculated using $\Delta\Delta Ct$ method. The mean of group is plotted and the error bars represent SE.

3.5. Ca^{2+} , Mg^{2+} , phosphor, and Troponin T concentrations in Plasma.

Dystrophic myocardial calcification is distinguished from metastatic calcification by the fact that it occurs independently from plasma calcium/phosphate homeostasis. To confirm this result, blood was collected from animals which were thought for heart mRNA expression analysis at different point of time and subjected to plasma calcium, magnesium and phosphor concentration determination. Using limited number of animals (2 animals per group), no changes in calcium and magnesium level were observed between sham operated mice and animals subjected to injury (Fig. 24A-B). The values obtained for mice were found within the normal human range, 2.10 – 2.60 for calcium and 0.70 – 1.1 mmol/l for magnesium, except C3H/He mice at day 5. However, significant decrease was observed in plasma phosphor concentration after injury in both strains and a return to base line was noticed after day 3 in C3H/He mice (Fig. 24C). To support this finding statistically, this experiment was repeated and ten animals from each strain were examined. Each strain of mice was divided into two groups of five animals. Changes of Ca^{2+} , Mg^{2+} and PO_4 plasma concentrations were measured at day 3 post injury (Fig. 24D-F). Day 3 was chosen because many changes were observed previously at this time point. The normal calcium/magnesium plasma level was a second time confirmed within the biological range in both strains after injury in comparison to sham operated animals (Fig. 24D-E). Also the decrease in plasma phosphor concentration was observed in both strains after day 3 post injury (Fig. 24F). C3H/He mice marked a strong decrease in plasma phosphor level after injury with a maximum of 23 % (2.09 ± 0.13 mmol/l in injured versus 2.71 ± 0.22 in sham operated animals) in comparison to C57BL/6 with only 8 % (1.88 ± 0.08 mmol/l in injured versus 2.06 ± 0.15 mmol/l in sham operated strains). These concentrations were found outside the human plasma phosphor normal range (0.85 - 1.45 mmol/l).

Troponin is a regulatory protein of the thin filament of striated muscle. Three subunits were identified: C, I and T. After myofibril degradation skeletal muscles mediated the release of these proteins into the blood. Thus, after myocardial infarct the cardiac-specific troponin T and I were released in the systematic system and were used as relevant diagnostic markers. The blood level of troponin T was examined after freeze-thaw injury in C57BL/6 and C3H/He mice

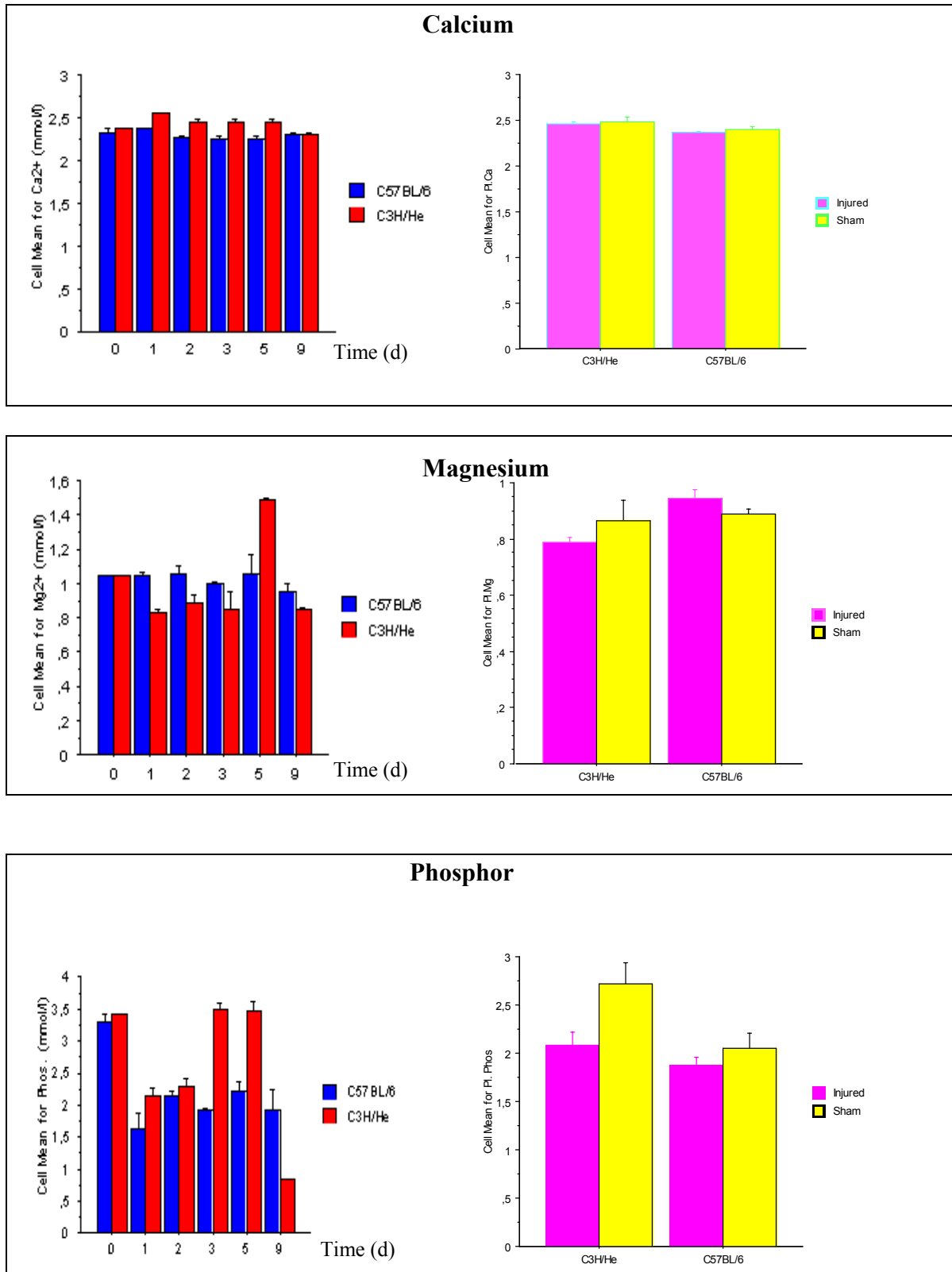


Fig. 24: Ca²⁺, Mg²⁺ and PO₄ plasma concentration. Mineral concentrations (mmol/l) of Calcium, A); magnesium, B) and phosphate C) in plasma of C57BL/6 (blue) and C3H/He inbred strains of mice (red). A number of two animals per group of each strain were screened after 0, 1, 2, 3, 5 and 9 days following myocardial infarct by freeze-thaw injury. For statistical prevalence a number of 5 animals per group were analysed and the concentration of different minerals were determined in plasma of C57BL/6 and C3H/He inbred strains of mice 3 days after myocardial infarction (pink) in comparison to the sham (yellow) (D-F).

using quantitative troponin T strip tests. The detection of troponin T in the blood of both strains was confirmed early as day 1 after myocardial infarct. This level remain high at day 2 and decline thereafter by day 3 (data not shown). By day 5, troponin T was not detected in plasma of both mice (data not shown).

Discussion

Dystrophic calcification is distinguished from pathological soft tissue calcification by the absence of a systemic mineral imbalance (Seifert, 1997; Black and Kanat, 1985). Although dystrophic calcification can occur in all soft tissues, it seems to affect mainly cardiovascular tissues. In arteries, calcification is correlated with the severity of atherosclerotic plaque load and with the risk of coronary events (Stallion et al., 1994; Catellier et al., 1990). Valvular calcification is particularly common in the elderly often requiring medical or even surgical therapies, which add up to considerable health costs (Mohler et al., 2001). Myocardial calcification, however, is associated with severe cardiomyopathy (D'agostino and Chiga, 1970; Bloom and Peric-Golia, 1989) or unknown hereditary causes (Bjelle and Sundstroem, 1975; Bosmann et al., 1977), and can occur in response to myocardial tissue injury (Vracko and Thorning, 1985; Brunnert and Altman, 1990). Despite the high prevalence and clinical significance of dystrophic cardiac calcification, little is known about the molecular genetic pathogenesis.

4.1. Gene targeting

DCC shares many features with physiological bone mineralization. It is associated with the accumulation of non-collagenous matrix proteins, such as osteopontin, osteonectin, osteocalcin, and transforming growth factor beta-1, one of the key regulators of proliferation and extracellular matrix synthesis by osteoblasts (Breen et al., 1994). In mouse models of targeted inactivation of the matrix Gla gene (Luo et al., 1997) as well as the osteoprotegrin gene, which is another member of the transforming growth factor receptor superfamily (Bucay et al., 1998), dystrophic vascular calcification was reported. Although, osteopontin, osteonectin and osteocalcin were reported to be associated with cardiovascular tissue mineralization, molecular understanding of cause and consequence is still very limited. Accumulated evidence suggested that these genes were indirectly involved in response to injury or as a result of calcium deposition rather than being involved in the initiation of dystrophic calcification as proposed recently (Gadeau et al., 2001). Other researchers, who studied knockout mice, supported the former hypothesis. In osteocalcin knockout mice bone formation was limited without impaired mineralization (Ducy et al., 1996). Osteonectin-null mice

exhibited cataracts (Gilmour et al., 1998, Norose et al., 1998) or, as reported recently, accelerated wound healing (Bradshaw et al., 2002). Osteopontin knockout mice, however, also exhibited altered wound healing (Liaw et al., 1998). Recently, Trueblood et al., 2001 reported left ventricular dilatation and reduced collagen deposition after myocardial infarction in osteopontin deficient mice. In summary, studies in mouse models with specific inactivation of osteocalcin, osteonectin, or osteopontin, failed to demonstrate dystrophic cardiac calcification, even in conditions of myocardial damage.

Dystrophic cardiac calcification, however, was demonstrated in several cardiomyopathy models, e.g. in mouse mutants of desmin (Mavroidis and Capetanaki, 2002), the alpha cardiac myosin heavy chain (Fatkin et al., 1999) and myosin-binding protein-C (McConnell et al., 1999), but the expression of the aforementioned non-collagenous bone matrix proteins not examined in these genetic mouse models.

4.2. Pathology

To elucidate the molecular mechanisms leading to DCC we examined C3H/He, an inbred mouse strain carrying a natural allele of the *Dyscalc1* locus predisposing to age-dependant spontaneous dystrophic cardiac calcification. In order to study the development of dystrophic calcification in a defined frame of time we employed transabdominal cryopexy to produce myocardial freeze-thaw injury and necrosis. The myocardial phenotype of the calcified lesions in these mice was compared to the phenotype in members of the resistant strain C57BL/6, which therefore served as a control in our experiments. In an attempt to determine the role of non-collagenous bone matrix proteins with respect to irreversible injury and calcium deposition we investigated the time course and spatial distribution of the mineralization process starting from its earliest stages after injury, which were studied employing transmission electron microscopy.

4.3. Initiation and progression of calcium phosphate deposits

Brunnert, 1997 reported precipitation of amorphous calcium within and around swollen mitochondria a few hours after myocardial damage. Subsequently, these electron-dense calcium deposits grew larger comprising the entire cytoplasm and eventually surrounding myofibrils (Eaton et al., 1978; Brunnert, 1997; Vracko and

Thorning, 1985; Burbach, 1987; Van Vleet and Ferrans, 1987). These findings prompted the authors to hypothesize that dystrophic calcification may actually result from altered mitochondrial function. The pivotal role of mitochondria for apoptosis and cell death has been amply documented (reviewed by Kim, 1995; Green and Reed, 1998; Chakraborti et al., 1999; Halestrap et al., 2000; Raha and Robinson, 2001). The leakage of cytochrome C from the mitochondrion into the cytoplasm appears to mark the point-of-no-return in apoptosis triggering a fatal cascade of caspases and other death effector proteins. However, ATP-dependent mitochondrial calcium sequestration contributes to physiological intracellular calcium homeostasis and may prevent cell death, which is always accompanied by large intracellular calcium shifts. The signal cascades leading to cell death in the presence of abnormally high concentrations of free intracellular calcium have been well studied (Kim, 1995; Chakraborti et al., 1999). Our own investigations in cooperation with PD Dr. M. Klinger (Institut für Anatomie, Universität Lübeck, Direktor Prof. Dr. Westermann) have principally confirmed the findings that were reported previously (Brunnert, 1997). After tissue damage mitochondria were swollen and formed conglomerations among disintegrating myofibrils and other debris. They exhibited some calcium precipitation in areas of irreversible tissue injury that was absent in mitochondria of normal appearance or in the surrounding necrosis. The localization of the precipitates excluded non-specific staining artifacts. Interestingly, within the first 24 hours after injury, the morphological changes in the necrosis were not obviously different between both predisposed C3H/He and resistant C57BL/6 strains. However, in later stages deposition of calcium continued spreading over larger areas in needle-like hydroxyapatite crystals only in the predisposed C3H/He strain, while resistant C57BL/6 did not exhibit any signs of progression. These data suggest a slightly different interpretation compared to what was reported by others. In both strains mitochondria may be able to sequester calcium and concentrate calcium salts beyond solubility in injured cells. In contrast, the formation of crystals may be explained with a deficiency of a cytoplasmic calcium binding inhibitor or a special mineral and matrix composition favouring apatite crystal formation in C3H/He mice. The physiological apatite mineral formation is initiated by the so-called matrix vesicles in bones. Once the calcification begun, Ca (PO₄) crystal serves as nuclei for the formation and growth of new crystals. This process is activated

by the availability of Ca^{2+} , $\text{PO}_4^{(3-)}$ and collagen (Anderson, 1989). Taken together, morphological similarity of the earliest stages of calcium deposition suggested that dystrophic calcification may not be due to primary mitochondrial differences as implied by other authors (Eaton et al., 1978; Brunnert 1997; Vracko and Thorning, 1985; Van Vleet and Ferrans, 1987). The strain-specific formation of hydroxyapatite may be an independent process that originated from mitochondria, because they offered high local calcium salt concentrations. Continued crystal formation may, however, be independent of mitochondrial function that appeared to have expired anyway at this stage of necrosis.

Subsequent stages of necrotic calcification extending from 1 to 5 days after myocardial injury were studied using primarily fluorescent calcein staining. Consistent with the findings in electron microscopy presented here, calcium deposits was noticed in the necrotic myocardium of both C57BL/6 and C3H/He strains since day 1. Calcein staining was noticed in areas of coagulative necrosis formed by denser remnants of debris in which agglomerations of mitochondria were clearly discernible by their intense fluorescence. Calcein fluorescence demonstrated that the mitochondria exhibited particularly high calcium concentrations and that debris appeared to bind some calcium as well. These islands of coagulative necrosis were surrounded by macrophages in which intensely stained phagocyte material could be seen sometimes. This histological phenotype was found in both strains at day 1, but appeared more pronounced in strain C3H/He. Interestingly, initially, calcein staining was mainly limited to a small zone interfacing healthy and necrotic tissue. This zone has special features suggesting different interpretations of the pathogenesis of DCC: 1) in this zone thermal injury may not have caused cell death immediately but may have produced a more protracted form of cell demise, such as apoptosis in irreversibly damaged cells. During this window of time the mitochondria of the dying cell may have accumulated large amounts of calcium that has leaked out of the sarcoplasmic reticulum before ATP-production ceased eventually. 2) an unknown component may have diffused from the interstitial space of the healthy myocardium into the necrotic core. This component may well be extracellular calcium but could also be secreted as a protein by the adjacent undamaged healthy myocardial tissue. 3) Calcium deposition in this zone was dependant on cellular components that infiltrated the necrotic zone from its exterior borders.

While the former two hypothetical pathways might have formed a more-or-less perfect ring shaped zone of initial calcification as a result of the distribution of the thermal gradient in the tissue or the easily diffusible nature of a liquid component, cellular infiltration may have produced calcification along the major interstitial routes of infiltration. In fact, we obtained evidence for the involvement of phagocytotic activity in the development of calcification because calcium staining assumed a patchy rather than a circular pattern in the periphery of the necrosis. This focal calcium deposition appeared to be strictly associated with remnants of debris (Murry et al., 1994). At day 2 calcein stained nearly the entire necrosis in C3H/He mice only. In the C57BL/6 strain, however, calcium deposition was restricted to small foci that were subsequently resolved completely suggesting a higher phagocytotic capacity in this strain.

More advanced stages of tissue calcification were assessed employing alizarin red S staining which forms a red complex with calcium in a chelating process. After day 3 calcium deposits were detectable only in C3H/He mice as crystals that formed larger spicular bundles with a gritty appearance. These focal calcifications were located predominantly in the periphery of the lesion adjacent to viable tissue or in the subepicardial areas of the necrosis. However, sometimes patches of calcification were found in necrotic cores as well. We could not readily determine an obvious association of calcium deposition with the extent of vascularisation, routes of inflammatory infiltration nor the composition and density of the cellular infiltrate, but we saw a relation with residual debris. A similar observation was reported by other investigators, yet without clear referral to the pathogenesis of dystrophic calcification (Murry et al., 1994).

4.4. DCC and biological bone mineralisation

Although the first histological studies focusing on the development of dystrophic calcifications in mice date back from the sixties (Bajusz et al., 1966 and 1969), only few evidence exists providing insights into the mechanisms leading to, or more precisely initiating, the pathological calcification. So far, only Gadeau et al. (2001) has addressed this specific question and co-workers studying the expression of non-collagenous bone matrix proteins in a rabbit balloon injury model of aortic calcification. Now, the initiation of the calcification processes was focused on myocardial tissue investigating the temporal and spatial expression

of several non-collagenous bone matrix proteins. In detail, the induction of Opn, Osc, Osn, and Tgf β 1, a major inducer of Opn, was determined on mRNA and protein expression level in susceptible C3H/He and resistant C57BL/6 mice after freeze-thaw injury.

Osteopontin is a sialic-acid rich phosphoprotein, which considered a potent regulator of osseous and ectopic calcification (Giachelli and Steitz, 2000) with high binding affinity to hydroxyapatite (Giachelli et al., 1995). An additional RGD-motif serves as a ligand for the integrin cell surface receptor family and contributes to its functions in cell adhesion, signaling, and migration (Oldberg et al., 1986). Immunohistological differences in Opn protein expression between C57BL/6 and C3H/He were observed at day 2 and more dramatically from day 3 on, when Opn was detectable in C3H/He myocardium only. Although we did not determine the amounts of Opn protein in the lesion, immunohistology revealed only a very slow decline in Opn antigen. Moreover, Opn immunostaining co-localized with calcification in the lesion as described previously by other authors (Mohler et al., 1997; Gadeau et al., 2001; Mavroidis and Capetanaki, 2002). Using double immunostaining and a macrophage specific antibody Murry et al. (1994) previously detected subpopulation of macrophages that stained positive with an anti-osteopontin antibody as well. The characteristic of this subpopulation is unclear. Further characterization of this subpopulation should be taken in order to determine whether these macrophages may have in fact differentiated to osteoclasts already. At the mRNA level, it was very encouraging to find that Opn was induced as early as day 1, which potentially implicated Opn in the initiation of the mineralization process. Interestingly, at day 1 Opn mRNA was induced about 13 -fold (compared to sham treated controls) in both strains as determined by real-time RT-PCR. At day 2, however, a marked differential regulation became evident. Whereas induction increased about linearly in C57BL/6 until day 3 (65 -fold induction) and then declined rapidly until day 5 (6 -fold), mRNA expression rose dramatically in C3H/He mice reaching a 1364 -fold peak induction at day 3 and further decreased to 458 -fold at day 5. In both strains initial levels as well as time course of mRNA induction were comparable, yet the response was much more dramatic in strain C3H/He. These data suggested that Opn was mainly up regulated at the transcriptional level. Known inducers of Opn include the transforming growth factor beta1, Tgf β 1, a key regulator of wound

healing and myocardial remodelling, which contributes to the extra cellular matrix synthesis and fibrosis (Border and Ruoslahti, 1992; Wahl, 1994). In an isolated cell system Watson et al. (1994) demonstrated the calcification of osteoblast-like vascular cells by Tgf β 1. The role of Tgf β 1 in DCC is unclear but Tgf β 1 may also mediate cardioprotection after severe injury (Lefer et al., 1990). Our results demonstrated higher mRNA levels in the lesions of C3H/He than in C57BL/6 mice starting at day1 (2.5 -fold vs. 1.7 -fold) and peaking at day 3 (7.5 -fold vs. 0.7 -fold). Consistently, immunohistology documented increased Tgf β 1 staining at day 1 already, which peaked at day 3 in both C57BL/6 and C3H/He mice. Although suggestive, these results could not determine whether the differential expression of Tgf β 1 was indeed responsible for the differences seen in Opn expression. Further extensive in vitro experiments are required to answer this question satisfactorily. Although Opn appeared to be differentially regulated mainly at the transcriptional level, it cannot be excluded that Opn mRNA and hence protein was increased so strikingly in C3H/He because it had also accumulated due to posttranscriptional mechanisms. These would include increased stability of Opn mRNA i.e. resistance to intracellular RNA degradation or greater resistance to protein degradation. Opn may undergo extensive posttranslational modification, such a sulfation, glycosylation, transglutamination, yet phosphorylation appears to be required for its function as a natural inhibitor of mineralization (Jono et al., 2000). First evidence that posttranslational modification might be involved in the DCC was reported from Mavroidis and co-worker (2002), who analysed desmin knock-out mice exhibiting altered mitochondria, extensive myocardial necrosis and calcification. By Western Blot analysis they demonstrated a rather abundant high molecular weight isoform in calcified myocardial tissue, which was absent in control bone extracts. It remained unclear whether this Opn isoform had in fact less inhibitory potency with respect to calcification or higher resistance against protein degradation let alone different biological effects on macrophage and osteoclast differentiation despite normal mouse development and osteogenesis (Rittling et al., 1998). Clearly, the biological function of Opn isolated from calcified myocardial lesions requires further investigation. It is, however, quite conceivable that the progression of calcification simply exceeded the inhibitory capacity of the secreted Opn despite maximal stimulation of the macrophages.

Apart from Opn, Osn and Osc possess calcium and hydroxyapatite binding capacity and were found in calcified vascular lesions. Although these non-collagenous bone matrix proteins may play a regulatory role in the bone mineralization processes (Chen et al, 1993; Denhardt and Guo, 1993), gene targeted inactivation in mice failed to prove an interference of these proteins with bone mineralization. The results presented here showed a slight increase in Osc expression at mRNA and protein levels which began at day 3 well after the initiation of calcification in susceptible C3H/He, but not in C57BL/6 mice. After day 5 Osc was markedly expressed at protein level and was co-localized to mineral deposits. These findings are in concordance with previous reports suggesting that Osc is produced in response to calcium deposition to limit the development of calcification. Using a polyclonal antibody against rat Osn we failed to detect osteonectin protein in calcified lesions although we saw a maximal 4-fold increase in mRNA expression. This may be explained e.g. by a lack of sensitivity of the immunohistological methodology used. Fell (2001) for example claimed that a two-fold change in protein expressions required at least a 10-fold change at the mRNA levels), a lack of cross reactivity of this antibody with respect to murine protein (this has not been tested by manufacturer, but mouse and rat share 97% identical amino acid sequence). Nevertheless, this data also confirmed previous investigations in a rabbit aorta balloon injury model where osteonectin protein was not detected either (Gadeau et al., 2001). In summary, for the first time this study showed that the temporal and spatial expression of osteopontin, osteocalcin and osteonectin in dystrophic cardiac calcification was comparable to the results obtained in an injury model of vascular calcification. This, in turn, provides support for the hypothesis that DCC and vascular calcification share the same molecular and genetic basis (Colinayo et al., 2002).

4.5. The genetic background

In light of the complexity of the DCC phenotype the distinction of primary causes of DCC from secondary consequences of calcium deposition posed a considerable problem. In support of histological data presented here, a genetic analysis of this trait helped to establish that the induction of bone matrix proteins was rather a secondary phenomenon than actually the reason for the

development of calcifications. Employing quantitative trait locus (QTL) analysis of an F2 intercross between DCC resistant C57BL/6- and susceptible C3H/He-mice the polygenic basis of this recessive trait was previously reported. These QTLs served as markers for closely linked genes that contributed to DCC as primary causal genetic factors. A major predisposing locus, designated *Dyscalc1*, was identified with a highly significant LOD score of 14.8 on proximal chromosome 7 and mapped it more exactly to an interval between the genetic markers D7Mit228 and D7Mit230 (Ivancic et al., 2001). This interval comprised approximately 10 million base pairs. Additional QTL for genetic modifiers were identified on chromosome 4 (*Dyscalc2*), 12 (*Dyscalc3*), and 14 (*Dyscalc4*). The gene loci of *Opn*, *Osc* and *Osn*, however, mapped on chromosomes 5, 3, and 11. Therefore, genomic sequence variants in these proteins (including promoter and coding sequence) are not likely to contribute to the development of DCC. However, it is very possible that *Dyscalc* loci may interact with *Opn*, *Osc* or *Osn* in an activating fashion like *Tgfb1*. The locus of *Tgfb1* maps on proximal chromosome 7 and therefore, the *Tgfb1* gene must be considered as potential candidate gene for the so far unknown *Dyscalc1* gene, if it actually mapped in the *Dyscalc1* interval. This chromosomal interval exhibits a particularly high density of genes, many of which must be also included as candidate genes because they are involved in pathways that might be relevant to DCC, such as apoptosis, intracellular calcium homeostasis, mitochondrial function, inflammation and bone formation/resorption or mineralization. Two simple mapping techniques can be applied to determine whether a locus of a gene in question actually maps in the *Dyscalc1* interval. Firstly, indirect evidence may be obtained by comparing the distribution of RFLP alleles of the gene under study with the distribution of genotypes at a marker for *Dyscalc1* (e.g. D7Mit229) in recombinant (C57BL/6 x C3H/He) BXH inbred strains. Complete co-segregation of RFLP and marker alleles and DCC phenotype in this set of strains would suggest close linkage or even potential identity of the respective gene with *Dyscalc1*. Secondly, high-resolution mapping of genetic loci can be performed by radiation hybrid (RH) mapping testing the distribution of sequence tagged sites (STS) of the genes under study in a panel of somatic cell hybrid lines against the distribution of STS already mapped in a public domain RH map (Rowe et al., 2000; Van Etten et al., 1999). This technique allows pinpointing the locus of a

gene down to less than one million base pairs. We applied both strategies to evaluate putative candidate genes. Informative intragenic RFLPs were obtained only for the muscle $\text{Na}^+/\text{Ca}^{2+}$ exchanger *Ncx2* or *Slc8a2* and the FBJ osteosarcoma oncogene B, *Fosb*. Within the set of existing BXH RI strains RFLP alleles were identical in both genes and did not co-segregate with DCC susceptibility in BXH RI-2 and -10. Separated from *Fosb* by 64 kb sequence only (GenBank accession number AC073787) *Ckmm* could be excluded as candidate gene as well. *Ckmm* maintains muscle energy reserve and was associated with apoptosis (Zamzami and Kroemer, 2001). The genes encoding the muscle ryanodine receptor (*Ryr1*), the transforming growth factor beta1 subunit (*Tgfb1*), the beta-subunit of the Nf-kappaB inhibitor I κ B (*Nfkbib*), the mitochondrial electron transferring flavoprotein b (*Etfb*), the Bcl2-associated X protein (*Bax*) and the histidine-rich calcium binding protein (*Hrc*) did not exhibit intragenic RFLPs between C57BL/6 and C3H/He inbred strains using a set of 26 restriction endonucleases. Therefore, STS of these genes were typed in a set of hybrid mouse/hamster cell lines and placed in a high-resolution RH map. This study excluded *Ryr1*, *Tgfb1* and *Nfkbib* as candidate genes because they were clearly located proximal to the *Dyscalc1* interval. However, within this interval *Hrc*, *Bax* and *Etfb* were identified as potential candidate genes attractive for further molecular studies. Next, mRNA induction of these genes was analysed by real time RT-PCR after freeze-thaw injury to obtain additional evidence of myocardial gene expression and potential involvement in calcification.

Hrc is a luminal sarcoplasmic calcium binding protein with unknown function (Diamiani et al., 1995; Lee et al., 2001; Ridgeway et al., 1999), which has been repeatedly implicated as candidate gene for *Dyscalc1* (Brunnert et al., 1999; Van den Broek et al., 1998) as well as a candidate gene for a human cardiac conduction disease (de Meeus, 1995). In contrast to previous reports mapping *Hrc* at 20.4 cM, RH mapping now located *Hrc* further distal, at 23 cM (Hofmann et al., 1991). Interestingly, an unstable GAG repeat in the coding region of *Hrc* was reported to exhibit larger expansions in DCC-susceptible DBA/2 mice compared to resistant C57BL/6 mice after freeze-thaw injury (Shi and Brunnert, 1999). The data presented here revealed less abundance of *Hrc* mRNA in the calcified lesions compared to the transcripts we determined in non-injured, healthy myocard. We could not exclude that the lower mRNA levels in the

necrosis were actually a consequence of the lack of viable myocytes rather than true down regulation of *Hrc*.

In this investigation Bax one of the potential genes involved in the pro-death stage (Wrogemann and Pena, 1976) was included. It was mapped by RH panel at 23 cM between D7Mit26 proximal and D7Mit81 distal within the region containing *Dyscalc1*. As proapoptotic member of Bcl-2 family, Bax is part of the Permeability Transition Pore Complex, PTPC, but may also form independently pores in mitochondrial membranes, which lead to the release of intramitochondrial molecules of up to 1.5 kDa size (Jurgensmeier et al., 1998). Triggered by intracellular calcium raises only transient opening of the PTPC may occur as long as production of energy is maintained in the mitochondrion. However, a sustained increase in intracellular calcium or energy depletion eventually leads to the release of mitochondrial cytochrome c, which, in turn, activates cytosolic death proteins including caspases (Halestrap et al., 2000; Zamzami and Kroemer, 2001). This event marks the point of no return in the response to reversible injury and the beginning of cell death. Interestingly, Bax mRNA levels were increased as early as day 2 reaching a plateau of 8 –fold compared to day 0, however, in C57BL/6 mice Bax mRNA expression reached a maximum of 4,5 –fold late at day 3.

Proximal chromosome 7 contains several members of mitochondrial substrate oxidation pathways that must also be included as potential candidate genes acknowledging that cell death occurs upon energy depletion (Williams et al., 2001). The electron-transferring flavoprotein, *Etfb* is an electron carrier of electrons between acyl-CoA dehydrogenase and the respiratory chain in the inner mitochondrial membrane. *Etfb* is a close neighbor of *Hrc* (Stubbs et al., 1996) and therefore linked to *Dyscalc1* as well. *Etfb* exhibited, similar to *Hrc*, marked decrease of mRNA levels in C3H/He in comparison to C57BL/6 mice at day 3 after myocardial injury. In humans *Etfb* deficiency produces a neurodegenerative phenotype associated with type II glutaric acidemia, but not with mitochondrial mineralization (White et al., 1996). Cytochrome oxidase is the terminal component of the chain of respiratory carriers and is responsible for the reaction whereby electrons resulting from substrate oxidation by dehydrogenase are transferred to their final acceptor, oxygen. Furthermore, several loci of

subunits of cytochrome oxidase have been mapped on chromosome 7, but none were identified within the *Dyscalc1* interval, so far.

In opposition to the data here and linkage studies in a larger DBA/2 (Brunnert et al., 1999), Gerhard and Kauffman suggested the myocyte enhancer factor 2a (Mef2a at 33 cM) as candidate gene for *Dyscalc1* based on the existence of a Mef2a-binding site in the desmin promoter and the observation of a DCC-phenotype in desmin knockout mice (Gerhard and Kauffman, 1997; Milner et al., 1996, Mavroidis and Capetanaki, 2002). Mef2a-mutant mice died early from sudden death and exhibited right ventricular dilation, a deficiency of cardiac mitochondria, but not cardiac calcinosis (Naya et al., 2002).

Taken together existing evidence and experimental data presented here, a modified hypothetical model of the pathogenesis of DCC was proposed including combined histological and molecular genetic mechanisms (Fig. 25). DCC is a recessively inherited disease characterized by rapid and marked calcium deposition in necrotic myocardial tissue irrespective of the nature of myocardial damage. The multi-step sequence of events initially requires irreversible cell injury. In response to injury mitochondrial calcium and phosphate sequestration ultimately exceeds the calcium x phosphate solubility product leading to amorphous calcium phosphate precipitation in these dying mitochondria. Then, strain-dependant differences in the progression of the calcium deposits become apparent. In strains with predilection to DCC, calcification spreads further involving surrounding debris. Debris and calcification, however, are both absent in resistant strains. This may be explained by rapid phagocytotic clearance of remnants of cell membranes that would otherwise serve as a nidus for hydroxyapatite crystal formation similar to matrix vesicles mediating bone mineralization. The reasons for persistence of debris in predisposed strains are not clear at present. On the one hand, macrophage differentiation and/or function may be impaired at the level of phagocytosis or lysosomal degradation; on the other hand, specific physico-chemical conditions may have promoted necrotic tissue coagulation known to be particularly prone to calcification. From this point on, secondary mechanisms of compensation prevail including maximal induction and secretion by macrophages of osteopontin, an inhibitor of bone mineralization, which appears to be incapable of coping with excessive hydroxyapatite crystal

precipitation. Similarly, involvement of another inhibitor, *Osc*, but not *Osn* was demonstrated. Our findings compared well to the results obtained in a rabbit model of aortic wall injury (Gadeau et al., 2001), yet investigations of atherosclerotic vascular calcification, which is caused by slow degenerative processes rather than rapid injury and death, have illustrated the abundance of these and additional non-collagenous bone matrix proteins. Our experimental data, however, showed a different pattern of induction of bone matrix proteins as well as absence of osteoblasts (electron microscopy, data not shown) in calcifying necrotic lesions. This emphasized that only certain limited aspects of DCC – in contrast to vascular calcification – may be compared to bone formation and mineralization.

The complex pathogenesis of DCC is also reflected by the results of the genetic studies identifying 4 QTLs for more advanced necrotic tissue calcification. The most influential of these *Dyscalc* loci resided in a region on proximal chromosome 7 with well conserved homology to human chromosome 19 and a small part of chromosome 11. In this region many genes may be considered candidate genes for this *Dyscalc* locus, because they are involved in calcium handling, apoptosis or mitochondrial function. Based on close linkage with this *Dyscalc* locus the histidine-rich calcium binding protein *Hrc*, the bcl-2 associated X protein *Bax* and the electron transferring flavoprotein beta as candidates of each of the aforementioned categories was further investigated. However, *Hrc* and *Etfb* exhibited no differential gene induction at the mRNA level in response to injury which disqualified them as putative candidate genes of relevance. *Bax* exhibited differential induction in the lesion and would therefore deserve further investigation as would be additional genes involved in phagocytosis and lysosomal degradation.

In this combined approach histological and molecular genetic studies will allow the distinction of primary causes of DCC from secondary consequences of calcium deposition and will eventually lead to the identification of more components of this disease and their underlying genes. A hypothetical pathogenetic model for DCC is shown in Fig. 25.

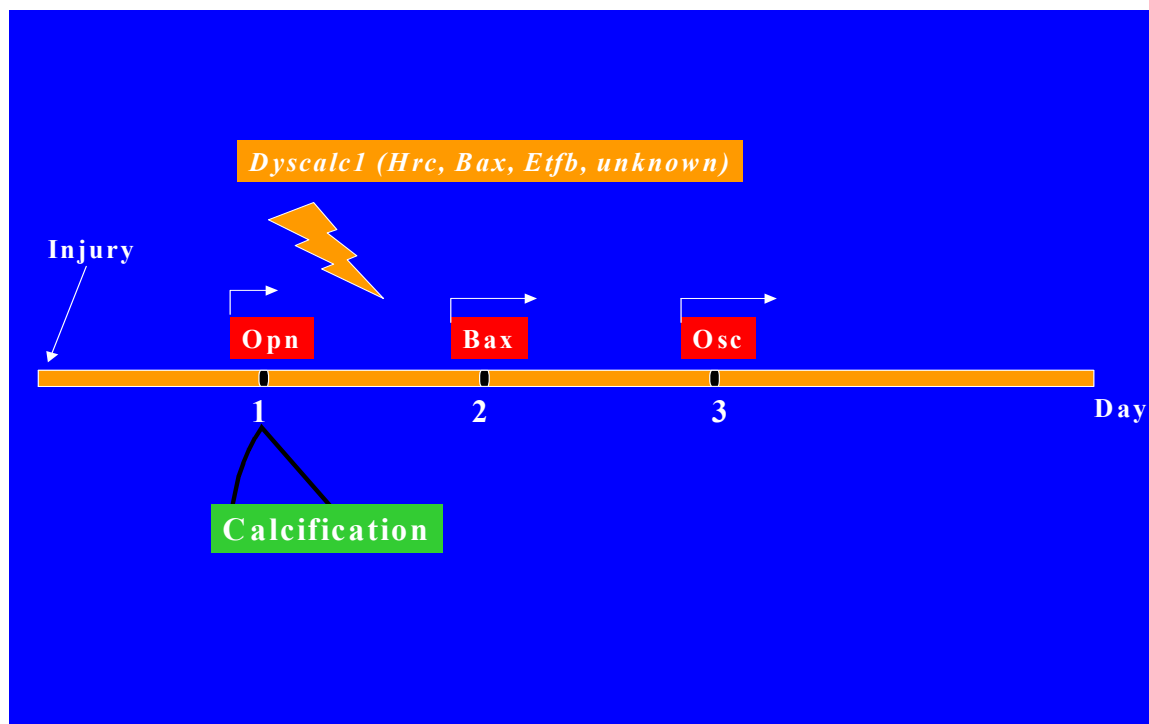


Fig. 25: Hypothetical pathogenetic model for DCC. In a primary phase after injury, calcification originate, independently from the genetic background, in mitochondria of the necrotic myocardial tissue of mice early at day 1. A second phase follow in which, depending on the predisposition of *dyscalc1* involving one of the potential candidate genes selected in this investigation or a not yet identified gene, initiation and development of DCC become irreversible and subsequent upregulation of genes coding for bone related proteins including *Opn* and *Osc* as a consequence to limit calcification progression become evident.

Summary

Myocardial calcification is observed in several inbred strains of mice including C3H/He, BALB/c and DBA/2 as response of myocardial tissue to injury. This abnormal response has been named dystrophic cardiac calcification (DCC). To elucidate the molecular mechanisms by which the observed phenotype take place, the mineralisation progression was investigated in a time course processes starting from its early stages in DCC-susceptible C3H/He and resistant C57BL/6 mice after freeze-thaw injury. Using calcein fluorescence staining the deposition of calcium phosphate was demonstrated early as day 1 between healthy and necrotic tissue in both strains as response to injury. Transmission electron microscopy demonstrated calcium depositions originating in mitochondria. This mineralization process develop and progress in C3H/He mice whereas it disappear completely in C57BL/6 after day 2 post injury.

Previous studies demonstrated similar features of dystrophic calcification with bone mineralisation. Here, the induction of bone related proteins including osteopontin, osteocalcin and osteonectin was examined at protein and RNA levels 0, 1, 2, 3, and 5 days after freeze-thaw injury in DCC -susceptible C3H/He in comparison to resistant C57BL/6 mice. In both strains Opn, a key regulator protein found in bone remodelling and inflammation, was detected in the lesions after the 1st day and peaked at day 3. Co-localised with calcium deposition, Opn remained dramatically upregulated in C3H/He mice while it disappeared in C57BL/6 at day 5. Opn gene induction confirmed this finding at the transcription level. Slight changes were observed in Opn plasma concentrations after freeze-thaw injury in both strains suggesting like this a general response of Opn to injury. In addition a high Opn plasma concentrations was revealed in C57BL/6 with a mean value of 3289 ± 40 (\pm SE) compared to C3H/He mice with only 839 ± 39 . The mechanism involving the accumulation of bone related proteins during the progression and development of DCC is still obscure but might involve Osc and not Osn. Tgf β 1, a determinant element in tissue remodelling, was highly expressed at mRNA level in the necrotic lesions of C3H/He compared to C57BL/6. The expression at protein level of Tgf β 1, however, appeared similar in both strains.

While results reported here and previous studies suggest that DCC occur in C3H/He mice early as day 1 after freeze-thaw injury, that calcification progression enhance the accumulation of bone related proteins among which osteopontin might play a potential inhibitory role, the ultrastructural evidence of calcium deposits originating in mitochondria is far to be understood. In mitochondria many processes and signalling pathways involving calcium phosphate homeostasis and apoptosis might lead to DCC. Previous genetic analysis revealed a major predisposing locus, *Dyscalc1*, on proximal chromosome 7. The molecular mechanisms leading to DCC are unknown and genes involved in myocyte function, calcium homeostasis or apoptosis must be considered as candidate genes. In this study more accurate gene mapping was included by radiation hybrid mapping and RFLP analysis in recombinant inbred BXH strains. Among the candidate genes, *Tgfb1*, *Dm15*, *Nfkb1b*, *Ncx2*, *Ryr1* and *Fosb* found distal to D7Mit228 were excluded for their C57BL/6 genotype in DCC-susceptible BXH-10 RI strains. However, the histidine-rich calcium binding protein (*Hrc*), the bcl₂-associated x-protein (*Bax*) and electron-transfer protein-beta (*Etfb*) loci that were mapped close to D7Mit229 at 23 cM between D7Mit228 and D7Mit230 were included. For supportive evidence of linkage with DCC, the induction of these potential candidate genes were studied in a time course by RT-PCR after freeze-thaw injury. *Hrc* and *Etfb* exhibited no differential gene induction at the mRNA level in response to injury which disqualified them as putative candidate genes of relevance. However, *Bax* exhibited differential induction in the lesion and should therefore deserve further investigation.

Taken together, for the first time, this study allow distinction of primary genetic causes initiating DCC from progressive secondary consequences. Thus, DCC originate in mitochondria as early as day 1 in both DCC-resistant and susceptible strains after freeze-thaw injury. Thereafter, initiation and progression of calcium phosphate mineral become apparent in strains with *Dyscalc* predisposition. The mechanism leading to crystal initiation is still unknown but include in a primary mechanism *dyscalc1* located at proximal chromosome 7 in a 5 cM interval between D7Mit228 and D7Mit230 marker. *Bax* was proposed as potential candidate. After initiation of crystal nidus, the progression and development of DCC take a process of no return. This process is associated with

the accumulation of bone proteins (secondary mechanism) among which osteopontin might play a critical role as inhibitor.

Reference List

- Anderson HC (1989) Biology of Disease Mechanism of Mineral Formation in Bone. *Lab Invest.* 60:320-330
- Bajusz E, Homburger F, Baker JR, Opie LH (1966) The heart muscle in muscular dystrophy with special reference to involvement of the cardiocascular system in the hereditary myopathy of the hamster. *Ann NY Acad Sci.* 138:213-229
- Bajusz E, Baker JR, Nixon CW, Homburger F (1969) Spontaneous hereditary myocardial degeneration and congestive heart failure in a strain of Syrian hamster. *Ann NY Acad Sci.* 156:105-129
- Bjelle AO, Sundstroem BKG (1975) An ultrastructural study of the articular cartilage in calcium pyrophosphate dihydrate (CPPD) crystal deposition disease (chondrocalcinosis articularis). *Calcif Tissue Res.* 19:261-264
- Black AS, Kanat IO (1985) A review of soft tissue calcification. *J Foot Surg.* 24:243-250
- Bloom S, Peric-Golia L (1989) Geographic variation in the incidence of myocardial calcification associated with acute myocardial infarction. *Human Pathol.* 20:726-731
- Border WA, Ruoslahti E (1992) Transforming Growth Factor- β in disease: The Dark Side of Tissue Repair. *J Clin Invest.* 90:1-7
- Boskey AL (1996) Matrix proteins and mineralization: an overview *Connect Tissue Res.* 35:357-363
- Bosman C, Bonucci E, Gugliantini P, Sagui L (1977) Ultrastructural aspects of chondrodystrophia calcificans congenital (syndrome of Conradi-hunermann). *Virchows Arch A pathol Anat Histol.* 373:23-35

- Bostrom K, Memer LL (2000) Regulatory mechanisms in vascular calcification. *Crit Rev Eukaryt Gene Expr.* 10:151-158
- Boström KI (2000) Cell differentiation in vascular calcification. *Z Kardiol.* 89 Suppl 2:69-74
- Bradshaw AD, Reed MJ, Sage EH (2002) SPARC-null Mice exhibit accelerated cutaneous wound closure. *J Histochem Cytochem* 50:1-10
- Breen EC, Ignatz RA, McCabe L, Stein JL, Stein GS, Lian JB (1994) TGF beta alters growth and differentiation related gene expression in proliferation osteoblasts in vitro, preventing development of the mature phenotype. *J Cell physiol.* 160:323-335
- Brunnert SR, Altman NH (1990) Dystrophic cardiac calcinosis in mice: abnormal myocardial response to freeze-thaw injury. *Lab Anim Sci.* 40:616-619
- Brunnert SR (1997) Morphologic response of myocardium to freeze-thaw injury in mouse strains with dystrophic cardiac calcification. *Lab Anim Sci.* 47:11-18
- Brunnert SR, Shi S, Chang B (1999) Chromosomal localisation of the loci responsible for dystrophic cardiac calcinosis in DBA/2 mice. *Genomics.* 59:105-107
- Bucay N, Sarosi I, Dunstan CR, Monrony S, Tarpley J, Capparelli C, Scully S, Tan H, Xu W, Lacey DL, Boyle WJ, Simonet WS (1998) Osteoprotegrin-deficient mice develop early onset osteoporosis and arterial calcification. *Genes Dev.* 12:1260-1268
- Burbach JA (1987) Ultrastructure of Cardiocyte Degeneration and Myocardial Calcification in the Dystrophic Hamster. *Am J Anat.* 179:291-307
- Catellier MJ, Chua GT, Youmans G, Waller BF (1990) Calcific deposits in heart. *Clin Cardiol.* 13:287-294

- Chakraborti T, Das S, Mondal M, Roychoudhury S, Chakraborti S (1999) Oxidant, Mitochondria and Calcium: an overview. *Cell Signal*. 11:77-85
- Chen J, Singh K, Mukherjee BB, Sodek J (1993) Developmental expression of osteopontin (OPN) mRNA in rat tissues: evidence for a role for OPN in bone formation and resorption. *Matrix*. 13:113-123
- Christoffersen J, Landis WJ (1991) A contribution with review to the description of mineralization of bone and other calcified tissues in vivo. *The Anat Rec*. 230:435-450
- Colinayo VV, Qiao JH, Demant P, Krass K, Lusic AJ, Drake TA (2002) Genetic characterization of the Dyscalc locus. *Mamm Genome*. 13:283-288
- Cotran RS, Kumar V, Robbins SL (1994) Cellular injury and cellular death: pathologic basis of disease. Philadelphia: WB Saunders. 1-34
- D'Agostino AN, Chiga M (1970) Mitochondrial mineralisation in human myocardium. *Am J clin Pathol*. 53:820-824
- Damjanovski S, Liu F, Ringuette M (1992) Molecular analysis of *Xenopus laevis* SPARC (Secreted Protein, Acidic, Rich in Cysteine). A highly conserved acidic calcium-binding extracellular-matrix protein. *Biochem J*. 281:513-517
- de Meeus A, Stephan E, Debrus S, Jean MK, Loiselet J, Weissenbach J, Demaille J, Bouvagnet P (1995) An isolated cardiac conduction disease Maps to chromosome 19q. *Circ Res*. 77:735-740
- Demer LL (1995) A Skeleton in the Atherosclerosis Closet. *Circulation*. 92:2029-2032
- Diamiani E, Picello L, Saggin L, Margreth A (1995) Identification of triadin and of histidin-rich Ca(2+)-binding protein as substrates of 60 KDa calmodulin-dependent protein kinase in junctional terminal cisternae of sarcoplasmic reticulum of rabbit fast muscle. *Biochem Biophys Res Commun*. 209:457-465

- Ducy P, Karsenty G (1995) Two distinct osteoblast-specific cis-acting elements control expression of a mouse osteocalcin gene. *Mol Cell Biol.* 15:1869
- Ducy P, Desbois C, Boyce B, Pinero G, Story B, Dunstan C, Smith E, Bonadio J, Goldstein S, Gundberg C, Bradley A, Karsenty G (1996) Increased bone formation in osteocalcin-deficient mice. *Nature.* 382:448-452
- Eaton GJ, Custer RP, Johnson FN, Stadenow KT (1978) Dystrophic cardiac calcinosis in mice: genetic, hormonal, and dietary influences. *Am J Pathol.* 90:173-186
- Everitt JI, Ross PW, Neptum DA, Mangum JB (1988) Effect of a purified diet on dystrophic cardiac calcinosis in mice. *Lab Anim Sci.* 38:426-429
- Everitt JI, Olson LM, Mangum JB, Visek WJ (1988) High mortality with severe dystrophic cardiac calcinosis in C3H/OUJ mice fed high fat purified diets. *Vet Pathol.* 25:113-118
- Fatkin D, Christe ME, Aristizabal O, McConnell BK, Srinivasan S, Schoen FJ, Seidman CE, Turnbull DH, Seidman JG (1999) Neonatal cardiomyopathy in mice homozygous for the Arg503Gln mutation in the alpha cardiac myosin heavy chain gene. *J Clin Invest.* 103:147-153
- Fell DA (2001) Beyond genomics. *Trends genet.* 17:680-682
- Flores ME, Norgard M, Heinegard D, Reinholt FP, Andersson G (1992) RGD-directed attachment of isolated rat osteoclasts to osteopontin, bone sialoprotein, and fibronectin. *Exp Cell Res.* 201:526-530
- Fujisawa R, Wada Y, Nodasaka Y, Kuboki Y (1996) Acidic amino acid-rich sequences as binding sites of osteonectin to hydroxyapatite crystal. *Biochem Biophys Acta.* 1292:53-60
- Gadeau AP, Chaulet H, Daret D, Kockx M, Lamaziere JMD, Desgranges C (2001) Time course of osteopontin, osteocalcin, and osteonectin

accumulation and calcification after acute vessel wall injury. *J Histochem Cytochem.* 49:79-86

Gang DL, Barrett LV, Wilson EJ, Rubin RH, Medearis DN (1986) Myopericarditis and enhanced dystrophic cardiac calcification in murine cytomegalovirus infection. *Am J Pathol.* 124:207-215

Gerhard GS, Kauffman EJ (1997) Refinement of the Dyscalc locus mapping interval and nomination of a candidate gene. 47th annual meeting of the American Society of Human Genetics. 1997. <http://www.faseb.org/ashg97/f6500.html>

Giachelli CM, Schwarz SM, Liaw L (1995) Molecular and cellular biology of osteopontin. *Trends Cardiovasc Med.* 3:88-95

Giachelli CM, Lombardi D, Johnson RJ, Murry CE, Almeida M (1998) Evidence for a role of osteopontin in macrophage infiltration in response to pathological stimuli in vivo. *Am J Pathol.* 152:353-358

Giachelli CM, Steitz S (2000) Osteopontin: a versatile regulator of inflammation and biomineralization. *Matrix Biol.* 19:615-622

Gilmour DT, Lyon GJ, Carlton MB, Sanes JR, Cunningham MJ, Anderson JR, Hogan BL, Evans MJ, Colledge WH (1998) Mice deficient for the secreted glycoprotein SPARC/osteonectin/BM40 develop normally but show severe age-onset cataract formation and disruption of the lens. *EMBO J.* 17:1860-1870

Green DR, Reed JC (1998) Mitochondria and Apoptosis. *Science.* 281:1309-1312

Green DR, Amarante-Mendes GR (1998) The point of no return: mitochondria, caspases, and the commitment to cell death. *Results Probl Cell Differ.* 24:45-61

- Halestrap AP, Doran E, Gillespie JP, O'Toole A (2000) Mitochondria and cell death. *Biochem Soc Trans.* 28:170-177
- Highman B, Daft FS (1965) Calcified lesions in C3H mice given purified low protein diets. *Arch Pathol.* 52:221-229
- Hofmann SL, Topham M, Hsieh CL, Francke U (1991) cDNA and genomic cloning of HRC, a human sarcoplasmic reticulum protein, and localization of the gene to human chromosome 19 and mouse chromosome 7. *Genomics.* 9:656-669
- Hunter GK, Hauschka PV, Poole AR, Rosenberg LC, Goldberg HA (1996) Nucleation and inhibition of hydroxyapatite formation by mineralized tissue proteins. *Biochem J.* 317:59-64
- Ivandic BT, Qiao JH, Machleder D, Liao F, Drake TA, Lusic AJ (1996) A locus on chromosome 7 determines myocardial cell necrosis and calcification (dystrophic cardiac calcinosis) in mice. *Proc Natl Acad Sci USA.* 93:5483-5488
- Ivandic BT, Utz HF, Kaczmarek PM, Aherrahrou Z, Axtner SB, Klepsch C, Lusic AJ, Katus HA (2001) New Dyscalc loci for myocardial cell necrosis and calcification (dystrophic cardiac calcinosis) in mice. *Physiol Genomics.* 6:137-144
- Jono S, Peinado C, Giachelli CM (2000) Phosphorylation of osteopontin is required for inhibition of vascular smooth cell calcification. *J Biol Chem.* 275:20197-203
- Jurgensmeier JM, Xie Z, Deveraux Q, Ellerby L, Bredesen D, Reed JC (1998) Bax directly induces release of cytochrome c from isolated mitochondria. *Proc Natl Acad Sci USA.* 95:4997-5002
- Kim KK (1976) Calcification of matrix vesicles in human aortic valve and aortic media. *Fed Proc.* 35:156-162

- Kim KM (1995) Apoptosis and calcification. *Scanning Microsc.* 9:1137-1175
- Klein BS, Liptay S, Schmid RM, Hameister H (1999) Assignment of Nfkbib to murine chromosome bands 7A3-B3 by in situ Hybridization. *Cytogenet Cell Genet.* 85 (3-4): 308-309
- Lee HG, Kand H, Kim DH, Park WJ (2001) Interaction of hrc (histidine-rich Ca²⁺-binding protein) and triadin in the lumen of sarcoplasmic reticulum. *J Biol Chem.* 276:39538
- Lefer AM, Tsao P, Aoki N, Palladino MA Jr (1990) Mediation of cardioprotection by transforming growth factor-beta. *Science.* 249:61-64
- Liaw L, Birk DE, Ballas CB, Whitsitt JS, Davidson JM, Hogan BL (1998) Altered wound healing in mice lacking a functional osteopontin gene (spp1). *J Clin Invest.* 101:1468-1478
- Lockard VG, Bloom S (1991) Morphologic features and nuclide composition of infarction-associated cardiac myocyte mineralisation in humans. *Am J Pathol.* 139:565-572
- Luo G, Ducey P, McKee MD, Pinero GJ, Evelyne L, Behringer RR, Karsenty G (1997) Spontaneous calcification of arteries and cartilage in mice lacking matrix GLA protein. *Nature.* 386:78-81
- Matsumori A, Okada I, Yamada T, Maruyama S, Kawai C (1991) Pathogenesis of myocardial injury in myocarditis and cardiomyopathy. *Jpn Circ J.* 55:1132-1137
- Mavroidis M, Capetanaki Y (2002) Extensive induction of important mediators of fibrosis and dystrophic calcification in Desmin-deficient cardiomyopathy. *Am J Pathol.* 160:943-952
- McConnell BK, Jones KA, Fatkin D, Arroyo LH, Lee RT, Aristizabal O, Turnbull DH, Georgakopoulos D, Kass D, Bond M, Niimura H, Schoen FJ, Conner D,

- Fischman DH, Seidman CE, Seidman JG (1999) Dilated cardiomyopathy in homozygous myosin-binding protein-C mutant mice. *J Clin Invest.* 104:1235-1244
- Milner DJ, Weitzer G, Tran D, Bradeley A, Capetanaki Y (1996) Disruption of muscle architecture and myocardial degeneration in mice lacking desmin. *J Cell Biol.* 134:1255-1270
- Miyauchi A, Alvarez J, Greenfield EM, Teti A, Grano M, Colucci S, Zambonin-Zallone A, Ross FP, Teitelbaum SM, Cheresch D, Hruska KA (1991) Recognition of osteopontin and related peptides by an alpha v beta 3 integrin stimulates immediate cell signals in osteoclasts. *J Biol Chem.* 266:20369-20374
- Mohler ER 3rd, Adam LP, McClelland P, Graham L, Hathaway DR (1997) Detection of osteopontin in calcified human aortic valves. *Arterioscler Thromb Vasc Biol.* 17:547-552
- Mohler ER 3rd, Gannon F, Reynolds C, Zimmerman R, Keane MG, Kaplan FS (2001) Bone formation and inflammation in cardiac valves. *Circulation.* 103:1522-1528
- Murry CE, Giachelli CM, Schwarz SM, Vracko R (1994) Macrophages express osteopontin during repair of myocardial necrosis. *Am J Pathol.* 145:1450-1462
- Naya FJ, Black BL, Wu H, Bassel-Duby R, Richardson JA, Hill JA, Olson EN (2002) Mitochondrial deficiency and cardiac sudden death in mice lacking the MEF2A transcription factor. *Nat Med.* 8:1303-1309
- Norose K, Clark JI, Syed NA, Basu A, Hebert-Katz E, Sage EH, Howe CC (1998) SPARC deficiency leads to early-onset cataractogenesis. *Invest Ophthalmol Visc Sci.* 39:2674-2680

- O'Brien ER, Garvin MR, Stewart DK, Hinohara T, Simpson JB, Schwartz SM, Giachelli CM (1994) Osteopontin is synthesized by macrophage, smooth muscle, and endothelial cells in primary and restenotic human coronary atherosclerotic plaques. *Arterioscler Thromb.* 14:1648-1656
- Oldberg A, Franzen A, Heinegrad D (1986) Cloning and sequence analysis of rat bone sialoprotein (osteopontin) cDNA reveals an Arg-Gly-Asp cell-binding sequence. *Proc Natl Acad Sci USA.* 83:8819-8823
- Raha S, Robinson BH (2001) Mitochondria, oxygen free radicals, and apoptosis. *Am J Med Genet.* 106:62-70
- Reddy S, Smith DB, Rich MM, Leferovich JM, Reilly P, Davis BM, Tran K, Rayburn H, Bronson R, Cros D, Balice-Gordon RJ, Housman D (1996) Mice lacking the myotonic dystrophy protein kinase develop a late onset progressive myopathy. *Nat Genet.* 13:325-335
- Ridgeway AG, Petropoulos H, Siu A, Ball JK, Skerjanc IS (1999) Cloning, tissue distribution, subcellular localization and overexpression of murine-rich Ca²⁺ binding protein. *FEBS Lett.* 456:399-402
- Rittling SR, Matsumoto HN, McKee MD, Nanci A, An XR, Novick KE, Kowalski AJ, Noda M, Denhardt DT (1998) Mice lacking osteopontin show normal development and bone structure but display altered osteoclast formation in vitro. *J Bone Miner Res.* 13:1101-1111
- Ross FP, Chappel J, Alvarez JI, Sander D, Butler WT, Farach-Carson MC, Mintz KA, Robey PG, Teitelbaum SL, Cheresch DA (1993) Interactions between the bone matrix proteins osteopontin and bone sialoprotein and the osteoclast integrin alpha v beta 3 potentiate bone resorption. *J Biol Chem.* 268:9901-9907

- Rowe LB, Barter ME, Eppig JT (2000) Cross-referencing radiation hybrid data to the recombination map: lessons from mouse chromosome 18. *Genomics*. 69:27-36
- Sambrook J, Fritsch EF, Maniatis T (1989) *Molecular cloning. A laboratory manual*. Cold Spring Harbour Laboratory Press, Cold Spring Harbor, NY 2nd ed
- Seifert G (1997) Heteropic (extraosseous) calcification (calcinosis) etiology, Pathogenesis and clinical importance. *Pathologie*. 18:430-438
- Shi S, Brunnert SR (1999) Molecular cloning and sequencing of the Hrc gene from mouse heart reveals a highly unstable GAG repeat. 13th International Mouse Genome Conference of the International Mammalian Genome Society. <http://im.gs.org/abstracts/99abstracts/shi.html>
- Stallion A, Rafferty JF, Warner BW, Ziegler MM, Ryckman FC (1994) Myocardial calcification: a predictor of poor outcome for myocarditis treated with extraporeal life support. *J Pediatr Surg*. 29:492-494
- Stubbs L, Carver EA, Shannon ME, Kim J, Geistler J, Generoso EE, Stanford BG, Dunn WC, Mohrenweiser H, Zimmerman W, Watt SM, Ashworth LK (1996) Detailed comparative map of human chromosome 19q and related regions of the mouse genome. *Genomics*. 35:499-508
- Termine JD, Kleinman HK, Whitson SW, Conn KM, McGarvey ML, Martin GR (1981) Osteonectin, a bone-specific protein linking mineral to collagen. *Cell*. 26:99-105
- Thellin O, Zorzi W, Lakaye B, De Borman B, Coumans B, Hennen G, Grisar T, Igout A, Heinen E (1999) Housekeeping genes as internal standards: use and limits. *Journal of Biotechnology* 75:291-295
- Trueblood NA, Xie Z, Communal C, Sam F, Ngoy S, Liaw L, Jenkins AW, Wang J, Sawyer DB, Bing OHL, Apstein CS, Colucci WS, Singh K (2001)

- Exaggerated left ventricular dilatation and reduced collagen deposition after myocardial infarction in mice lacking osteopontin. *Circ Res.* 88:1080-1070
- Van den Broek FA, Beems RB, van Tintelen G, Lemmens AG, Fielmich-Bouwman AX, Beynen AC (1997) Co-variance of chemically and histologically analysed severity of dystrophic cardiac calcification in mice. *Lab Anim.* 31:74-80
- Van den Broek FA, Bakker R, den Bieman M, Fielmich-Bouwman AX, Lemmens AG, van Lith HA, Nissen I, Ritskes-Hoitinga JM, van Tintelen G, van Zutphen LF (1998) Genetic analysis of dystrophic cardiac calcification in DBA/2 mice. *Biochem Biophys Res Commun* 253:204-208
- Van Etten WJ, Steen RG, Nguyen H, Castle AB, Slonim DK, Ge B, Nusbaum C, Schuler GD, Lander ES, Hudson TJ (1999) Radiation hybrid map of the mouse genome. *Nature genetics.* 22:384-387
- Van Vleet JF, Ferrans VF (1987) Ultrastructural changes in inherited cardiac calcinosis of DBA/2 mice. *Am J Vet Res.* 48:255-261
- Veldtman GR, Blackburn ME, Wharton GA, daCosta P, Gibbs JL (1999) Dystrophic calcification of the fetal myocardium. *Heart.* 81:92-93
- Vracko R, Thorning D (1985) Freeze-thaw injury of rat heart across an intact diaphragm: a new model for the study of the response of myocardium to injury. *Cardio-vasc Res.* 19:76-84
- Wahl SM (1994) Transforming Growth Factor β : The Good, the Bad, and the Ugly. *The Journal of Experiment Medicine.* 180:1587-1590
- Watson KE, Bostrom K, Ravindranath R, Lam T, Norton B, Demer LL (1994) Tgf-beta 1 and 25-hydroxycholesterol stimulate osteoblast-like vascular cells to calcify. *J Clin Invest.* 93:2106-2113

- Weinreb M, Shinar D, Rodan GA (1990) Different pattern of alkaline phosphatase, osteopontin, and osteocalcin expression in developing rat bone visualized by insitu hybridization. *J Bone Miner Res.* 5:831-842
- White RA, Dowler LL, Angeloni SV, Koeller DM (1996) Assignment of Etfhd, Etfb, and EtfA to chromosomes 3, 7, and 13: the mouse homologs of genes responsible for glutaric acidemia type II in human. *Genomics.* 33:131-134
- Williams RW, Gu J, Qi S, Lu L (2001) The genetic sturcture of recombinant inbred mice: high-resolution consensus maps for complex trait analysis. *Genome Biology* 2: research0046.1-0046, 18, 2001.
<http://genomebiology.com/2001/2/11/research/0046>
- Winer J, Jung CK, Shackel I, Williams PM (1999) Development and validiation of real-time quantitative reverse transcriptase-polymerase chain reaction for monitoring gene expression in cardiac myoytes in vitro. *Anal Biochem.* 270:41-49
- Wrogemann K, Pena SD (1976) Mitochondrial calcium overload: A general mechanism for cell-necrosis in muscle diseases. *Lancet.* 1:672-674
- Wu AH, Feng Y, Moore R, Apple FS, McPherson PH, Buechler KF, Bodor G (1998) Characterization of cardiac troponin subunit release into serum after acute myocardial infarction and comparison of assays for troponin T and I. *Clinical Chemistry.* 44:1198-1208
- Yamamura Y, Hua X, Bergelson S, Lodish HF (2000) Critical role of Smads and AP-1 complex in transforming growth factor- β -dependent apoptosis. *J Biol Chem.* 275:36295-36302
- Yin Y, Shackel NA, Zekry A, McGuinness PH, Richards C, Putten KV, McCaughan GW, Eris JM, Bishop GA (2001) Real-time reverse transcriptase-polymerase chain reaction (RT-PCR) for measurement of cytokine and

growth factor mRNA expression with fluorogenic probes or SYBR Green I.
Immunol cell biol. 79:213-221

Zamzami N, Kroemer G (2001) The mitochondrion in apoptosis: how Pandora's
box opens. Nature Rev Mol Cell Bio. 2:67-71

Acknowledgement

This thesis was prepared at the department of medicine II at the Medical University of Lübeck and was a part of a project sponsored by DFG grant (ref. Iv10/3-1) in the research group of Dr. med. T. B. Ivandic to whom I would like to express my profound gratitude and appreciation for his hearted diligent co-operation, criticism, and advice throughout the entire period of this investigation.

I would like to take this opportunity to thank the Director of the department of medicine II Prof. Dr. med. H. A. Katus and his representative Prof. Dr. med. G. Richardt for their continual financial support.

A special thanks goes to Prof. Dr. med. H. Schunkert, recently Director of the department of medicine II, and PD Dr. rer. nat. D. Reinhardt from the molecular biology institute for their fruitful advice and discussions during the last period of this thesis.

For technical assistance I would like to extend my thanks to S. B. Axtner at the department of medicine II during the genotyping analysis and J. Alex at the department of medicine I for ELISA analysis.

I also would like to thank PD Dr. med. M. Klinger and Prof. Dr. rer. nat. U. Schramm at the institute of anatomy for their precious cooperation and discussions on transmission electron microscope analysis and Dr. Dibbelt at the institute of clinical chemistry for plasma mineral determination.

Last but the most important I thank all my laboratory staff, P. M. Kaczmarek and L. C. Doehring and colleagues PD. Dr. S. O. Peters, and Dr. rer. nat. S. Stölting for their encouragement, valuable help and fruitful discussions during the period of this research.

Finally, I must express my gratitude to my family and relatives both at home and abroad for their encouragement and moral support.

Name	Zouhair Aherrahrou
Geburtsdatum	15.09.1968
Geburtsort	Rich/Marokko
Staatsangehörigkeit	Deutsch
Familienstand	verheiratet
Wohnort	Weidenkamp50, 25436 Uetersen
Ehefrau	Dr. Sandra Liedtke-Aherrahrou, Sinologin

Ausbildung:

April 2000-April 2003	Promotionsarbeit als Dr. hum. Biol.
Sept. 1997-Juni 1998	Weiterführende Studien im Bereich Biopharmazie
Sept. 1994-Juli 1997	Studium der Bio-Pharmazie an der China Pharmaceutical University. Abschluß mit dem Grad Master of Science
Sept. 1993-Juli 1994	Studium der chin. Sprache an der pädagogischen Hochschule Nanjing
Sept. 1989-Juli 1991	Studium an der Faculte des science Fes. Abschluß mit dem Bachelor in Biologie
Sept. 1986-Juli 1989	Studium an der Faculte des science Meknes. Abschluß mit DEUG in Biogeologie
Sept. 1983-Juli 1986	Gymnasium My Ali Cherif, Schwerpunkt: experimentelle Wissenschaften

Akademische Ausbildung:

Nov 2002 – Dec 2002	Mausgenetik Fortbildung (Institut Pasteur, Paris) Inhalt: Genetic recombination, gene mapping of complex traits, transgenesis and homologous recombination, conditional mutagenesis, chemical mutagenesis, X-inactivation, imprinting, epigenetic, cloning in mammals, embryogenesis.
seit April 2000	Biologischen Vorbereitung zur Promotion, Untersuchung der Ursachen dystropher kardiovaskulärer Verkalkungen am Menschen sowie am Mausmodell mittels molekulargenetischen und –biologischen Methoden, unter anderem mittels Immunohistologie, Genkartierung (RFLPs, Radiation Hybrid), Maus-Züchtung zum kongenen Mausmodell. PCR und RT-PCR, Klonierung und Sequenzierung

1994-1998

Abt. Biochemie/-pharmazie, Abschluß mit dem Grad Master of science **Thema:** Preparation of glutathione by biosynthesis reaction from yeast.

Publikation und Abstracts

- **Aherrahrou Z**, Axtner SB, Kaczmarek PM, Jurat A, Korff S, Doehring LC, Weichenhan D, Katus HA, Ivandic BT (2004) A locus on chromosome 7 determines Dramatic Up-Regulation of osteopontin in Dystrophic Cardiac Calcification in mice. *Am J Pathol.* 164: 1379-1387
- Ivandic BT, Utz UF, Kaczmarek PM, **Aherrahrou Z**, Axtner SB, Klepsch C, Lusic A, Katus HA (2001) New Dyscalc loci for myocardial cell necrosis and calcification (dystrophic cardiac calcinosis) in mice. *Physiol Genomics.* 28;6(3):137-44.
- **Zouhair Aherrahrou**, Xu Jiyang, Wu Wutong (1997) Determination of Glutathione in Biosynthesis Reaction by Paper Chromatography. *Journal of China Pharmaceutical University.* 28 (3): 176-17.

Richardt, B.T. Ivandic: Dystrophic cardiac calcification is associated with early upregulation of osteopontin in mice with genetic predisposition. Symposium on Phenotyping Mouse Cardiovascular Function and Development, National Institute of Health, Bethesda, MD, USA (October 10-11, 2002).

- G. Heinze, K. Terres Bauermeister, P.M. Kaczmarek, S. Stölting, R. Nadrowitz, **Z. Aherrahrou**, T. Wagner, S.O. Peters: Endothelial Cells in Solid Growing Wehi 164 and JC Tumors Derive from Bone Marrow Progenitor Cells. *Blood* 100, 2002, (44th ASH Annual Meeting 2002).
- B.T. Ivandic, P.M. Kaczmarek, **Z. Aherrahrou**, H.F. Utz: Genetische Basis der Myokardzellnekrose und -verkalkung, einer "response-to-injury"-Reaktion bei Mäusen. 67. Jahrestagung der Deutschen Gesellschaft für Kardiologie-, Herz- und Kreislaufforschung, Mannheim (19.-21. April 2001).